CEX-59.14

CIVIL EFFECTS STUDY

DETERMINATIONS OF AERODYNAMIC-
DRAG PARAMETERS OF SMALL
IRREGULAR OBJECTS BY MEANS
OF DROP TESTS

E. R. Fletcher, R. W. Albright,
V. C. Goldizen, and I. G. Bowen

Issuance Date: October 1961

CIVIL EFFECTS TEST OPERATIONS

U.S. ATOMIC ENERGY COMMISSION

DTIC QUALITY INSPECTED 4

20000911 093

NOTICE

This report is published in the interest of providing infor nation which may prove of value to the reader in his study of effects data derived principally from nuclear weapons tests and from experiments designed to duplicate various characteristics of nuclear weapons.

This document is based on information available at the time of preparation which may have subsequently been expanded and re-evaluated. Also, in preparing this report for publication, some classified material may have been removed. Users are cautioned to avoid interpretations and conclusions based on unknown or incomplete data.

DETERMINATIONS OF AERODYNAMIC-DRAG PARAMETERS OF SMALL IRREGULAR OBJECTS BY MEANS OF DROP TESTS

By

E. R. Fletcher, R. W. Albright,
V. C. Goldizen, and I. G. Bowen

Approved by: R. L. CORSBIE
Director
Civil Effects Test Operations

ABSTRACT

During the 1955 and 1957 Test Operations at the Nevada Test Site (NTS), masses and velocities were determined for more than 20,000 objects, such as glass fragments from windows, stones, steel fragments, and spheres, which were energized by blast winds resulting from nuclear explosions. Following the field tests, a mathematical model was devised to help explain quantitatively the experimental results. This model required certain aerodynamic-drag information in regard to the displaced objects. It was the purpose of the study outlined in this report to determine the necessary drag properties for the objects by means of drop tests.

In addition to the objects mentioned above, small laboratory animals, mice, rats, guinea pigs, and rabbits, were used in the drop tests. The data obtained from these tests were extrapolated to estimate the drag properties for man, and the results compared favorably with data from other sources. Also a method was developed to estimate the average drag properties of man from his total surface area, assuming that every possible orientation of a straight, rigid man with respect to the wind was equally likely.

ACKNOWLEDGMENTS

NOMENCLATURE

a = acceleration

C_D = drag coefficient

D = sphere diameter or other characteristic dimension

$°F$ = temperature, degrees Fahrenheit

F_d = drag force

F_g = force of gravity

g = acceleration of gravity

h = height of fall at time t or velocity v

H = total height of fall

K = acceleration-coefficient numeric $\equiv (\rho/g)\,(A/m)\,(\nu/D)^2$

m, M = mass

m_0 = reference mass

P_0 = atmospheric pressure, ambient

R_d = Reynolds number = vD/ν

R_V = a function concerned with error in computed velocity

R_α = a function concerned with error in computed α

R'_α = an approximation to R_α

R''_α = an approximation to R_α

s = frontal area of the object

t = instantaneous time

t = thickness of plate-like objects

t_0 = a reference thickness

T = total time of fall

T_{ND} = total time of fall assuming no drag forces

ΔT = $T - T_{ND}$

δT = timing error

v = instantaneous velocity

V = impact velocity

V_{ND} = "no-drag" impact velocity

ΔV = error in computed impact velocity

X = time numeric $\equiv tg(D/\nu)$

ΔX = increment of X

Y = height-of-fall numeric $\equiv hg(D/\nu)^2$

ΔY = increment of Y

Z = velocity numeric $\equiv R_d \equiv vD/\nu$

α = acceleration coefficient $\equiv sC_D/m$

α_0 = reference acceleration coefficient

$\Delta\alpha$ = error in computed α

θ_T = T/T_{ND}

θ'_T = an approximation to θ_T

θ''_T = an approximation to θ_T

θ_V = V/V_{ND}

7

θ'_V = an approximation to θ_V

ν = kinematic viscosity of the air

ρ = density of air

$'\rho$ = density of plate-like objects

ρ_0 = a reference density of plate-like objects

CONTENTS

CONTENTS (Continued)

ILLUSTRATIONS

ILLUSTRATIONS (Continued)

APPENDIX   DERIVATION OF EQUATIONS

TABLE

CHAPTER 4   ANALYSIS OF DATA

Chapter 1

INTRODUCTION

1.1 OBJECTIVES

During the 1955 and 1957 Test Operations at the Nevada Test Site (NTS), masses and velocities of more than 20,000 objects,[1-5] such as glass fragments from windows, stones, steel fragments, and spheres, which were energized by blast winds were experimentally determined, and the time-displacement history of an anthropometric dummy simulating man[6] was measured. The availability of such a mass of data stimulated an analytical study calculated to arrive at a mathematical formulation capable of predicting the translation of objects by blast winds. The model[7] designed to predict this translation assumed that certain aerodynamic properties of the objects displaced were known. The purpose of this report is to describe the drop-test studies, both theoretical and experimental, which were undertaken to determine the aerodynamic properties of interest.

1.2 HISTORICAL BACKGROUND

When objects dropped in air were first observed to fall at varying rates, it was presumed that the difference was inherent in the nature of the materials of which the objects were composed. In the early 16*th* century, Galileo disproved this theory and established the true cause of the observed variations. Small spheres of different substances were dropped at the same instant from the Leaning Tower of Pisa, and all hit the ground at nearly the same time. Next, Galileo dropped objects composed of the same materials in a variety of shapes and observed that they then fell at different rates. Galileo concluded that gravity acted upon all objects with the same intensity but that the air resisted their fall in varying degrees, depending on the object being dropped. It then followed that all objects would fall at the same rate in a vacuum.

After the invention of the air pump, Newton verified Galileo's theory with his famous "guinea and feather" experiment. A gold coin, called a "guinea," and a feather were placed in a tube about 5 ft long. When the tube was turned on end, they were observed to fall at different rates. When most of the air was removed from the tube with an air pump, no difference in the rates of fall of the guinea and the feather was perceivable.

The force with which the air acts upon a falling object came to be known as a drag force since it always resisted the motion of the object. The first experiments to determine the nature of this drag force were performed in 1853 by Piobert, Morin, and Didion,[8] who observed an object falling in air and recorded its velocity until it reached terminal velocity. Since the object at that point was not undergoing acceleration, the drag force equaled the force of gravity. They were able to obtain terminal velocities up to about 30 ft/sec. In 1892 Cailletet and Colardeau[9] dropped plane surfaces of various shapes from the Eiffel Tower and recorded the descent times; they obtained velocities up to 90 ft/sec. In 1905, Eiffel[10] conducted a series of experiments that involved attaching the object to be tested to an apparatus that slid down a

stretched wire. This apparatus actually recorded both the distance dropped and the drag force as a function of time, measured by the vibrations of a tuning fork. Velocities up to 130 ft/sec were obtained.

Today most experiments involving drag measurements are conducted in an artificial air stream.[11] This method possesses many advantages over the drop test. In addition to improving accuracy, the use of an artificial air stream makes it easier to vary the environment of the object being tested. The drop technique is, however, still used to determine air density,[12-15] to study parachute descents,[16-18] and to determine the drag force on bombs at high subsonic speeds.[19] It has also been used to study impact damage to small laboratory animals.[20-23]

REFERENCES

1. I. Gerald Bowen, Allen F. Strehler, and Mead B. Wetherbe, Distribution and Density of Missiles from Nuclear Explosions, Project 33.4, Operation Teapot Report, WT-1168, December 1956.
2. I. Gerald Bowen et al., Biological Effects of Blast from Bombs; Glass Fragments as Penetrating Missiles and Some of the Biological Implications of Glass Fragmented by Atomic Explosions, Report AECU-3350, Lovelace Foundation for Medical Education and Research, June 18, 1956.
3. I. Gerald Bowen et al., Secondary Missiles Generated by Nuclear-produced Blast Waves, Project 33.2, Operation Plumbbob Report, WT-1468, in preparation.
4. V. C. Goldizen et al., Missile Studies with a Biological Target, Project 33.4, Operation Plumbbob Report, WT-1470, Jan. 23, 1961.
5. V. C. Goldizen et al., Missile Studies with a Biological Target, Project 33.4, Operation Plumbbob Report, WT-1470, Jan. 23, 1961.
6. R. V. Taborelli, I. G. Bowen, and E. R. Fletcher, Tertiary Effects of Blast—Displacement, Project 33.3, Operation Plumbbob Report, WT-1469, May 1959.
7. I. Gerald Bowen et al., A Model Designed to Predict the Motion of Objects Translated by Classical Blast Waves, Report CEX 58.9, June 1961.
8. Memoirs on the Laws of Air Resistance (French), Memorial de l'Artillerie, No. 5, 1842; see also O. G. Tietjens (based on the lectures of L. Prandtl), *Applied Hydro- and Aeromechanics*, Chap. VII, p. 247, McGraw-Hill Book Company, Inc., New York, 1934.
9. L. Cailletet and E. Colardeau, Recherches expérimentales sur la chute des corps et sur la résistance de l'air à leur mouvement; expériences exécutees à la tour Eiffel, *Compt. rend.*, *115:* 13 (1892); see also O. G. Tietjens (based on the lectures of L. Prandtl), *Applied Hydro- and Aeromechanics*, Chap. VII, p. 247, McGraw-Hill Book Company, Inc., New York, 1934.
10. G. Eiffel, Experimental Researches on Air Resistance Conducted at the Eiffel Tower (French), Paris, 1907; see also O. G. Tietjens (based on the lectures of L. Prandtl), *Applied Hydro- and Aeromechanics,* Chap. VII, p. 248, McGraw-Hill Book Company, Inc., New York, 1934.
11. O. G. Tietjens (based on the lectures of L. Prandtl), *Applied Hydro- and Aeromechanics*, Chap. VII, p. 251, McGraw-Hill Book Company, Inc., New York, 1934.
12. L. M. Jones, Transit-time Accelerometer, *Rev. Sci. Instr.*, 27: 374-377 (1956).
13. L. M. Jones et al., Upper-air Density and Temperature: A Simplified Falling-sphere Method, Engineering Research Institute, The University of Michigan, Ann Arbor, Mich., undated.
14. F. L. Bartman et al., Upper-air Density and Temperature by the Falling-sphere Method, *J. Appl. Phys.*, 27: 706-712 (1956).
15. F. L. Bartman, Falling-sphere Method for Upper-air Density and Temperature, *J. Atmospheric and Terrest. Phys.*, Vol. 1, Spec. Suppl. (1954).
16. F. J. Stimler and R. S. Ross, Drop Tests of 16,000-sq in. Model Parachutes, Vol. VIII, Summary Report, AFTR-5867, Wright Air Development Center, May 1954.
17. A. P. Webster, Free Falls and Parachute Descents in the Standard Atmosphere, Report NACA-TN-1315, National Advisory Committee for Aeronautics, June 1947.

18. K. E. Penrod, G. L. Maison, and J. E. McDonald, The Rate of Descent of Parachutes from Various Altitudes, *J. Aeronaut Sci., 14:* 303-310 (1947).

19. B. Göthert, Comparison of Drop and Wind-tunnel Experiments on Bomb Drag at High Subsonic Speeds, Report NACA-TN-1186, National Advisory Committee for Aeronautics, May 1948.

20. R. F. Rushmer, Internal Injury Produced by Abrupt Deceleration of Small Animals, Report No. 1, Project 241, School of Aviation Medicine, Randolph AFB, Tex., Sept. 2, 1944.

21. R. F. Rushmer, E. L. Green, and H. D. Kingsley, Internal Injuries Produced by Abrupt Deceleration of Experimental Animals, Report No. 1, Project No. 401, School of Aviation Medicine, Randolph AFB, Tex., Jan. 15, 1946.

22. R. F. Rushmer, The Changes in Pressure in the Peritoneal Cavity Produced by Sudden Deceleration of Experimental Animals, Report No. 1, Project No. 472, School of Aviation Medicine, Randolph AFB, Tex., Apr. 19, 1946.

23. D. R. Richmond, I. G. Bowen, and C. S. White, Tertiary Blast Effects: The Effects of Impact on Mice, Rats, Guinea Pigs, and Rabbits, Technical Progress Report on Contract DA-49-146-XZ-055, submitted to the Defense Atomic Support Agency for publication on June 27, 1961; also to be published in *Aerospace Medicine* (September issue).

Chapter 2

EQUATIONS OF MOTION

2.1 INTRODUCTORY REMARKS

To predict the motion of an object displaced by the movement of the surrounding air, one must know the object's acceleration coefficient (α). The quantity α has been defined as the product of the presenting area and the drag coefficient divided by the mass of the object.[1] The same quantity is, of course, involved in the equations of motion of an object in free fall, where the object is moving instead of the air. It will be shown in this chapter by development of equations of motion that α can be determined experimentally by drop tests if the time of fall, height of drop, acceleration of gravity, and air density are known. Analysis of experimental data involves the assumptions that (1) no vertical air motion existed, (2) the air density remained constant over the entire drop interval, and (3) the α of the falling object did not change during the fall. Measures were taken to reduce air motion during the drop tests (see Chap. 3). Since the total drop height was less than 50 ft, the assumption of constant air density is reasonable. Changes in α may occur during fall by two processes: First, the presenting area may change for objects other than spheres because of rotation, and, second, the drag coefficient, a function of Reynolds number and thus of velocity of fall, may change. A further discussion of these topics will be found in Chap. 4.

2.2 BASIC EQUATIONS

A free-falling object is subjected to two forces: a drag force (F_d) resulting from the drag of the air on the object and the force of gravity (F_g). For the case of free fall in still air,

$$F_d = (^1\!/_2)\rho v^2 C_D s \tag{2.1}$$

and

$$F_g = mg \tag{2.2}$$

where F_d = drag force
ρ = air density
v = velocity of object
C_D = drag coefficient
s = frontal area of object
F_g = force of gravity
m = mass of object
g = acceleration of gravity

These two forces (F_d and F_g) act in opposition. By Newton's second law of motion, their algebraic sum is equal to the product of the mass and the acceleration (a) of the object, or

$$ma = mg - (\tfrac{1}{2})\rho v^2 C_D s$$

which can be written in the form:

$$a = g - (\tfrac{1}{2})\rho v^2 \frac{s C_D}{m} \tag{2.3}$$

The quantity $s C_D/m$ is the acceleration coefficient (α). Its units are area/mass (ft^2/lb is used throughout this report). Thus

$$\alpha = \frac{s C_D}{m} \tag{2.4}$$

Alpha has a special significance since it combines the significant parameters of the object which influence the drag force and consequently the acceleration of the object, i.e., if two objects with the same α were dropped at the same time under identical conditions, their accelerations and velocities would remain the same throughout the fall.

Therefore Eq. 2.3 can now be written as

$$a = g \left(1 - v^2 \frac{\rho \alpha}{2g} \right) \tag{2.5}$$

By definition, v and a can be written in differential form:

$$v = \frac{dh}{dt} \tag{2.6}$$

and

$$a = \frac{dv}{dt} \tag{2.7}$$

where t = time and h = height.

By combining Eqs. 2.6 and 2.7,

$$dh = \frac{v\,dv}{a} \tag{2.8}$$

and substituting a from Eq. 2.5 into Eq. 2.8,

$$dh = \frac{v\,dv}{g \left(1 - v^2 \dfrac{\rho \alpha}{2g} \right)} \tag{2.9}$$

Now, if α is assumed to be constant throughout the low-velocity range $v_1 < v < v_2$, Eq. 2.9 can be integrated (see Appendix, Sec. A.1.1) over the range $h_1 < h < h_2$ and $t_1 < t < t_2$ to give the following equations:

$$h_2 - h_1 = (\rho \alpha)^{-1} \ln \left\{ [1 - v_1 (\rho \alpha/2g)^{\frac{1}{2}}] [1 + v_1 (\rho \alpha/2g)^{\frac{1}{2}}] \right\}$$
$$- (\rho \alpha)^{-1} \ln \left\{ [1 - v_2 (\rho \alpha/2g)^{\frac{1}{2}}] [1 + v_2 (\rho \alpha/2g)^{\frac{1}{2}}] \right\} \tag{2.10}$$

and

$$t_2 - t_1 = (2g\rho\alpha)^{-\frac{1}{2}} \ln \{[1 - v_1 \ (\rho\alpha/2g)^{\frac{1}{2}}] \ [1 + v_2 \ (\rho\alpha/2g)^{\frac{1}{2}}]\}$$
$$- (2g\rho\alpha)^{-\frac{1}{2}} \ln \{[1 - v_2 \ (\rho\alpha/2g)^{\frac{1}{2}}] \ [1 + v_1 \ (\rho\alpha/2g)^{\frac{1}{2}}]\} \quad (2.11)$$

Before these equations were used for numerical computations, they were transformed to a more convenient nondimensional form, which is explained in the Appendix (Sec. A.1.2). Figure 2.1 illustrates how the drag coefficient of a sphere varies with Reynolds number.[2] The Reynolds number (R_d) is a dimensionless quantity defined by

$$R_d = \frac{vD}{\nu} \quad (2.12)$$

where R_d = Reynolds number
$\quad$ v = velocity of the sphere
$\quad$ D = diameter of the sphere
$\quad$ ν = kinematic viscosity of the air

Figure 2.2 shows the Reynolds number as a function of velocity and characteristic dimension (diameter for a sphere, length of side for a square plate, etc.). The characteristic dimension is read directly in inches; whereas, velocity is read directly only if the kinematic viscosity of the air is 0.000179 ft^2/sec. This value was chosen because it represents the average kinematic viscosity at 5300 ft above sea level,[3] the approximate altitude of the southeast section of Albuquerque, N. Mex., where the experiments were performed. If the kinematic viscosity has any other value, the velocity variable must be modified by the appropriate factor, as indicated in Fig. 2.2, to convert it to its true velocity. If the velocity, diameter of a sphere, and the kinematic viscosity of the surrounding medium are known, Fig. 2.2 can be used to find the Reynolds number. Then for that Reynolds number, the corresponding drag coefficient can be determined with the aid of Fig. 2.1.

2.3 EQUATIONS FOR CONSTANT α

If α is assumed to be constant throughout a fall; if the initial conditions are $v_1 = h_1 = t_1 = 0$; and if $v_2 = V$, $h_2 = H$, and $t_2 = T$ (see Appendix, Sec. A.1.1), Eqs. A.3 and A.5 become

$$V = (2gH)^{\frac{1}{2}} \ [(1 - e^{-\rho\alpha H})/\rho\alpha H]^{\frac{1}{2}} \quad (2.13)$$

and

$$T = [(2H/g)^{\frac{1}{2}} (\rho\alpha H)^{\frac{1}{2}}/2] + (2H/g)^{\frac{1}{2}} (\rho\alpha H)^{-\frac{1}{2}} \ln [1 + (1 - e^{-\rho\alpha H})^{\frac{1}{2}}] \quad (2.14)$$

An alternative way of writing Eq. 2.14 is

$$T = (2H/g)^{\frac{1}{2}} (\rho\alpha H)^{-\frac{1}{2}} \cosh^{-1} e^{\rho\alpha H/2} \quad (2.15)$$

An explicit solution of Eq. 2.13 for α in terms of V and H was not possible; however, for a fixed value of H, V can be plotted as a function of α. Such a plot, illustrated in Fig. 2.3, was found to be useful in a previous study of the impact loading of small anesthetized laboratory animals[4] in which impact velocity was determined by means of high-speed photography. The experimental data shown on this chart (Fig. 2.3), however, were determined in the present study (Sec. 4.5).

Acceleration as a function of height of fall can be found by substituting V from Eq. 2.13 into Eq. 2.5 to give

$$a = g \ e^{-\rho\alpha H} \quad (2.16)$$

2.4 EQUATIONS WITHOUT DRAG *

The equations for free fall with no-drag force and initial conditions $V = H = 0$ when $T = 0$ are

$$a_{ND} = g \tag{2.17}$$

$$V_{ND} = gT_{ND} \tag{2.18}$$

and

$$H = g\,(T_{ND})^2/2 \tag{2.19}$$

Equation 2.19 can be solved for T to give

$$T_{ND} = (2H/g)^{1/2} \tag{2.20}$$

Substituting T from Eq. 2.20 into Eq. 2.18 gives

$$V_{ND} = (2gH)^{1/2} \tag{2.21}$$

2.5 COMPARISON OF EQUATIONS OF MOTION WITH AND WITHOUT DRAG

A summary of the preceding equations is given here:

For any initial conditions:

(a) With drag (for constant α)

$$a = g\left(1 - v^2\,\frac{\rho\alpha}{2g}\right) \tag{2.5}$$

(b) No drag

$$a_{ND} = g \tag{2.17}$$

For initial conditions $v = h = 0$ when $t = 0$:

(a) With drag (for constant α)

$$V = (2gH)^{1/2}\,[(1 - e^{-\rho\alpha H})/\rho\alpha H]^{1/2} \tag{2.13}$$

$$a = g\,e^{-\rho\alpha H} \tag{2.16}$$

$$T = [(2H/g)^{1/2}\,(\rho\alpha H)^{1/2}/2] + (2H/g)^{1/2}\,(\rho\alpha H)^{-1/2}\;\ln\,[1 + (1 - e^{-\rho\alpha H})^{1/2}] \tag{2.14}$$

(b) No drag

$$V_{ND} = (2gH)^{1/2} \tag{2.21}$$

$$a_{ND} = g \tag{2.17}$$

$$T_{ND} = (2H/g)^{1/2} \tag{2.20}$$

---

*The subscript ND is used to indicate the no-drag value of the parameter; i.e., T_{ND} is the time an object would take to fall, assuming the object did not experience drag force.

For the initial conditions $v = h = 0$ when $t = 0$, the quantities with drag are arranged so that they differ from those without drag by a factor that is a function of the dimensionless quantity $\rho\alpha H$.

Figure 2.4 shows these results in a different form. Theta (θ) is defined as the ratio of a variable (V, T, or a) with drag to the same variable without drag and is a dimensionless quantity expressed as a function of the $\rho\alpha H$. For example, θ_V is the final or impact velocity divided by the velocity for a drop with no drag. The final or impact velocity can be computed from Fig. 2.4 and measured values of H, g, and T (assuming α, g, and ρ are constant). This calculation can be made by computing T_{ND} and θ_T and then using the θ_T curve to determine $\rho\alpha H$. For that value of $\rho\alpha H$, θ_V is then read and multiplied by the computed value of V_{ND} to determine the impact velocity. If the values for ρ and α are known and H is measured, θ_T and θ_V can be read directly from Fig. 2.4.

The dotted curves in Fig. 2.4, which are approximations to the solid curves, are good over certain ranges of $\rho\alpha H$ and are useful to simplify computations. They were computed from the following equations:

$$\theta_T' = [(\rho\alpha H)^{1/2}/2] + (\rho\alpha H)^{-1/2}\ln 2 \tag{2.22}$$

and

$$\theta_V' = (\rho\alpha H)^{-1/2} \tag{2.23}$$

These approximate relations depend upon the fact that $e^{-\rho\alpha H} \to 0$ very fast as $\rho\alpha H \to \infty$. Hence zero was substituted for $e^{-\rho\alpha H}$ in the equations for θ_T and θ_V (Fig. 2.4) to arrive at the approximations. Using Eq. A.16 from the Appendix (Sec. A.2) and the definition $\theta_V = V/V_{ND}$, one can write

$$V/V_t = \theta_V \, (2gH)^{1/2} \, (2g/\rho\alpha)^{-1/2}$$
$$= \theta_V \, (\rho\alpha H)^{1/2} = \theta_V/\theta_V'. \tag{2.24}$$

where V_t is the terminal or limiting velocity as $\rho\alpha H \to \infty$. Thus the convergence of θ_V' to θ_V indicates $V \to V_t$ or the approach of the velocity of an object to terminal velocity as the height of fall increases. Another approximation to θ_T,

$$\theta_T'' = 1 + (\rho\alpha H/12) \tag{2.25}$$

for low values of $\rho\alpha H$ was found by expanding θ_T in a Maclaurin's series as follows:

$$\theta_T(\rho\alpha H) = \theta_T \, |_0 + d\theta_T/d(\rho\alpha H) \, |_0 \, (\rho\alpha H) + d^2\theta_T/d(\rho\alpha H)^2 \, |_0 \, (\rho\alpha H)^2/2! + \dots$$
$$= 1 + (\rho\alpha H/12) + (\rho\alpha H)^2/480 + \dots \tag{2.26}$$

The approximation shown by Eq. 2.25 is then the first two terms of the Maclaurin's series for $\theta_T(\rho\alpha H)$.

Although impact velocity can be computed from height of fall with Fig. 2.4, as described in the preceding paragraphs, Fig. 2.5 represents a simpler way to accomplish the same thing. It is especially useful if $g = 32.174$ ft/sec^2, in which case, V, T, and H can be read directly. This value for g was chosen because it represents the acceleration of gravity[5] at sea level. If the acceleration of gravity has any other value, the velocity and time variables must be modified by the appropriate factors, as indicated in Fig. 2.5, to convert them to actual velocity and time.

2.6 ESTIMATIONS OF ERRORS

To estimate the percentage of error in computed impact velocity (V) introduced by a timing error (δT), the following equation was used:

$$100\Delta V/V = 100(\Delta V/\Delta T)(1/V)\ \Delta T = 100(a/V)\ \delta T \tag{2.27}$$

Substituting for a and V from Eqs. 2.16, 2.13, and 2.20 in Eq. 2.27 gives

$$100\Delta V/V = [(\rho\alpha H)^{\frac{1}{2}} e^{-\rho\alpha H}(1 - e^{-\rho\alpha H})^{-\frac{1}{2}}]\ 100\delta T/T_{ND}$$

$$= R_V \cdot 100\delta T/T_{ND} \tag{2.28}$$

where R_V is the dimensionless quantity in brackets. Figure 2.6 is a plot of R_V vs. $\rho\alpha H$. To find the estimated percentage of error in computed impact velocity due to error in measured time of fall, determine R_V from Fig. 2.6 and use this value in Eq. 2.28. It is interesting to note that $100\Delta V/V < 100\delta T/T_{ND}$ for all values of $\rho\alpha H$; indeed, by substituting

$$T_{ND} = T\{[(\rho\alpha H)^{\frac{1}{2}}/2] + (\rho\alpha H)^{-\frac{1}{2}} \ln [1 + (1 - e^{-\rho\alpha H})^{\frac{1}{2}}]^{-1}\}$$

from Eqs. 2.14 and 2.20 into Eq. 2.28, it can be shown that $\Delta V/V < \delta T/T$ for all values of $\rho\alpha H$. Thus impact velocity can be determined with greater accuracy, percentagewise, than the measurement of time of drop from which it is computed.

A similar procedure was used to estimate the percentage of error in computed α introduced by a timing error δT.

$$100\Delta\alpha/\alpha = 100(\Delta\alpha/\Delta T)(1/\alpha)\Delta T = 100\left(\frac{dt}{d\alpha}\ \alpha\right)^{-1}\delta T \tag{2.29}$$

Differentiate Eq. 2.14 with respect to α and substitute in Eq. 2.29 to obtain

$$100\Delta\alpha/\alpha = 2\{[(\rho\alpha H)^{\frac{1}{2}}/2] - (\rho\alpha H)^{-\frac{1}{2}} \ln [1 + (1 - e^{-\rho\alpha H})^{\frac{1}{2}}] + (\rho\alpha H)^{\frac{1}{2}} e^{-\rho\alpha H}[(1 - e^{-\rho\alpha H})$$

$$+ (1 - e^{-\rho\alpha H})^{\frac{1}{2}}]^{-1}\}^{-1}\ 100\delta T/T_{ND}$$

$$= R_\alpha\ 100\delta T/T_{ND} \tag{2.30}$$

where the dimensionless quantity in braces is given the symbol R_α.

Figure 2.7 is a plot of R_α vs. $\rho\alpha H$. To find the estimated percentage of error in computed α resulting from error in measured time of fall, determine R_α from Fig. 2.7 and use this value in Eq. 2.30. The two dashed curves are reasonable approximations to the solid curve over certain ranges of $\rho\alpha H$. The R_α'' approximation was formed in the same way the θ_T' and θ_V' approximations were formed (Eqs. 2.22 and 2.23). The R_α' approximation for low values of $\rho\alpha H$ was obtained by differentiating Eq. 2.25 and substituting it into Eq. 2.29 to obtain

$$R_\alpha' = 12/\rho\alpha H \tag{2.31}$$

Equation 2.31 was used to approximate the timing accuracy needed for the experiment, where $\rho \approx 0.06\ lb/ft^3$, $H \approx 50\ ft$, $g \approx 32\ ft/sec^2$, and $\alpha \approx 0.03\ ft^2/lb$. Since the timing requirement is greatest for low values of α, the value used in this report was the lowest one anticipated for the objects to be dropped. From Eq. 2.31, $R_\alpha \approx 12/\rho\alpha H = 12/0.09$. If this value of R_α is used for the quantity in braces in Eq. 2.30,

$$100\Delta\alpha/\alpha = (12/0.09)100\delta T[2(50)/32]^{-\frac{1}{2}} \approx 7500\delta T$$

Thus, if $\delta T = 0.2$ msec, then $100\Delta\alpha/\alpha \approx 1.5$ per cent. Therefore to limit the error in computed α to about 1 per cent, the timing mechanism would need to determine the drop time to the nearest 0.1 msec.

REFERENCES

1. I. Gerald Bowen et al., A Model Designed to Predict the Motion of Objects Translated by Classical Blast Waves, Report CEX 58.9, June 1961.
2. S. F. Hoerner, author and publisher, *Fluid-dynamic Drag*, pp. 3-8 and 3-15, Midland Park, N. J., 1958.
3. Internal Civil Aviation Organization, Montreal, Can., and Langley Aeronautical Laboratory, Langley Field, Va., Manual of the ICAO Standard Atmosphere Calculations by the NACA, NACA-TN-3182, May 1954.
4. D. R. Richmond, I. G. Bowen, and C. S. White, Tertiary Blast Effects: The Effects of Impact on Mice, Rats, Guinea Pigs and Rabbits, Technical Progress Report on Contract DA-49-146-XZ-055, submitted to the Defense Atomic Support Agency for publication on June 27, 1961; also to be published in *Aerospace Medicine* (September issue).
5. Robert W. Knox, Coast and Geodetic Survey, Department of Commerce, letter to the Lovelace Foundation for Medical Education and Research, Aug. 9, 1955.
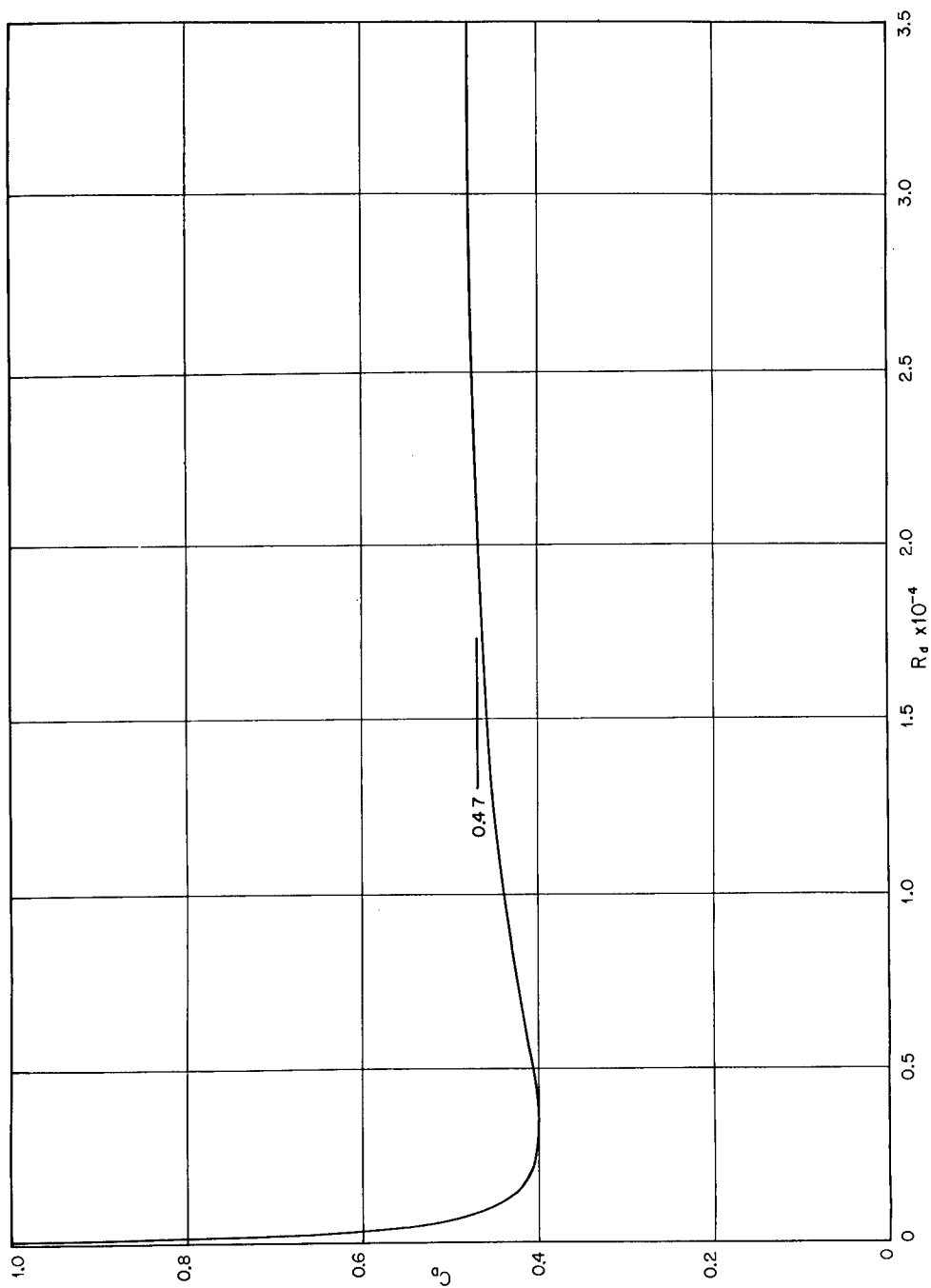
Fig. 2.1—Drag coefficient of spheres vs. Reynolds number. Over a large range of Reynolds numbers, C_D is nearly constant at 0.47. (Data from Ref. 2.)
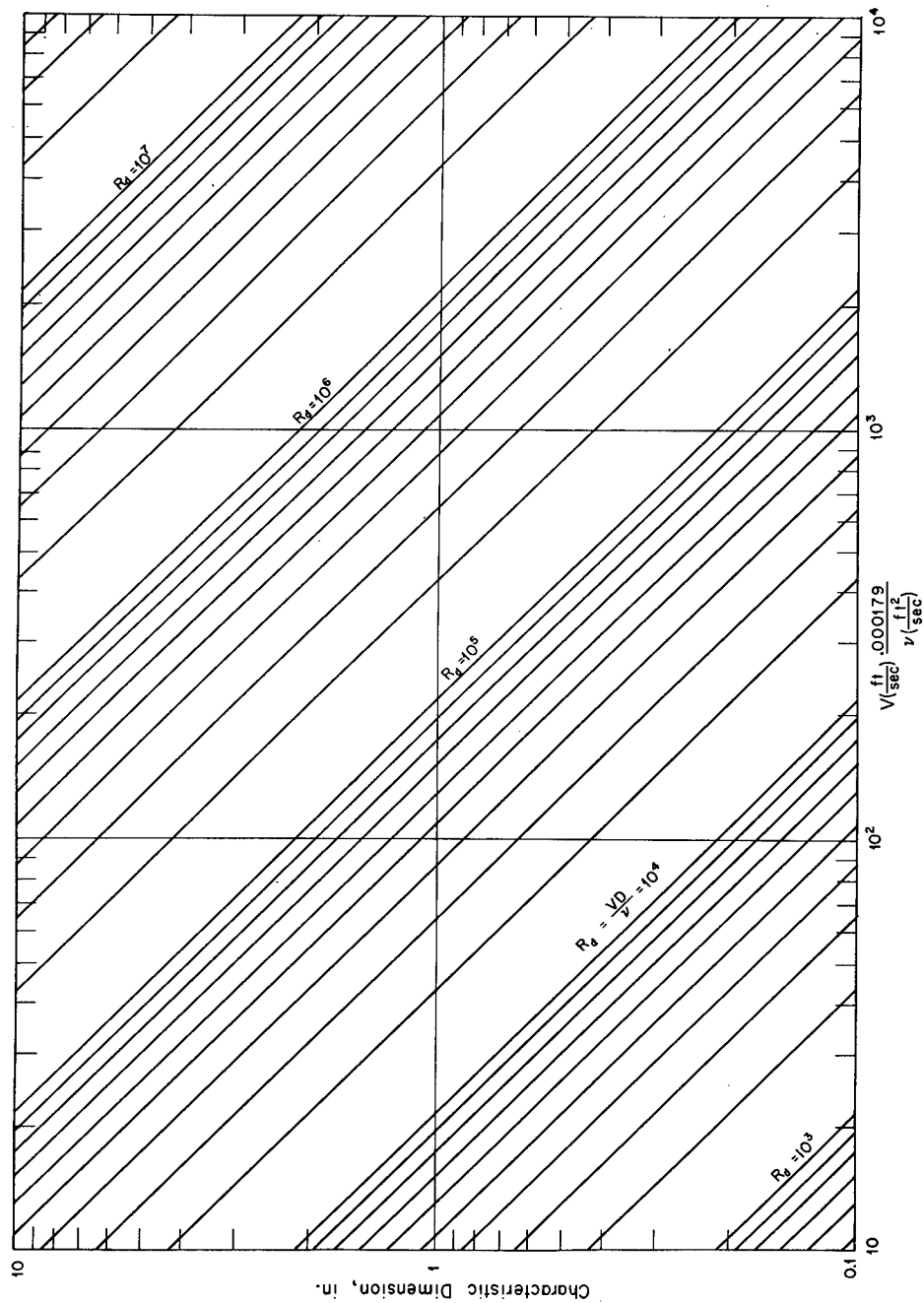
Fig. 2.2.— Reynolds number vs. velocity, characteristic dimensions, and kinematic viscosity. Characteristic dimension is the diameter of a sphere, length of side of a square plate, etc.
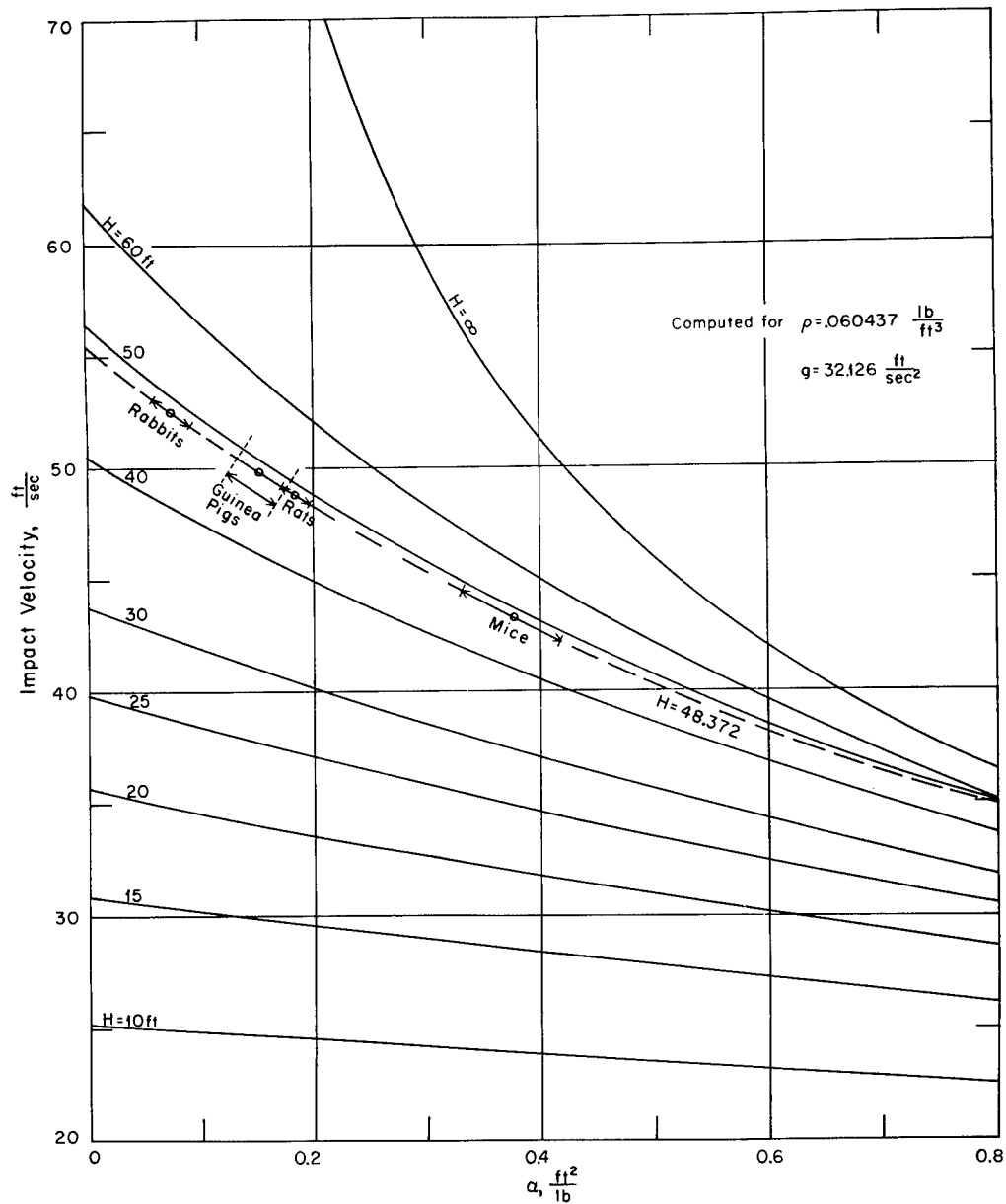
Fig. 2.3 — Impact velocity vs. height of fall and α. Included in the figure are the animal data from the present report showing mean values (represented by o) and standard deviations (represented by ⟷) of the experimentally determined α.

$$\theta_a = \frac{a}{a_{ND}} = \bar{e}^{\rho \alpha H}$$

$$\theta_V = \frac{V}{V_{ND}} = \sqrt{\frac{1 - \bar{e}^{\rho \alpha H}}{\rho \alpha H}}$$

$$\theta_T = \frac{T}{T_{ND}} = \frac{\sqrt{\rho \alpha H}}{2} + \frac{1}{\sqrt{\rho \alpha H}} \ln_e \left(1 + \sqrt{1 - \bar{e}^{\rho \alpha H}}\right)$$

$$\theta = \frac{\sqrt{\rho \alpha H}}{2} + \frac{\ln_e{(2)}}{\sqrt{\rho \alpha H}}$$

$$\theta = 1 + \frac{\rho \alpha H}{12}$$

$$\theta = \frac{1}{\sqrt{\rho \alpha H}}$$

WHERE $a_{ND} = g$

$V_{ND} = \sqrt{2gH}$

$T_{ND} = \sqrt{\frac{2H}{g}}$
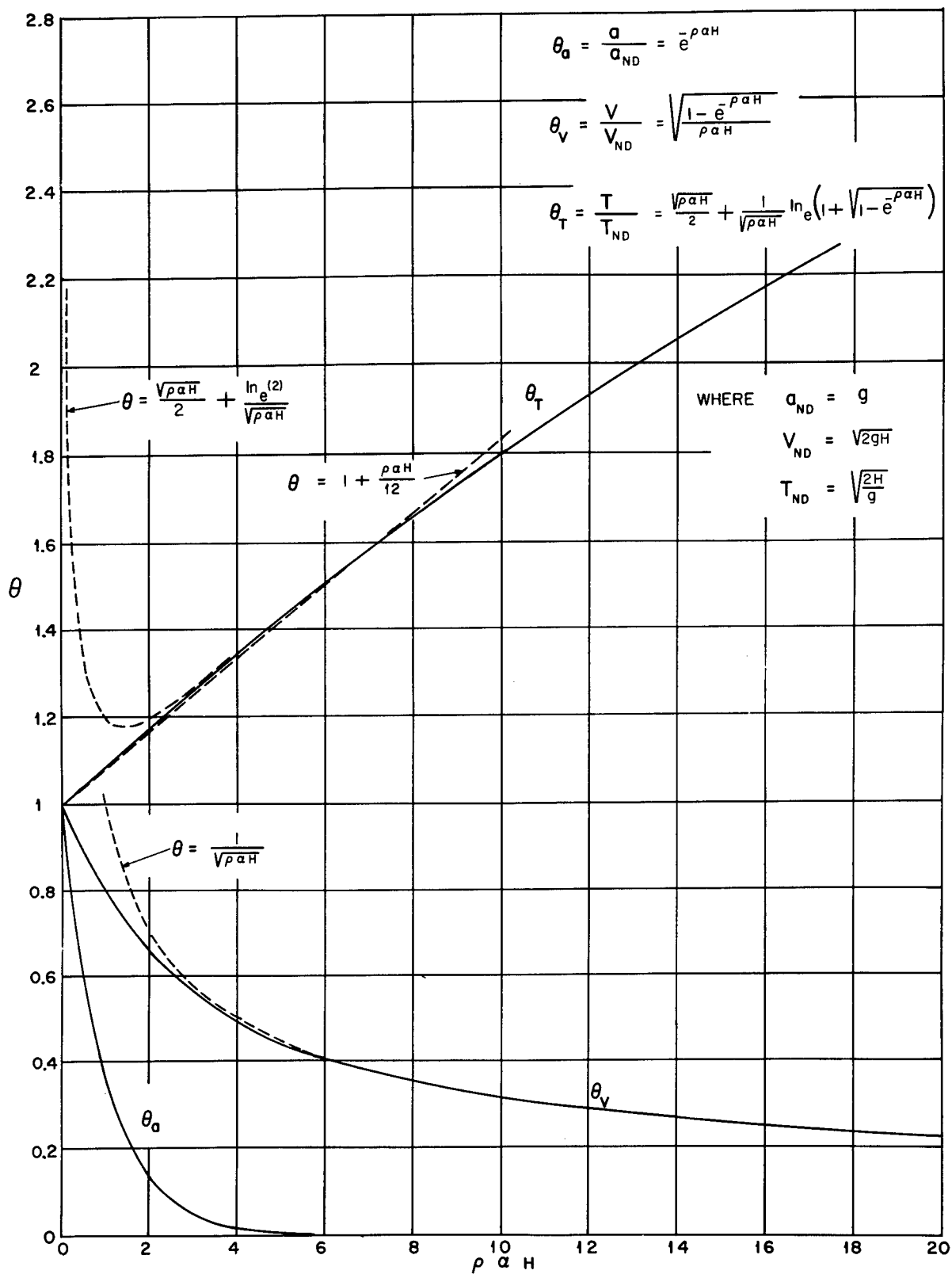
Fig. 2.4—Comparison of the drop parameters for the drag and no-drag cases. The dotted lines, which are approximations to the solid lines, are good over certain ranges of $\rho \alpha H$ (see text).
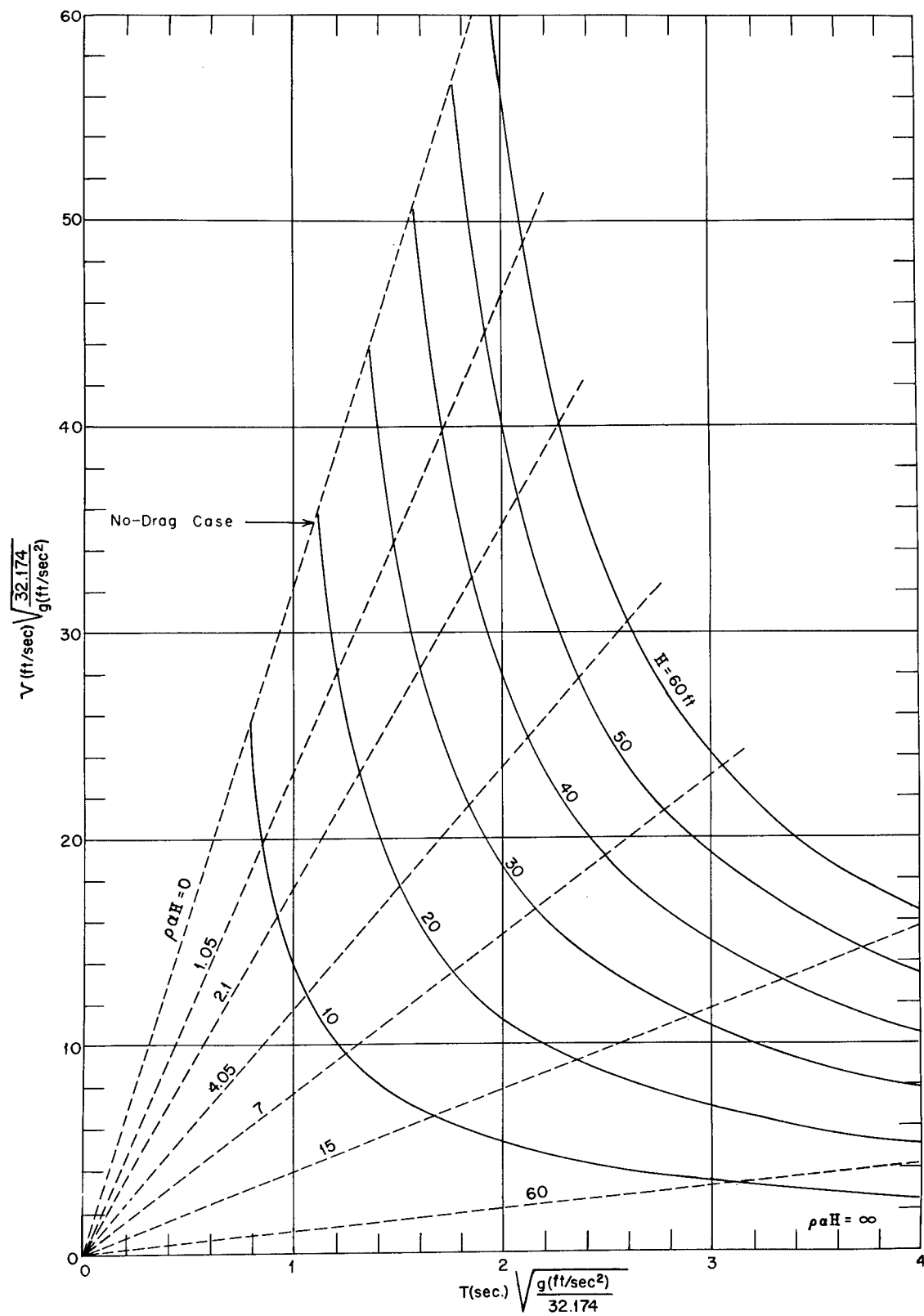
Fig. 2.5—Impact velocity vs. time of fall computed for several drop heights. Velocity and time can be evaluated for any acceleration of gravity. $\rho\alpha H$ lines are included for orientation.
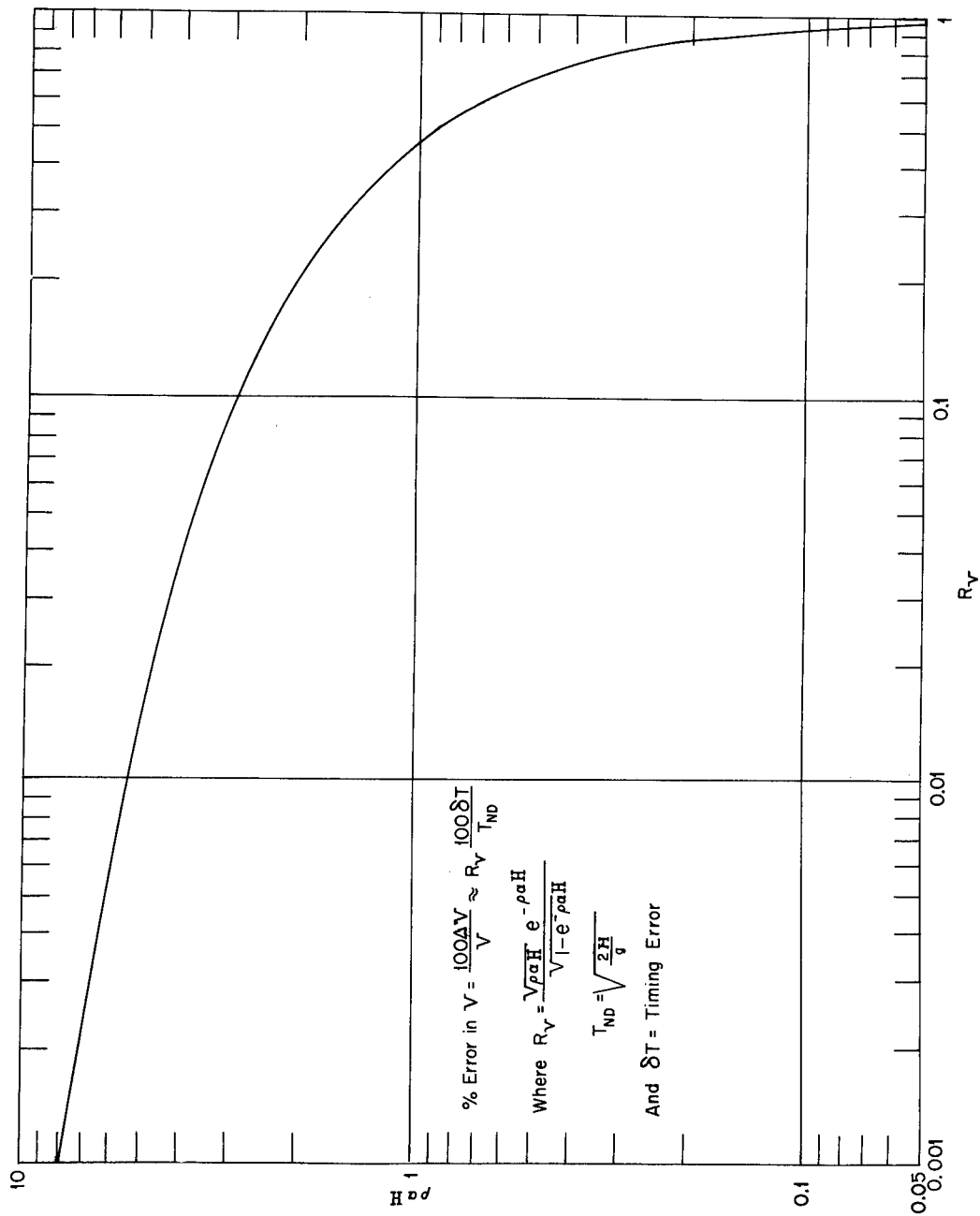
Fig. 2.6 — Method for estimating error in computed impact velocity resulting from error in measured time of fall. Find R_V from curve and percentage of error in V from equation shown.

% Error in $V = \dfrac{100 \Delta V}{V} \approx R_V \dfrac{100 \delta T}{T_{ND}}$

Where $R_V = \dfrac{\sqrt{\rho a H}\ e^{-\rho a H}}{\sqrt{1 - e^{-\rho a H}}}$

$T_{ND} = \sqrt{\dfrac{2H}{g}}$

And δT = Timing Error
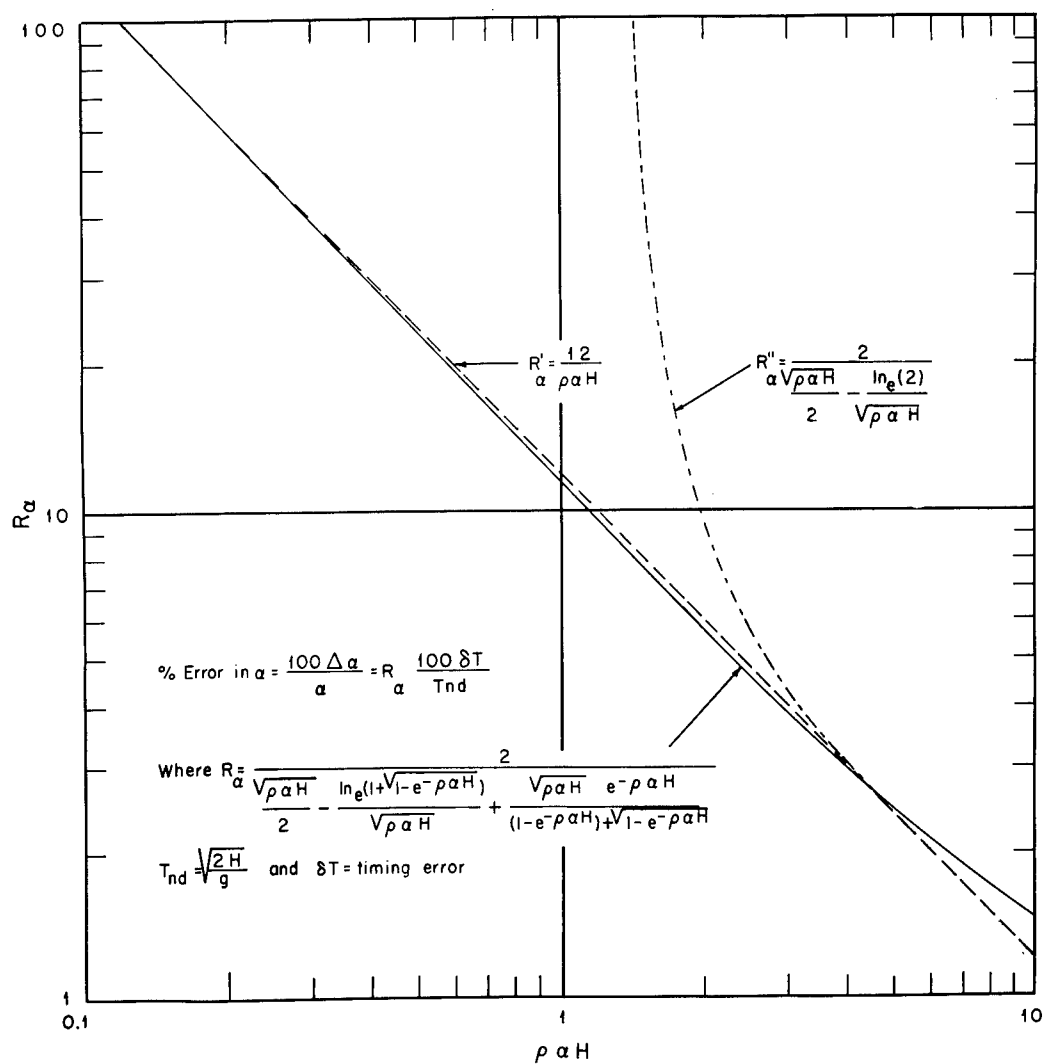
Fig. 2.7—Method for estimating error in computed α resulting from error in measured time of fall. Find R_α from curve and percentage of error in α from equation shown.

Chapter 3

EXPERIMENTAL PROCEDURE

The experimental system used to measure the time required for various objects to fall a measured distance is shown diagrammatically in Fig. 3.1. The object to be dropped was placed near the end of a bar that was designed to swing about its mid-point (see drop device in upper right of Fig. 3.1). The drops were initiated manually by tripping the catch shown just left of the microswitch. This action allowed a helical spring to rotate the bar about its mid-point. As the bar began to move, the test object was left free to fall; and, at the same time, the micro- switch was activated, starting an electronic timer (Hewlett Packard Electronic Counter, model 522-B). At the termination of the fall, the test object struck an aluminum plate, creating a noise, which was detected by a contact microphone placed on the underside of the impact plate. The signal from the microphone then stopped the electronic timer.

Figure 3.2 is a picture of the drop apparatus and a close-up view of the release mecha- nism. The dropping bar, supported on both sides by vertical members, was made thin ($\frac{3}{8}$ in.) to minimize air disturbance during release of the test object. Plates of various sizes were made to be attached to the right end of the dropping bar, whose total length was 32 in., so that objects as large as a rabbit could be conveniently dropped. A helical spring, hidden from view by the vertical support, was designed to ensure that the downward acceleration of the right side of the bar would be greater than the acceleration of gravity. After the bar moved approxi- mately 90°, its energy was partially dissipated by impact with a small pad of Ensolite (a product of the U. S. Rubber Co.) placed between the upright supports; thus rebound was less- ened, preventing interference of the bar with the falling object.

It was necessary to pay particular attention to the design and construction of the release mechanism. If any motion had been imparted to the dropping bar during the process of release, then the times of drop would not have been reproducible. Therefore, the sliding parts of the latch were made of blocks of tool steel, precision ground and clamped at the ends of the drop- ping bar; and the vertical bar, shown on the left side of Fig. 3.2, was designed to pivot about a point near the base of the apparatus. Even after taking these precautions in design, it was found that more reproducible times of drop could be obtained if the catch were released slowly by means of the knurled nut shown at the left in Fig. 3.2, thus minimizing motion induced in the dropping bar.

Tests were conducted in an elevator shaft in which objects were dropped 48.372 ft. Pre- cautions were taken to minimize vertical air currents by keeping all access doors to the shaft closed.

The impact plate shown schematically in Fig. 3.1 consisted of a $\frac{1}{4}$-in.-thick 2-ft^2 alumi- num plate. The plate was fastened to a table-like support about 6 in. high made of $\frac{3}{4}$-in.-thick plywood in which a hole was made in the center to accommodate the contact microphone. It is pertinent to note that the impact plate made a relatively small target for irregular objects dropping 48 ft. Occasional "misses" were experienced, especially by the smaller asymmetri- cal objects. Plate-like objects dropped flat also tended to veer away from the impact plate if

a small degree of rotation occurred. Surprisingly enough, the release operator could usually observe the object's fall well enough to detect the presence or absence of rotation. Thus the data included in this report are for objects that had little or no rotation while falling.
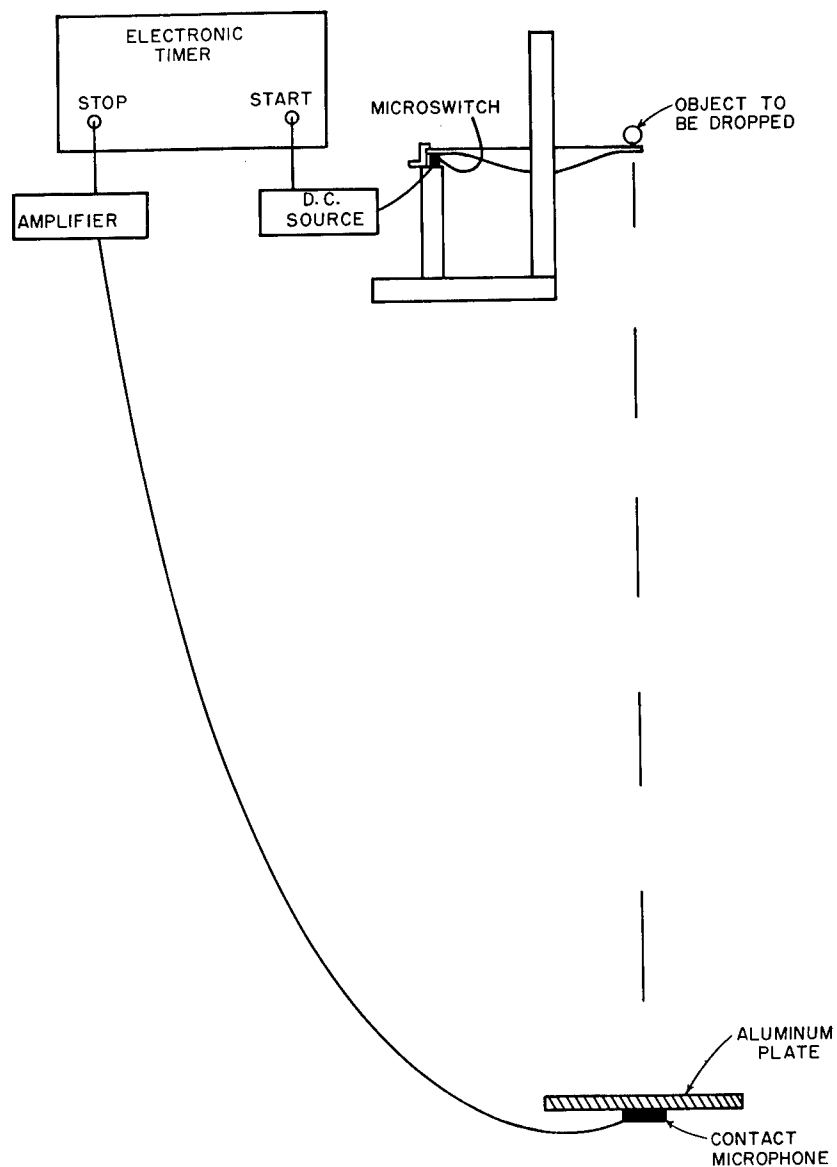
Fig. 3.1 — Block diagram of the drop-test equipment showing release apparatus and starting and stopping circuits.
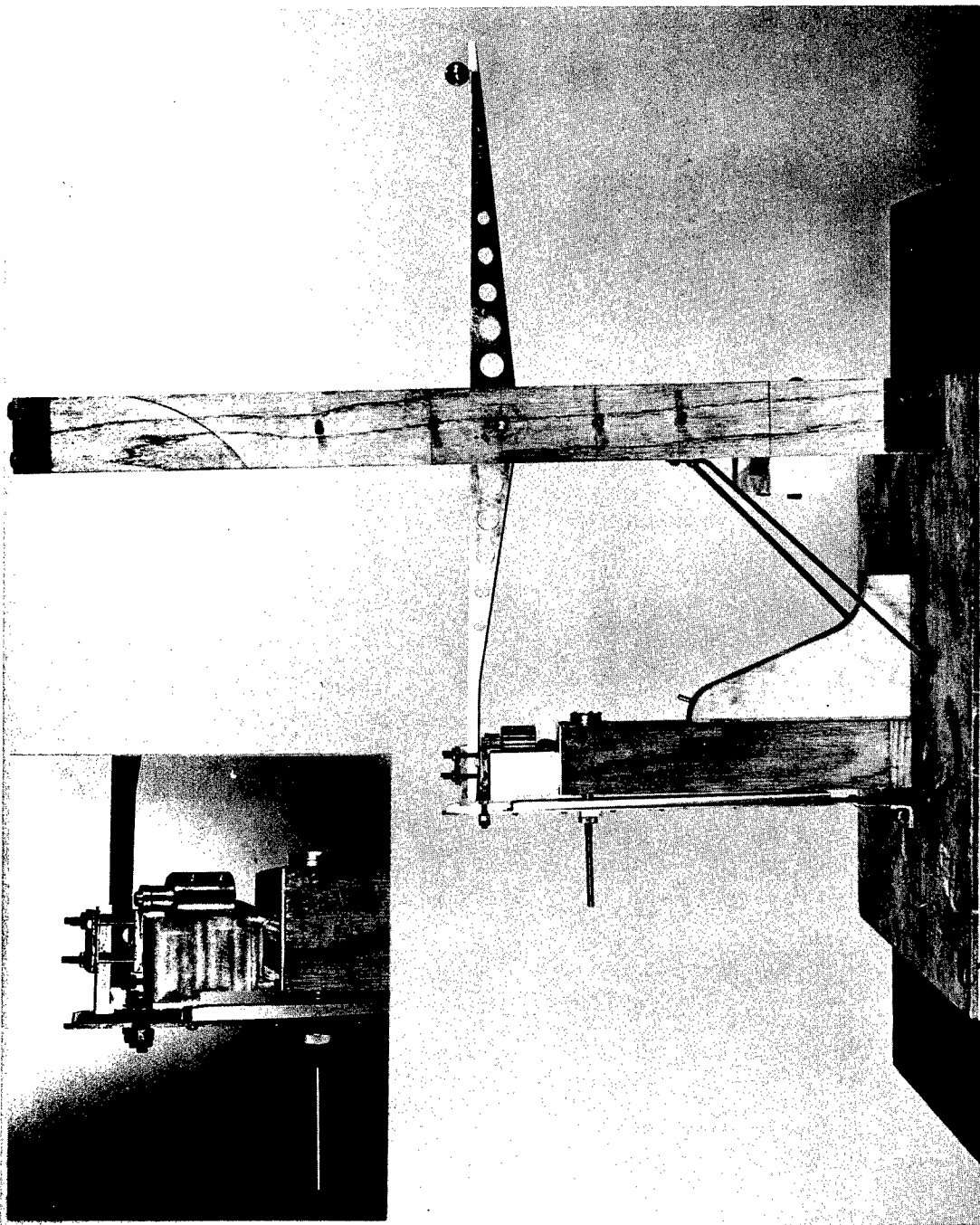
Fig. 3.2—Release apparatus used in the drop tests. The helical spring designed to accelerate the motion of the dropping bar (shown in horizontal position) is hidden from view behind the vertical support. The inset is an enlargement of the release mechanism (see text).

Chapter 4

ANALYSIS OF DATA

4.1 CONSTANTS FOR THE DROP TESTS

The constants for the drop tests were

$$g = 32.126 \text{ ft/sec}^2$$

$$H = 48.372 \text{ ft}$$

$$\rho = 0.060437 \text{ lb/ft}^3$$

$$\nu = 0.0002071 \text{ ft}^2/\text{sec}$$

The value of g was obtained from the Coast and Geodetic Survey, Department of Commerce.[1] H was measured directly; whereas, ρ and ν were computed by measuring the air pressure and temperature and substituting them in the following derived equations:[2]

$$\rho \left(\frac{\text{lb}}{\text{ft}^3}\right) = \frac{2.6954 \, p_0 \, (\text{psi})}{459.69 + t(°F)} \tag{4.1}$$

$$\nu \left(\frac{\text{ft}^2}{\text{sec}}\right) = \frac{2.7803 \, (10)^{-7} \, [456.69 + t(°F)]^{5/2}}{p_0 \, (\text{psi}) \, [675.69 + t(°F)]} \tag{4.2}$$

Since the drop tests were conducted over a period of three days, the above values of ρ and ν are averages; however, the deviations about these average values from day to day were small, the range in both cases being less than 1 per cent.

4.2 TIME CORRECTIONS

Steel spheres, $7/16$ and $3/16$ in. in diameter, were dropped during each of the three days when drop tests were conducted. Although the drop times for a particular sphere on a given day were quite consistent (low standard error), the mean drop time varied significantly from day to day. Since the air density remained nearly constant, the differences were probably due to minor adjustments that had been made on the microswitch and the release apparatus between daily tests.

The circumstance stated above pointed to the need for accurately computed drop times for the two "calibration" spheres in order to determine the timing deviations inherent in the experimental equipment. This was accomplished by the stepwise integration of Eqs. 2.10 and 2.11, the height of drop and time of drop being computed for small steps in velocity for which

C_D (and thus α) could be considered to have a constant value (see Fig. 2.1). Thus the following values were computed for time above no-drag time (ΔT): For a $\frac{3}{16}$-in.-diameter steel sphere, $\Delta T = 35.05$ msec; and for a $\frac{7}{16}$-in.-diameter steel sphere, $\Delta T = 14.91$ msec.

These values, when compared to the measured times of drop, indicated that the timing error for each day was essentially the same for the two spheres. The average corrections to be added to the measured times of fall were calculated to be: first day, $+3.45$ msec; second day, -0.14 msec; and third day, -1.65 msec.

In addition to these corrections, another correction was needed for the tests when heavy objects were dropped on a pad of Ensolite. This 1-in.-thick pad was used on the third day to help protect the contact microphone. Several spheres were dropped both with and without the pad. The differences in times of fall produced by the pad were plotted against the uncorrected times of fall with the pad. The points indicated a linear relation. This correction was then combined with the constant correction previously determined for the third day to give a total time correction (Fig. 4.1).

4.3 DATA FOR SPHERES, STONES, AND MILITARY DEBRIS

4.3.1 Introductory Remarks

It was implied in Sec. 4.2 that to determine an accurate time of drop relation for spheres, it was necessary to allow for a varying α dependent on the Reynolds number, which changes throughout the fall. If this were true for irregular objects, then the drop-test technique would be doomed to failure since the relation between drag coefficient and Reynolds number is not known for objects of interest to this study. In this section it will be shown that the dependence of α upon Reynolds number for irregular stones is evidently quite different from that for spheres. This difference makes it reasonable to assume for experimental purposes that α for stones can be considered to be constant for the entire drop interval.

4.3.2 Sphere Data

First, it will be necessary to examine the test data for the spheres. Figure 4.2 shows a plot of "theoretical" α (based on $C_D = 0.47$) for spheres vs. measured time of drop in excess of the no-drag time. The curve shown was computed assuming a constant α by using Eq. 2.14. For most of the spheres, the times measured were either too low or too high when compared to the constant α curve. An examination of the lower curve in Fig. 4.3 will help explain those deviations. Marked on this chart are the Reynolds numbers computed for the final or impact velocities for various spheres. The position of the $\frac{1}{16}$-in.-diameter steel sphere, for instance, indicates that high drag coefficients existed for a large percentage of the fall. The effect of this was that the measured time of drop was longer than that expected assuming a constant drag coefficient of 0.47 (Fig. 4.2). Times for the $\frac{1}{8}$-in.-diameter steel spheres, on the other hand, corresponded reasonably well with the constant α assumption. Undoubtedly the reason for this was that the effect of the initially high drag coefficients were compensated for by coefficients lower than 0.47 near the termination of the drop[3] (Fig. 4.3). For spheres still larger in diameter (e.g., $\frac{3}{4}$-in.-diameter aluminum spheres), the drop times were less than expected since a larger percentage of the drop-interval involved low drag coefficients (Fig. 4.3). The sphere drop involving the highest Reynolds numbers was that of a 3.34-in.-diameter croquet ball whose weight had been increased with a brass plug. In this instance a large portion of the drop entailed drag coefficients whose values were near 0.47. Thus the measured drop time corresponded closely to that expected for a constant coefficient of this value. It is interesting to note that the "effective" drag coefficient for the entire drop interval can be approximated in each individual instance by the coefficient corresponding to one-half the Reynolds number.

4.3.3 Stones Compared to Spheres

To study the differences in the Reynolds number–drag relation between spheres and irregular objects, it was necessary to analyze the two groups of data similarly. This involved

computing effective α for each sphere drop, assuming that the drag coefficient was constant for the entire drop (Eq. 2.14). The α values so computed were then plotted as a function of sphere mass, as illustrated in Fig. 4.4. If the drag coefficient is assumed to be constant, it can be shown that α for spheres of a constant density varies inversely as mass to the $\frac{1}{3}$ power. Thus, if the drag coefficient had the same constant value for all sizes of like-density spheres, the least-squares regression lines shown in Fig. 4.4 would have slopes of $-\frac{1}{3}$. Deviations from this value indicate that the smaller spheres had effective drag coefficients somewhat greater than those for the larger spheres.

Statistical data pertinent to the slopes of the least-squares regression lines for spheres and stones are recorded in Table 4.1. In addition to the slopes, the standard deviations of the slopes were computed; and from these data the probability (pr) that the measured slopes could have been deviations from the "true" slope of $-\frac{1}{3}$ was computed. Although the probabilities for the individual cases varied considerably, that for a combination of all spheres proved to be only 0.034. Stated in physical terms, the Reynolds number–drag relation for spheres is such that, for the purposes of the present study, the effective drag coefficient varies from one size sphere to another.

Table 4.1 also presents the results of a similar statistical treatment for six types of irregular stones. With one exception, pumice, the probabilities that the measured slopes could have been deviations from the "true" slope of $-\frac{1}{3}$ were quite high. This finding indicated that the computed slopes are likely to be random variations from the true slope. The variation of the pumice data from the $-\frac{1}{3}$ slope was probably due to the absorption of moisture from the air in the outer layer. If this layer were of uniform thickness, the smaller stones would suffer a larger relative increase in weight than would the larger stones.

4.3.4 Stone Data

The reasoning presented above seemed to justify a constant-α assumption. The α values for individual objects were, therefore, determined graphically from a curve of α vs. ΔT similar to that shown in Fig. 4.2.

Figure 4.5 is a plot of experimentally determined α for 41 pieces of painted gravel as a function of mass. These stones were taken from a sample of stones that was marked for identification and used in secondary-missile experiments in Nevada during the Operation Plumbbob weapons tests.[4] Since the stones actually used in these experiments had masses less than 1500 mg, a separate analysis was made for these. In addition, another analysis was made for all stones, assuming a slope of the least-squares regression line of $-\frac{1}{3}$ (Sec. 4.3.3). The results of both analyses are shown in Fig. 4.5.

Drop tests were made with limestone fragments so that there could be a comparison of the results with stones whose densities were less uniform. The slope of the least-squares regression line determined for these data (Fig. 4.6) is reasonably near the expected value of $-\frac{1}{3}$.

The data shown in Figs. 4.7, 4.8, and 4.9 are for stones obtained at three different locations (10P4, 1S1A, and 4.3 GTS) at NTS during Operation Plumbbob.[4] An analysis was made of the combined data for stones at the 10P4 and 1S1A locations because the individual analyses were remarkably similar.

Figure 4.10 contains the data for the pumice fragments that were discussed in Sec. 4.3.3. The least-squares regression lines for all the stone data are displayed in Fig. 4.11. An examination of this figure points to the similarity between pumice and stones at the 4.3 GTS location, both having higher α for given stone masses than the other samples.

4.3.5 Military-debris Data

The military debris used in the drop tests consisted of steel shrapnel and a few other irregular pieces of steel, all of which had been used and recovered as secondary missiles in the Operation Plumbbob study.[4] The α-mass data for these steel fragments are shown in Fig. 4.12. For comparison purposes, the theoretical α-mass relation for steel spheres, assuming $C_D = 0.47$, is shown on the same chart. It is apparent and reasonable that, for a given mass, a fragment of steel has a much larger α than does a steel sphere. The slope of the least-squares

regression line is less than that for the theoretical line for spheres; however, it is not as flat as a line for plates (Sec. 4.4).

4.4 DATA FOR PLATES, CUBES, AND GLASS FRAGMENTS

4.4.1 Introductory Remarks

Drag properties of window- and plate-glass fragments were of interest to this study because they constitute biological hazards when hurled through the air by the action of a blast wave on a structure containing windows.[4] Regular plates and cubes were studied only for the purpose of better interpretation of the glass-fragment data obtained in full-scale nuclear tests.

4.4.2 Regular Plates and Cubes

It should be pointed out that the plates referred to in this study are really "thick" plates, i.e., no attempt was made to sharpen the edges in order to achieve the "thin" plate that is usually used in wind-tunnel studies. For this reason the Reynolds number–drag relation shown in the upper part of Fig. 4.3 does not strictly apply to the experimental data reported here. However, it is useful to note in Fig. 4.3 that within the region of interest the variation in drag coefficient is less than 5 per cent (from 1.13 at $R_d = 2 \times 10^4$ to 1.17 at $R_d = 8 \times 10^4$).

Figure 4.13 presents drag coefficients for regular plates in normal flow determined from drop-test data, assuming that α was constant throughout the fall. If the plates used had been thin plates, those with the smallest area could have been expected to have the highest drag coefficients (Fig. 4.3). Since the reverse was true, it can be concluded that the thickness effect must outweigh the effect of Reynolds number. It is interesting to note that no difference in C_D could be detected between plates that were square, circular, or triangular (equilateral).

Similar data are presented in Fig. 4.14 for cubes made of various materials. Although a considerable change in terminal Reynolds number from the smallest to the largest cubes was noticed, no significant trend in the drag coefficient data was apparent.

With information obtained from the same drop tests for cubes, α was plotted as a function of the length of the cube on logarithmic paper (Fig. 4.15). If drag coefficient were constant, then the following relation can be stated for cubes made of material of constant density: $\alpha \sim (s/M) \sim (\text{length of side})^{-1}$. Thus a comparison of the data points in Fig. 4.15 to the lines drawn with a slope of -1 indicate the degree to which drag coefficient is constant for the different types of cubes.

4.4.3 Data for Glass Fragments

Two types of glass fragments were used in this study: those originating from window panes (0.125 in. thick) and those from plate-glass panes (0.225 in. thick). Figure 4.16 illustrates the random shapes of typical window-glass fragments. The number appearing with each fragment indicates its mass in grams.

Drop times obtained for 380 window-glass fragments were used to determine individual α by the method previously described, assuming constant α throughout the fall. When α was plotted as a function of mass on logarithmic paper, it was apparent that the points tended to form not one, but several line segments. The following procedure was used to determine the mass boundaries for each line segment. The data were divided into small mass groups, and the mean α and standard deviation in α were determined for each group. These data were plotted as illustrated in Fig. 4.17. The mass limits for each line segment were then estimated, and these limits used to determine the least-squares regression equations for each segment. These segments are shown in Fig. 4.18, along with the data points used in their determination. Because the smaller fragments were approximately spherical, the regression line for them was given a theoretical slope of $-\frac{1}{3}$ (Sec. 4.3.3). Another group of window glass was dropped edgewise (shown as triangles in Fig. 4.18). The regression line for these data passed near the intersection of the first two segments. For the sake of simplicity, another regression line was computed for the data, with the requirement that it pass through the intersection of the first two segments. The standard error of estimate was increased very little by this procedure.

Alpha data for plate glass (0.225 in. thick) dropped flat are presented in Fig. 4.19. It is interesting to note that a larger scatter is shown in the data for small fragments than for large. This, no doubt, can be attributed to the greater mechanical stability during fall of large plates than of small ones. This scatter also was observed at the time of the experiments. The same distribution of scatter can be detected in the data for window glass dropped flat as illustrated in Fig. 4.18.

A summary of all glass-fragment data is shown in Fig. 4.20. The data represented by line segment 1 for the smaller fragments can be used for either plate or window glass in any orientation since the fragments were small enough that their flat dimensions were not appreciably different from their thickness dimensions. Thus for plate glass line segment 1 was extended to higher masses until it intersected line segment 6 for plate-glass fragments dropped flat. This extension was possible because the densities of the window and plate glass were the same.

4.4.4 Analysis for Thick Plates of Random Shape

The purpose of this section is to derive relations that make it possible to determine drag coefficient (and thus α) for plates of any thickness and presenting area within the limits of the experimental data. The results apply to plates of random shapes such as those which have been described (see Fig. 4.16). The assumption is made, and verified by the experimental data, that plates with the same characteristic length-to-thickness ratio have the same drag coefficient, at least for the experimental conditions being considered here.

The characteristic length of a plate of random shape was taken to be the length of a side of a square plate of an equivalent area, i.e., the square root of the area.

It has been shown (see Figs. 4.19 and 4.20) for wide ranges of masses and for plates of constant thickness and density that the relation between the acceleration coefficient and mass can be expressed by an equation of the form

$$\log \alpha_0 = J + B \log m_0 \tag{4.3}$$

where J and B are constants. With this expression, the relation between C_D and $s^{1/2}/t$, where s represents the area of a plate in normal flow and t represents its thickness, can be determined.

The subscript zero is used to designate the parameters of the plates used in this study. The same terms without subscripts represent quantities that can vary between limits determined by the experimental data. Thus α, the acceleration coefficient, may be defined as $\alpha_0 = s_0 C_D / m_0$ and $\alpha = s C_D / m$ (Sec. 2.2), where the drag coefficients (C_D) are identical for the condition that $s_0^{1/2}/t_0 = s^{1/2}/t$. For each value of $s^{1/2}/t$ and, therefore, for each value of C_D, it can be stated that $s = k_1 t^2 \rho$, $s_0 = k_1 t_0^2 \rho_0$, $m = k_2 t^3 \rho$, and $m_0 = k_2 t_0^3 \rho_0$, where k_1 and k_2 are constants, t is the thickness of the plate, and ρ is the density of the material from which the plate is made. If these relations are used, the following equations can be derived: $m_0 = m \rho_0 (t_0/t)^3$ and $\alpha_0 = \alpha(\rho t / \rho_0 t_0)$. By the use of these equations to eliminate m_0 and α_0 from Eq. 4.3, the following equation is obtained:

$$\log \left[\alpha(t\rho/t_0 \rho_0) \right] = J + B \log \left[m(t_0/t)^3 (\rho_0/\rho) \right] \tag{4.4}$$

Since $m = t\rho s$ and $\alpha = s C_D / m$, Eq. 4.4 can be reduced to

$$\log (C_D/t_0 \rho_0) = J + B \log \left[\rho_0 t_0^3 (s^{1/2}/t)^2 \right] \tag{4.5}$$

Since t_0 and ρ_0 were assumed to have constant values in the analysis expressed by Eq. 4.3, Eq. 4.5 can be simplified to

$$\log C_D = K_1 + K_2 \log (s^{1/2}/t) \tag{4.6}$$

where K_1 and K_2 are constants. Thus $\log C_D$ is a linear function of $\log s^{1/2}/t$ if $\log \alpha$ can be assumed to be a linear function of $\log m$ (Eq. 4.3).

37

To verify the relation derived above, a plot was made of C_D vs. $s^{1/2}/t$, using all the data for plates obtained in this study. Figure 4.21 shows this plot, along with the results of a least-squares regression analysis. The data presented here are for 40 regular plates, referred to in Fig. 4.13, and 77 irregular plates, referred to in line segments 4 and 6 in Fig. 4.20. It is instructive to note that the drag coefficients for regular plates tend to be slightly higher than those for the irregular ones. Nevertheless, the standard error of estimate in C_D for all plates was only approximately 5.6 per cent, being between that for window-glass fragments (3.4 per cent) and that for plate-glass fragments (7.8 per cent). The areas for both types of glass fragments were computed from mass, thickness, and the measured glass density (39.657 g/in.[3]).

4.5 SMALL-ANIMAL DATA

Six mice, six rats, six guinea pigs, and five rabbits were dropped during these tests. The animals, which had been given lethal doses of Nembutal before the drops, were dropped as many as five times each.

The animals were dropped in two different initial orientations: first, with one side toward the direction of fall (lateral) and, second, with the abdomen toward the direction of fall (ventral). Figure 4.22 is a photograph of the presented areas of a few of the animals in these positions. The areas of most of the animals were measured from similar photographs and are recorded in Fig. 4.23, with circles representing the lateral areas and squares representing the ventral areas. The straight line on this plot has a slope of $2/3$. It tends to show that, at least for the mice, rats, and guinea pigs, the area is proportional to the mass to the $2/3$ power (see Ref. 5). It should be remembered that, although the animals tended to hold their initial orientations as they fell, the areas on Fig. 4.23 are larger than those "seen" by the wind since the hair tends to lie close to the body as the animal falls.

Figure 4.24 is a plot of the experimentally determined α as a function of mass; the circles represent the α of animals dropped laterally and the squares represent the α of animals dropped ventrally. The regression line was computed using all the points. The slope of -0.3240 is near the theoretical slope of $-1/3$, which was determined by assuming a constant density and a constant drag coefficient for any group of similar objects (see Secs. 4.3.3 and 4.3.4).

Figure 2.3 shows the impact velocity as a function of drop height and α. The α values, determined experimentally from the animal data, are plotted on the theoretical line for the actual height of drop. In addition, the means and standard deviations of the experimentally determined α are tabulated in Fig. 4.24. They are shown in Fig. 2.3 and can be used to estimate the means and standard deviations of the impact velocities of the various animals.

4.6 DRAG PROPERTIES FOR MAN

The least-squares regression line in Fig. 4.24 can be extrapolated up to a mass of 168 lb (75,977 g) to give an estimation of the α for man (0.0269 ft^2/lb).

The extrapolated value for the α for man was compared to Schmitt's report on wind-tunnel investigations of air loads on human beings[6] whose average weight was 168 lb. The data from this report were used to compute and average the α for a group of eight nude men in the lateral and ventral positions. A value of 0.0336 ft^2/lb was obtained. This value is higher than the 0.0269 ft^2/lb obtained from the extrapolation of the animal data, but this can be explained if the fact is taken into consideration that the animals tested were much more spherically shaped than man and thus have a lower α for the maximum presented-area position.

Another way to estimate the α of man is by the concept of the total surface area. For a sphere the total surface area is $4\pi r^2$ and the average presented area is πr^2. For a cube the total surface area is six times the area of one face, and the average presented area of a cube in random orientation is $3/2$ times the area of one face.[7] The ratio of the average presented area to the total surface area is $(\pi r^2/4\pi r^2)$ sphere $= 1/4$ and $[(3/2)/6]$ cube $= 1/4$.

In general, if an object has no cavities (ellipsoid, cube, etc.), its average presented area in random orientation is one-fourth the total surface area (see Appendix, Sec. A.3, for proof).

Since a man does have concavities, it is not actually the total surface area that should be considered, but rather an effective surface area.

Bohnenkamp's work with effective radiating surface area of an erect man has shown this area to be from 83 to 85 per cent of the total surface area.[5] The total surface area can be obtained from various sources,[8-9] but for this study the figures given in the Schmitt report[6] were used (an average of 20.7525 ft^2 total surface area and 167.5 lb weight). With these data the average value of s/m was found to be $\frac{1}{4} \times 84\% \times (20.7525$ ft$^2/167.5$ lb$) = 0.0260$ ft^2/lb. If C_D is assumed to be equal to unity, this figure (0.0260 ft^2/lb) can be compared to the extrapolated value for α of 0.0269 ft^2/lb (Fig. 4.24).

The α values derived from the Schmitt report for various orientations of the men relative to the wind were used to calculate the average α for a rigid, clothed man, giving a value of 0.0281 ft^2/lb (see Appendix, Sec. A.4). The average drag coefficient for a rigid, clothed man would then be the average α divided by the average s/m, or $0.0281/0.0260 = 1.08$. This value compares very well with the approximate values listed by Hoerner,[10] which include drag coefficients of 1.0 for a parachutist in free fall, 1.0 for a ski runner on a slope, and 1.2 for a ski jumper in air. It should be remembered that the average α of man would be lowered if those positions where a man is doubled up, instead of being rigid, were also considered.

REFERENCES

1. Robert W. Knox, Coast and Geodetic Survey, Department of Commerce, letter to the Lovelace Foundation for Medical Education and Research, Aug. 9, 1955.
2. Internal Civil Aviation Organization, Montreal, Can., and Langley Aeronautical Laboratory, Langley Field, Va., Manual of the ICAO Standard Atmosphere Calculations by the NACA, NACA-TN-3182, May 1954.
3. S. F. Hoerner, author and publisher, *Aerodynamic Drag*, pp. 3-8 and 3-15, Midland Park, N. J., 1951.
4. I. Gerald Bowen et al., Secondary Missiles Generated by Nuclear-produced Blast Waves, Project 33.2, Operation Plumbbob Report, WT-1468, in preparation.
5. Otto Glasser (Ed.), *Medical Physics*, Vol. 1, pp. 1490-1494, The Year Book Publishers, Chicago, 1944.
6. Thomas J. Schmitt, Wind-tunnel Investigation of Air Loads on Human Beings, Report DTMB-892, The David Taylor Model Basin Aerodynamic Laboratory, January 1954.
7. G. E. Hansche and J. S. Rinehart, Air Drag on Cubes Fired at Mack Numbers 0.5 to 3.5, *J. Aeronaut. Sci.*, *19*(2): 83-84 (February 1952).
8. Julius Sendroy, Jr., and Louis P. Cecchini, The Determination of Human Body Surface Area from Height and Weight, Report NM 004 006.05.01, Vol. 12, pp. 385-410, Naval Medical Research Institute, Oct. 19, 1954.
9. Delafield DuBois and Eugene F. DuBois, A Formula to Estimate the Approximate Surface Area if Height and Weight be Known (Clinical Calorimetry, Tenth Paper), *Arch. Internal Med.*, *17*: 863 (1916).
10. S. F. Hoerner, author and publisher, *Fluid-dynamic Drag*, p. 3-14, Midland Park, N. J., 1958.

TABLE 4.1—ALPHA VARIATION WITH MASS DERIVED FROM EXPERIMENTAL
DATA FOR SPHERES AND STONES*

Missile	N	b	σ_b	$b - \sigma_b$	$b + \sigma_b$	pr
Nylon spheres	5	−0.3561	0.0106	−0.3667	−0.3455	0.1
Glass spheres	6	−0.3432	0.0132	−0.3564	−0.3300	0.5
Aluminum spheres	7	−0.3530	0.0065	−0.3595	−0.3465	0.02
Steel spheres	7	−0.3763	0.0078	−0.3841	−0.3685	0.001
All spheres	25	−0.3578	0.0105	−0.3683	−0.3473	0.034
Painted gravel	41	−0.3563	0.0229	−0.3792	−0.3334	0.3
Limestone fragments	45	−0.3216	0.0258	−0.3474	−0.2958	0.7
1S1a (natural stones)	34	−0.3126	0.0240	−0.3366	−0.2886	0.4
10P4 (natural stones)	35	−0.3283	0.0200	−0.3483	−0.3083	0.8
4.3 GTS (natural stones)	29	−0.3076	0.0398	−0.3474	−0.2678	0.5
Pumice	39	−0.2547	0.0259	−0.2806	−0.2288	0.01

*Explanation of terms:

N = number of different types of spheres used (each type was dropped 10 to 20 times) or the number of stones dropped.

b = least-squares regression slope defined by $\log \alpha = a + b \log$ (mass).

σ_b = standard deviation of b.

pr = probability that measured slopes b do not deviate significantly from $-\frac{1}{3}$, assuming that the latter is the "true" or "population" slope.
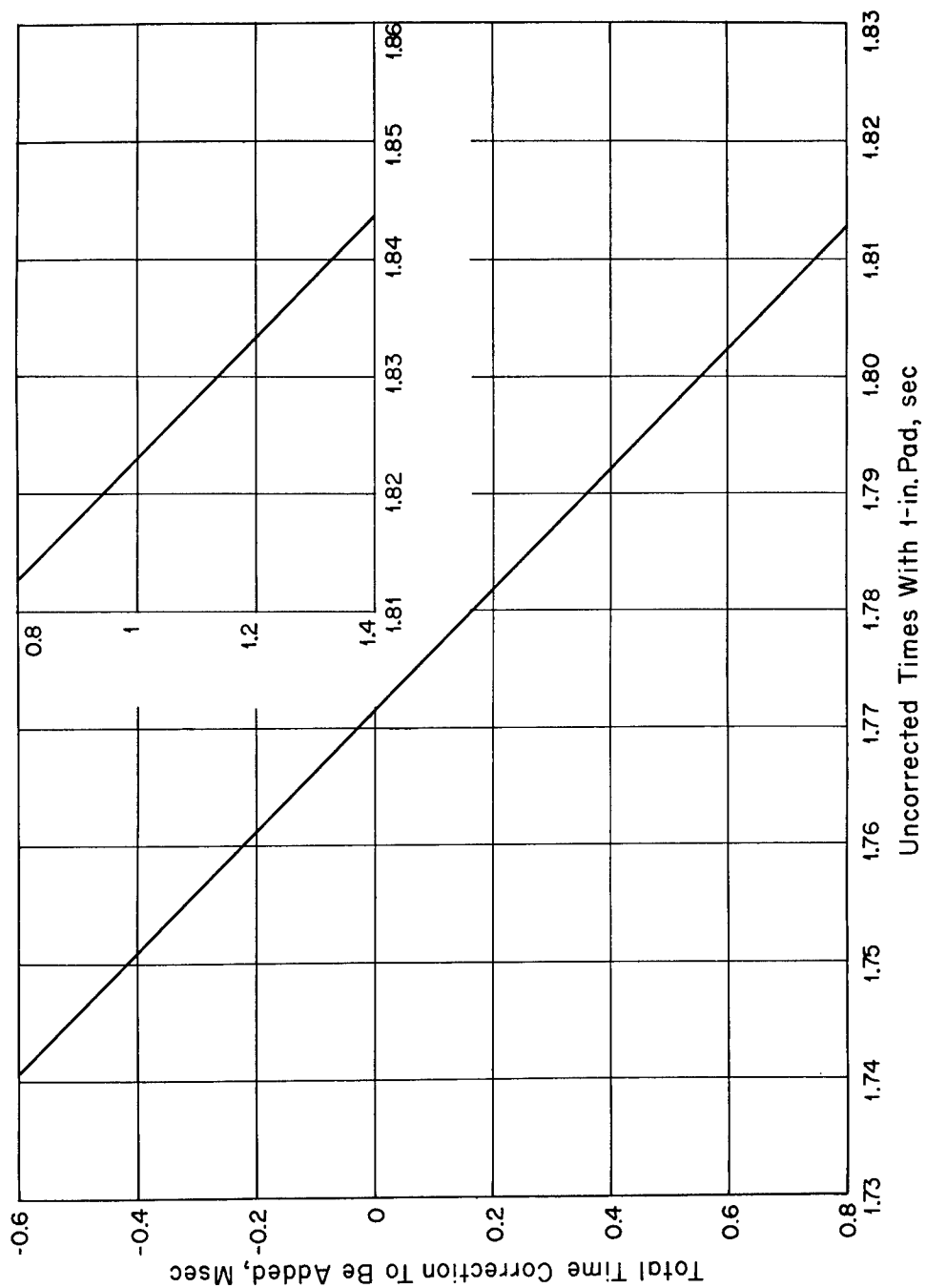
Fig. 4.1 — Time correction for times measured on the third day of testing when the Ensolite pad was used.
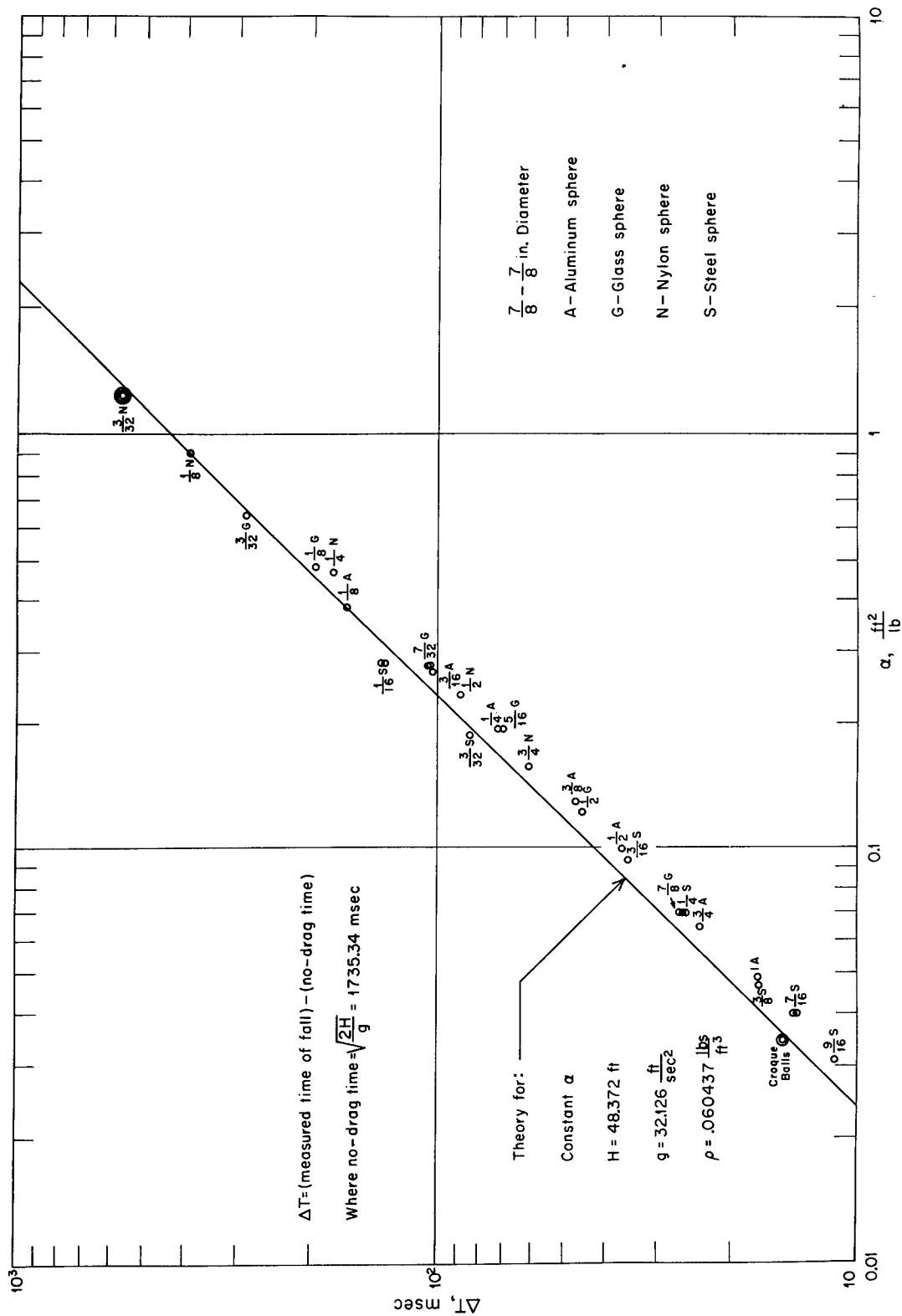
Fig. 4.2—Measured time of fall for spheres minus no-drag time of fall for spheres vs. α based on $C_D = 0.47$. The line is the theoretical curve, assuming constant α throughout a fall computed from Eq. 2.14.

42

√Area Plates table:

√Area	Plastic .125	Plastic .25	Glass Window .125	Glass Plate .225	Brass .125	Brass .25	Thickness in inches
1/2"	a		b(1.24)*	c(2.23)*	d	e	
1"	f	g	h(4.96)*	i(892)*	j	k	
2"	l	m	n(19.8)*	o(35.7)*	p	q	
4"	r	s	t(79.3)*	u(143)*	v		
8"	w						

Plates

Spheres

$C_D = 1.17$

$C_D = .47$

3.34 Croquet Ball

* (average weight in grams of pieces of glass in each group)

Numbers refer to sphere diameter in inches.
A = Aluminum sphere
N = Nylon sphere
S = Steel sphere

$R_d \times 10^{-4}$

C_D

Fig. 4.3—Drag coefficients vs. Reynolds number for spheres and plates (maximum area presented to the wind). Included on the figure are the terminal points of some of the plates and spheres dropped. The dashed lines represent average drag coefficients often used for these objects (see Ref. 3).

Fig. 4.4—Effective α vs. sphere mass. The least-squares regression lines were computed from test data assuming constant CD.

44
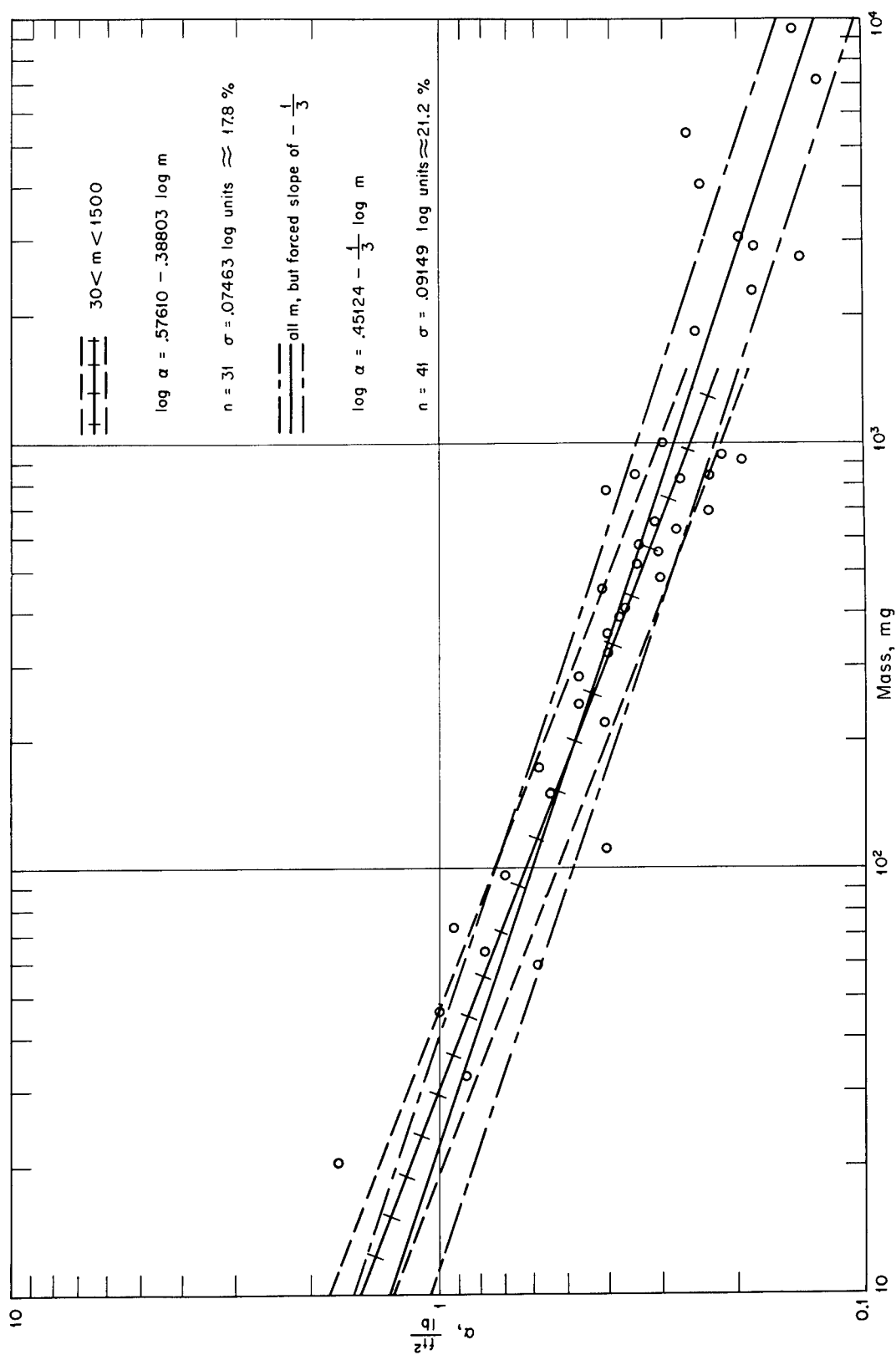
Fig. 4.5—Experimentally determined α vs. mass for painted gravel. Included are two least-squares regression lines prepared for two sets of conditions as stated on figure.
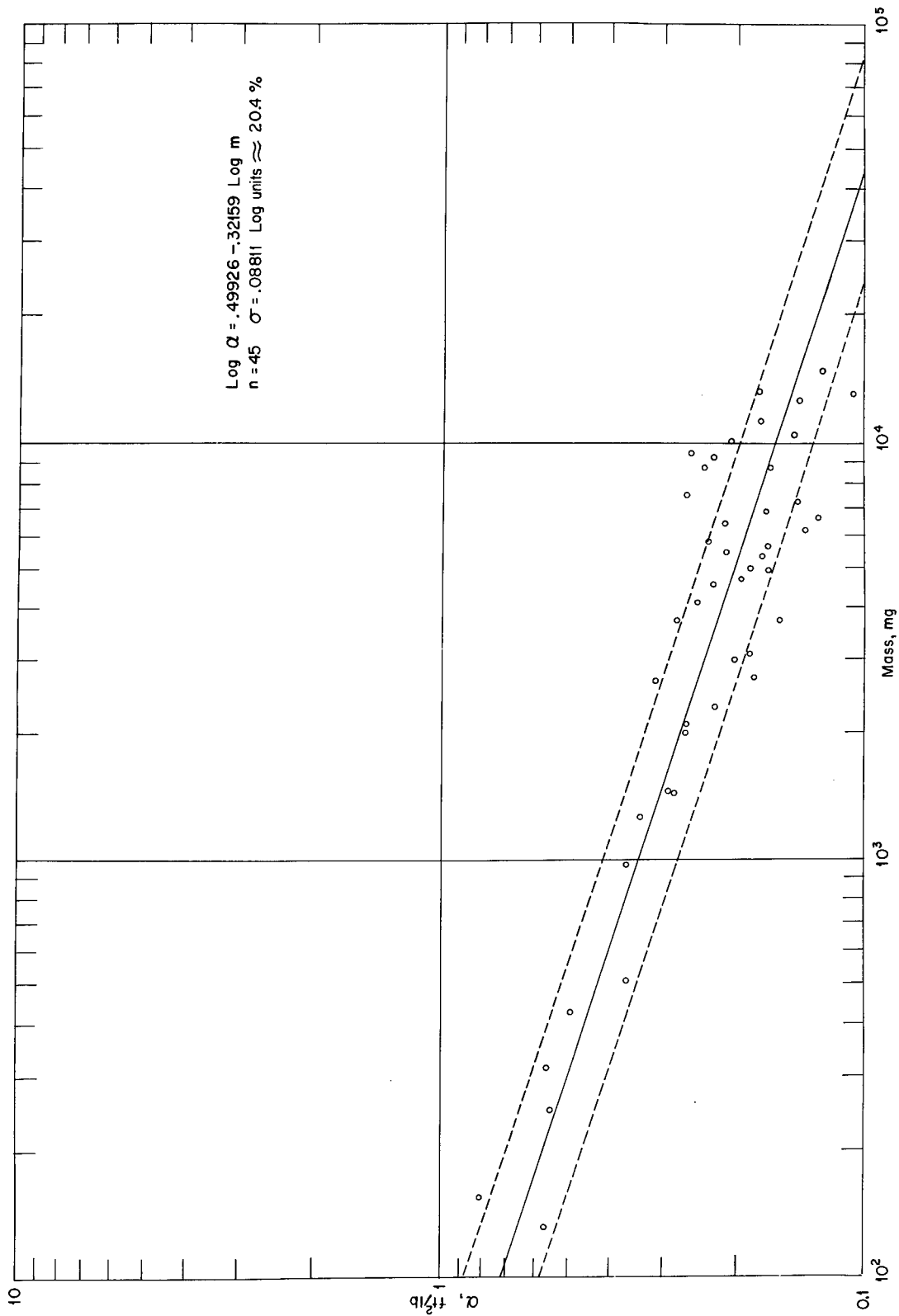
Fig. 4.6—Experimentally determined α vs. mass for limestone fragments. Results of the least-squares analysis are shown.

Log α = .49926 -.32159 Log m

n = 45 σ = .08811 Log units $\approx$ 20.4 %

Mass, mg

α, ft³/lb
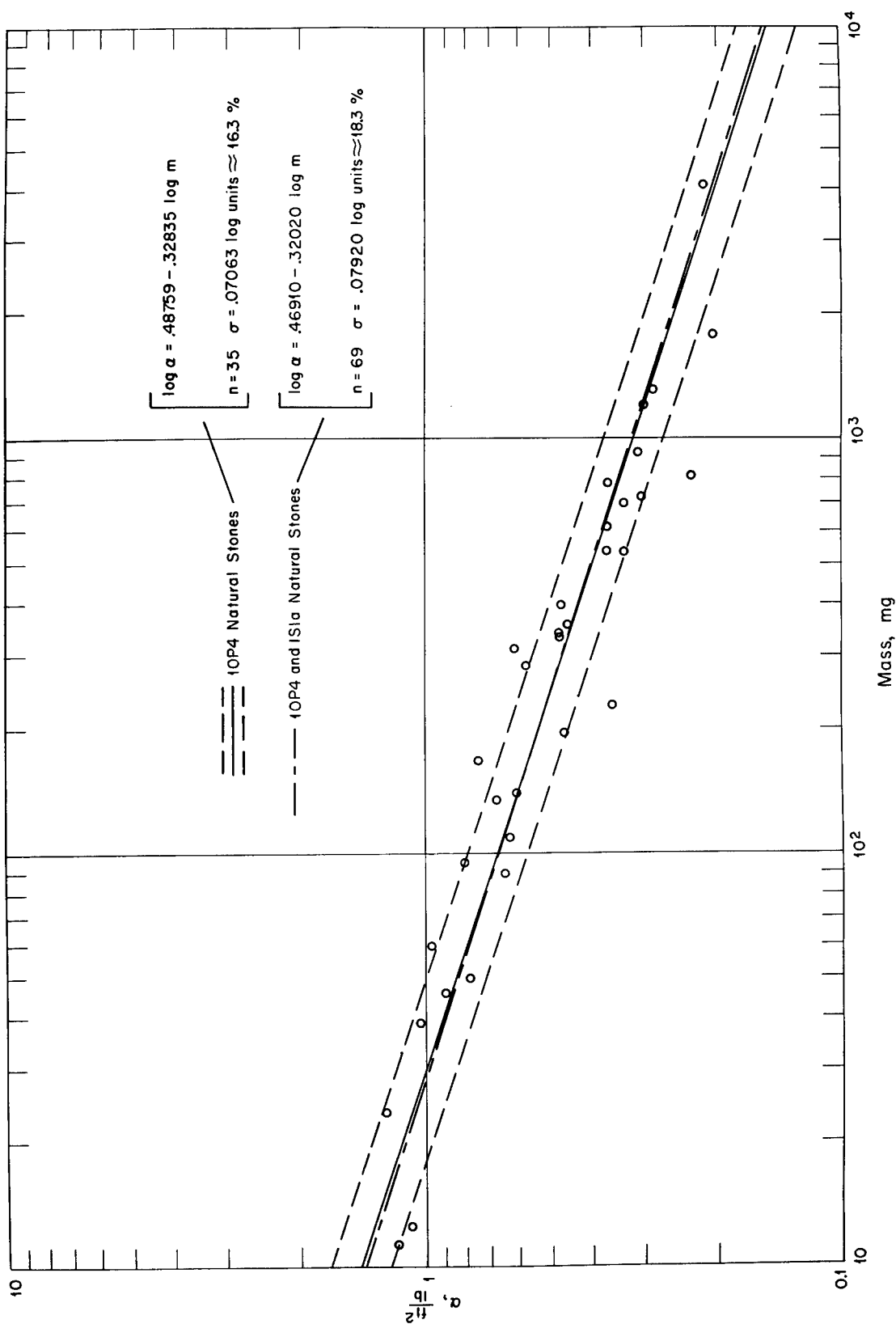
Fig. 4.7—Experimentally determined α vs. mass for 10P4 natural stones. Results of the least-squares regression analysis for natural stones from 10P4 and 1S1a locations at NTS are shown.
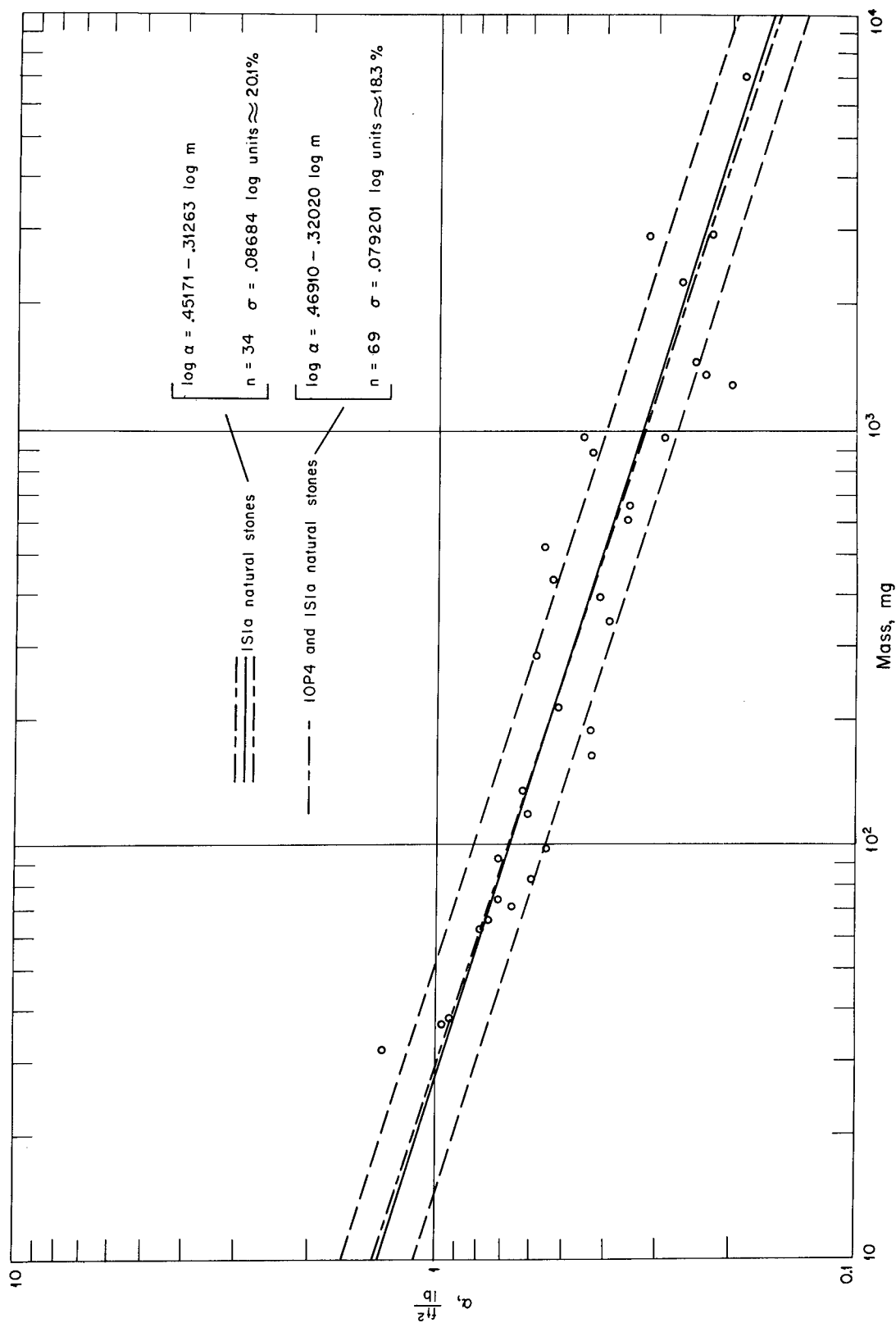
Fig. 4.8——Experimentally determined α vs. mass for 1S1a natural stones. Included are results of the least-squares regression analysis for natural stones from 10P4 and 1S1a locations at the NTS.
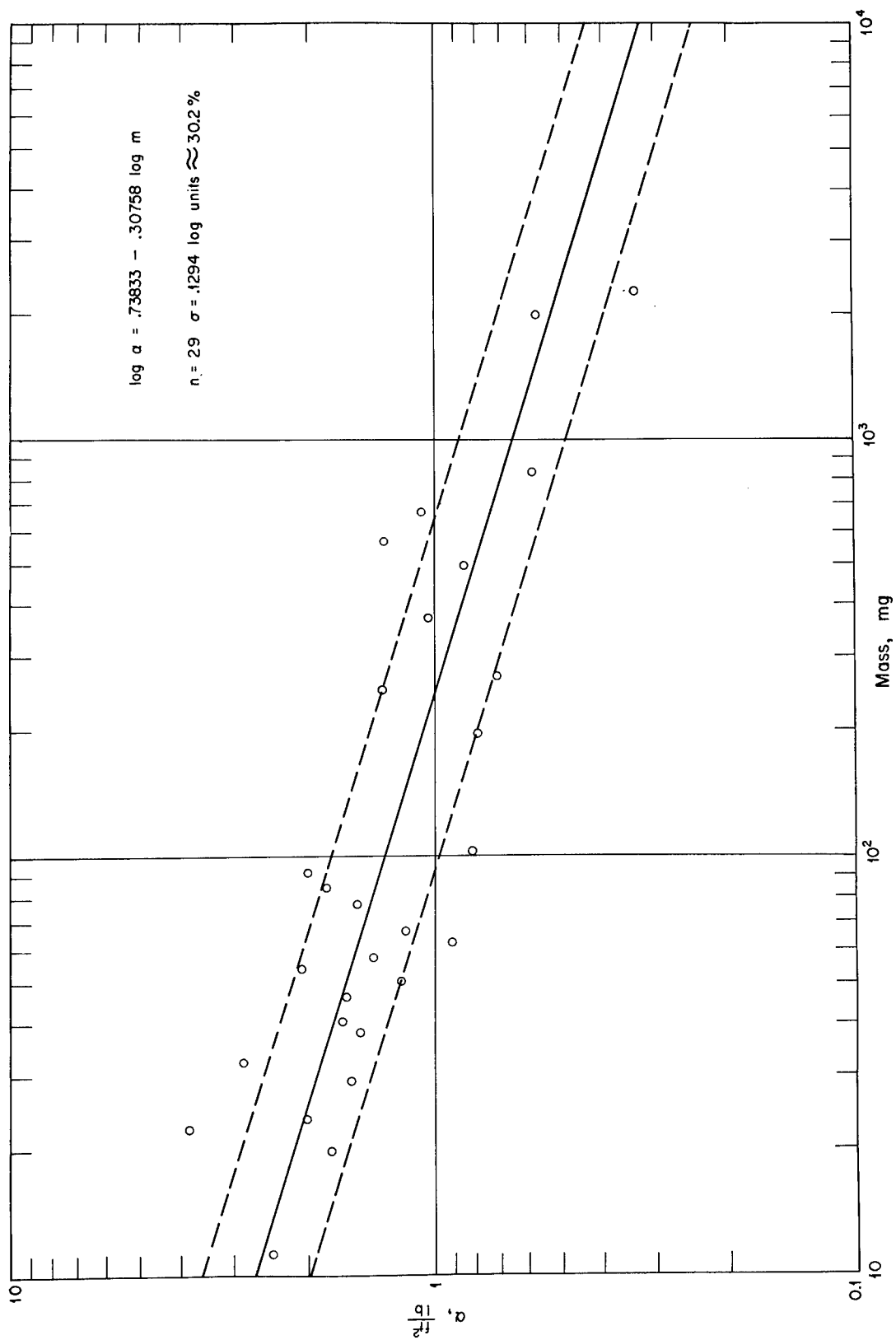
Fig. 4.9—Experimentally determined α vs. mass for natural stones from NTS at 4.3GTS location.

$\log \alpha = .73833 - .30758 \log m$

$n = 29 \quad \sigma = .1294 \text{ log units} \approx 30.2\%$

Mass, mg

$\alpha, \dfrac{ft^2}{lb}$
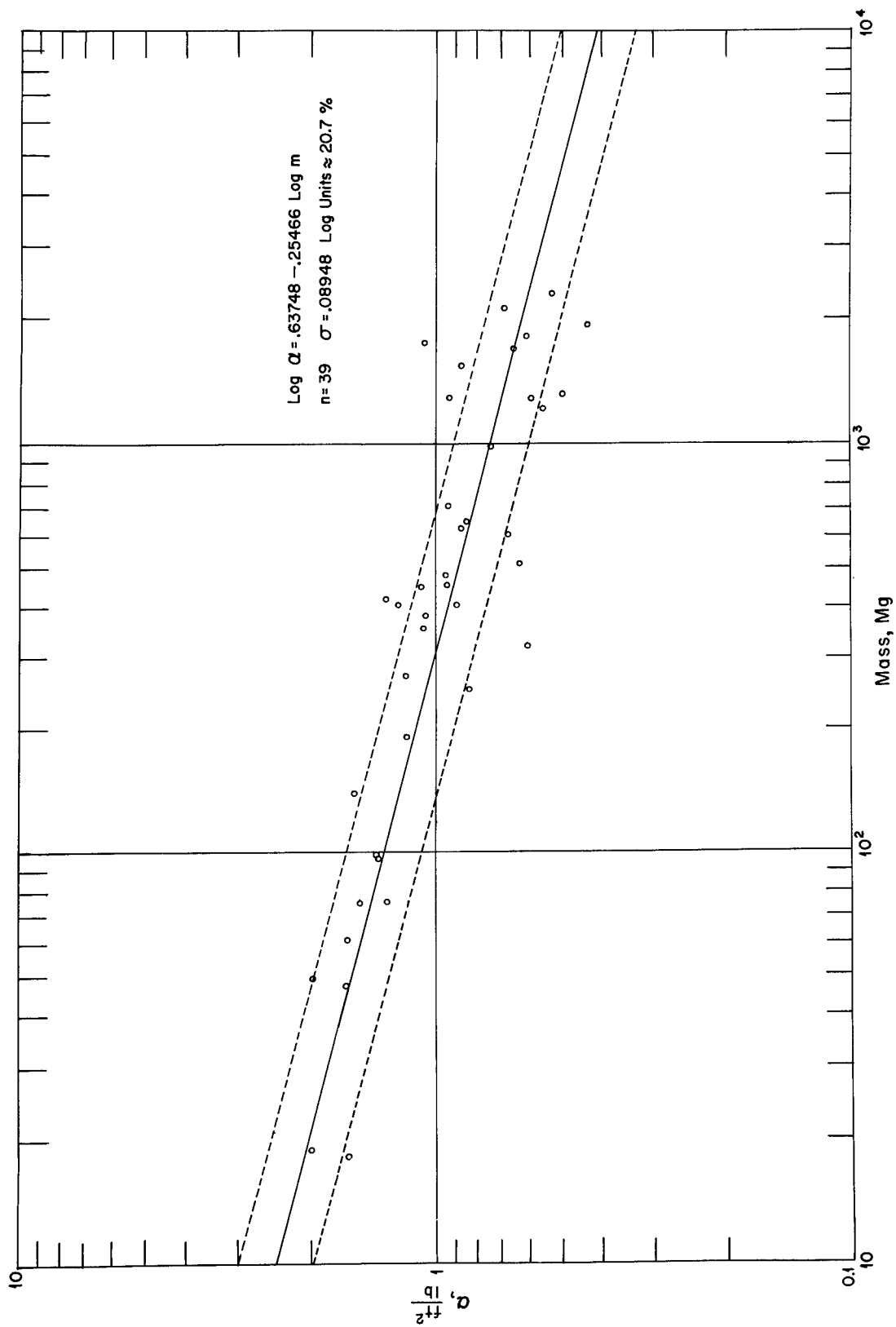
Fig. 4.10—Analysis of experimentally determined α vs. mass for pumice fragments.

Log α = .63748 − .25466 Log m

n = 39   σ = .08948 Log Units ≈ 20.7 %
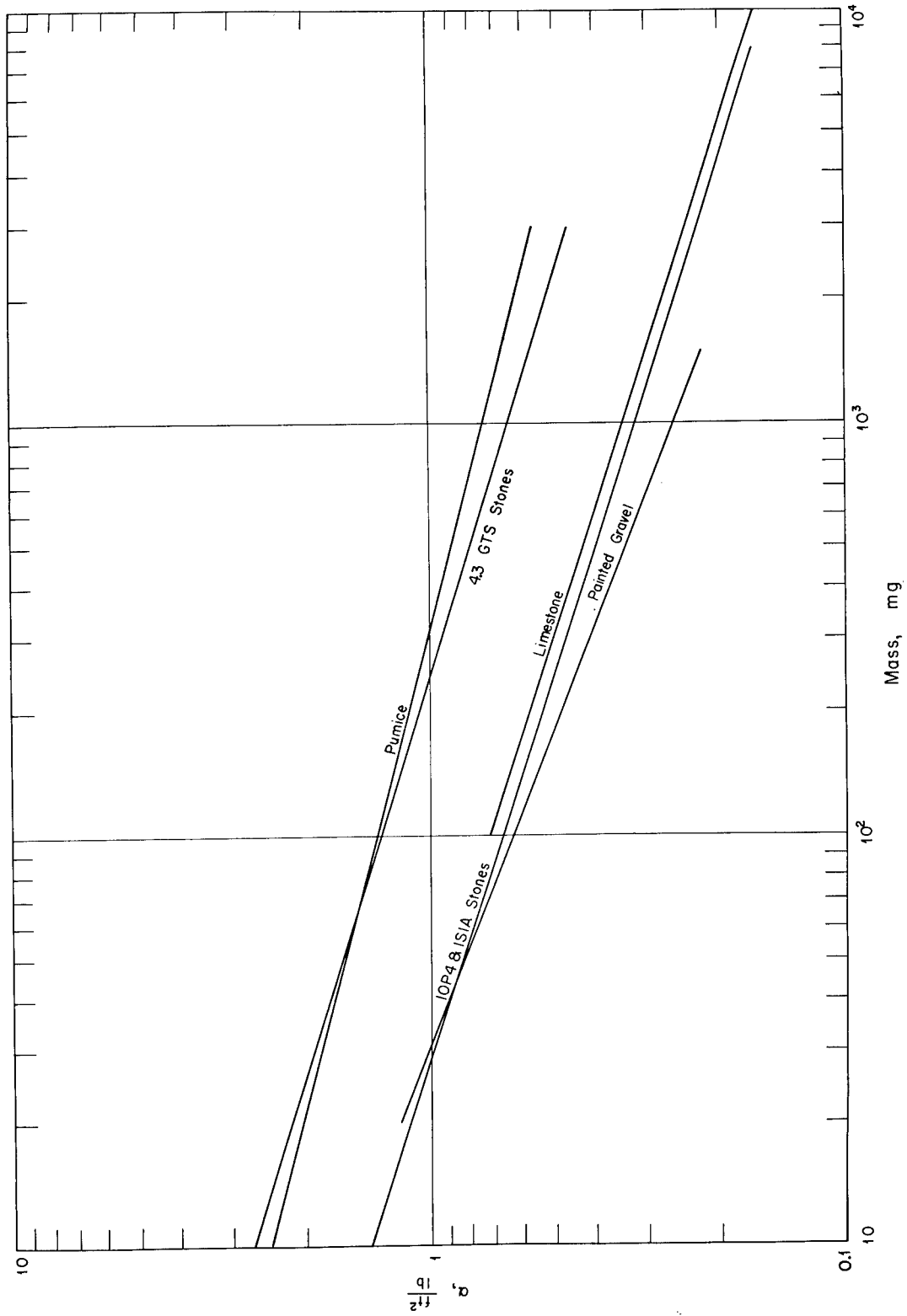
Fig. 4.11 — A summary of the stone analysis showing the least-squares regression lines describing α vs. mass for the various stone groups tested.
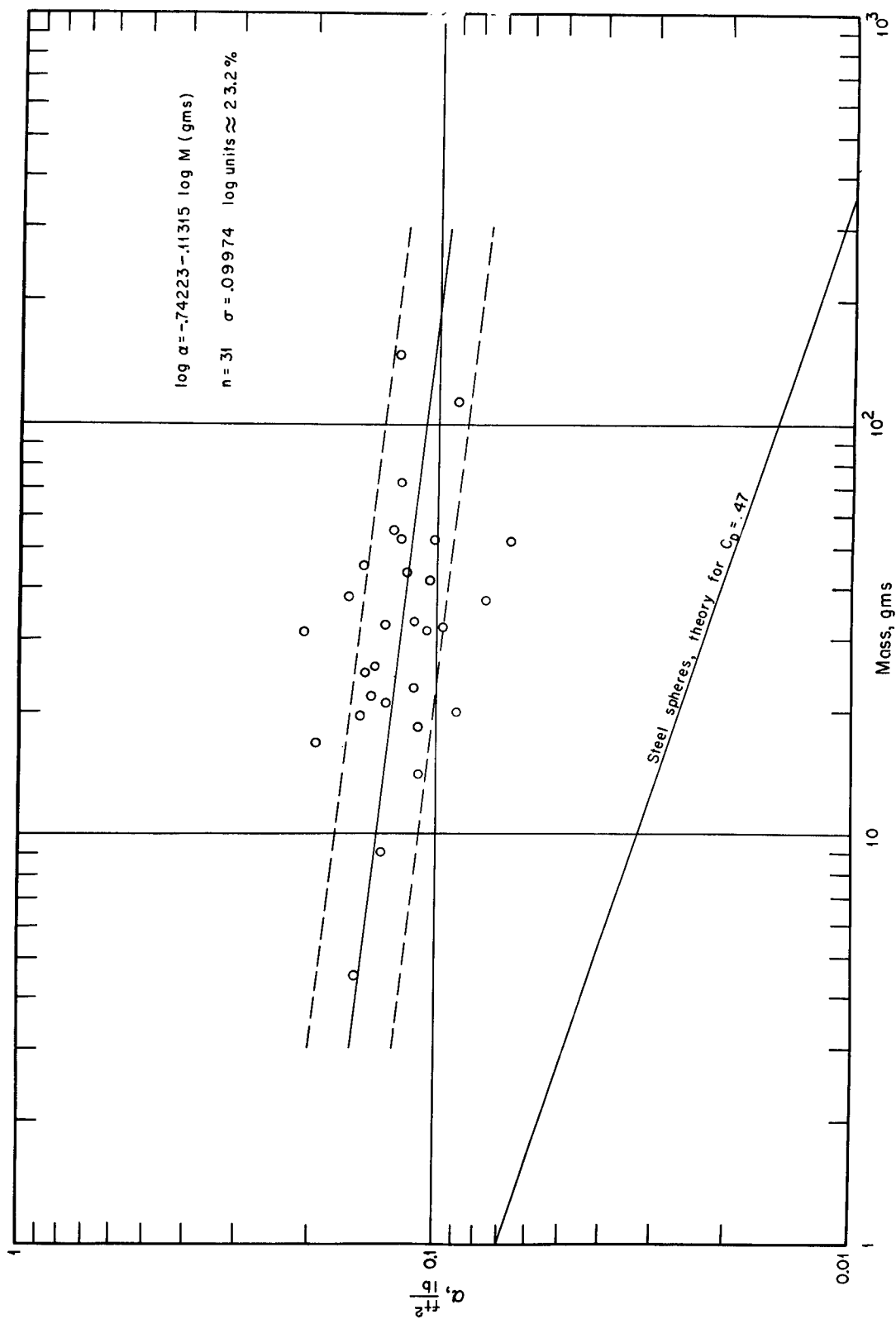
Fig. 4.12—Experimentally determined α vs. mass for military debris showing results of least-squares analysis. The theoretical line for steel spheres is included for comparison.
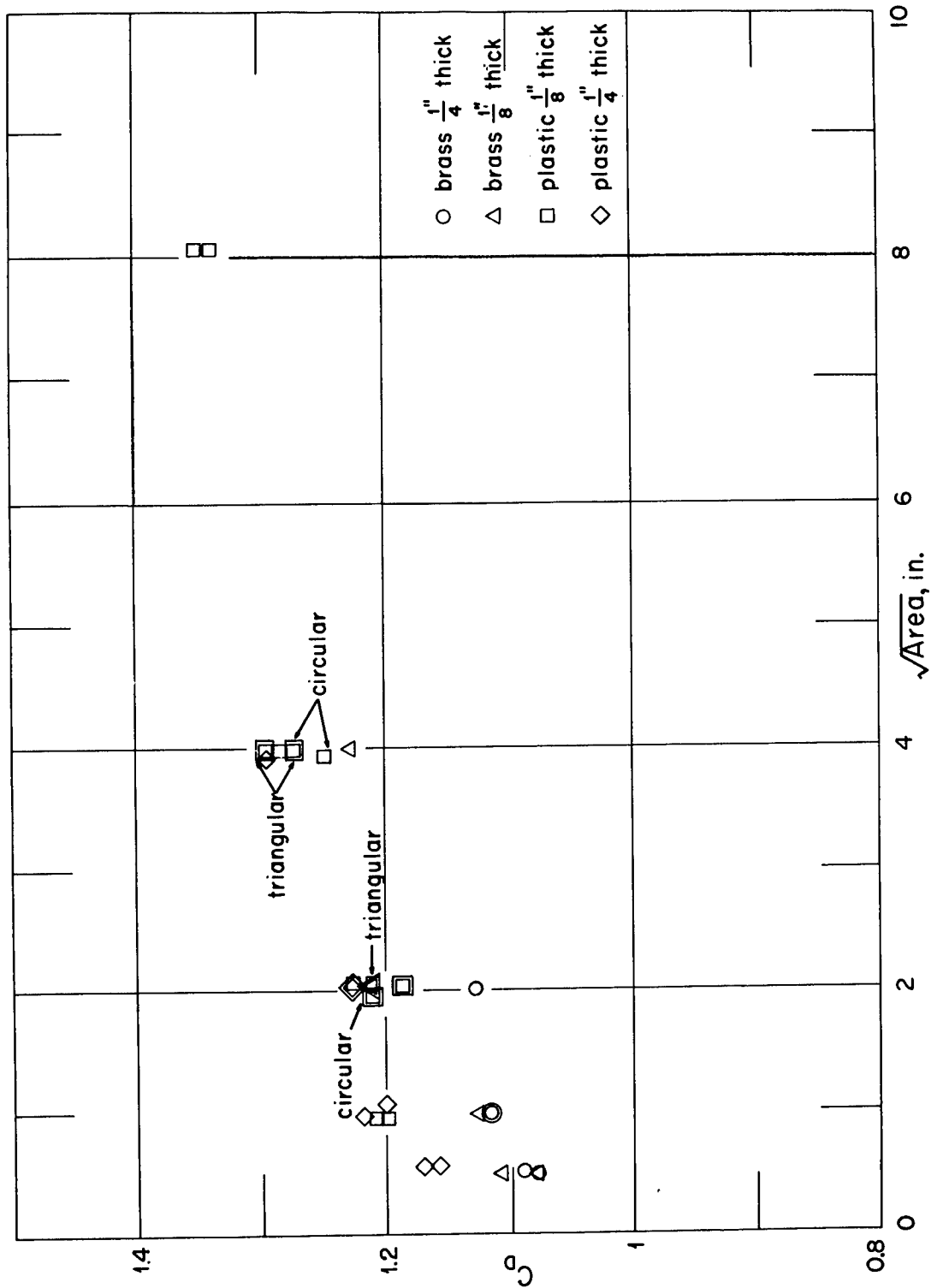
Fig. 4.13—Drag coefficients of regular plates (various simple geometric shapes) computed from their times of fall. The plates were dropped flat. The shapes of the plates not indicated were square.

Fig. 4.14—Drag coefficients of cubes (dropped with one face down) computed from their times of fall.
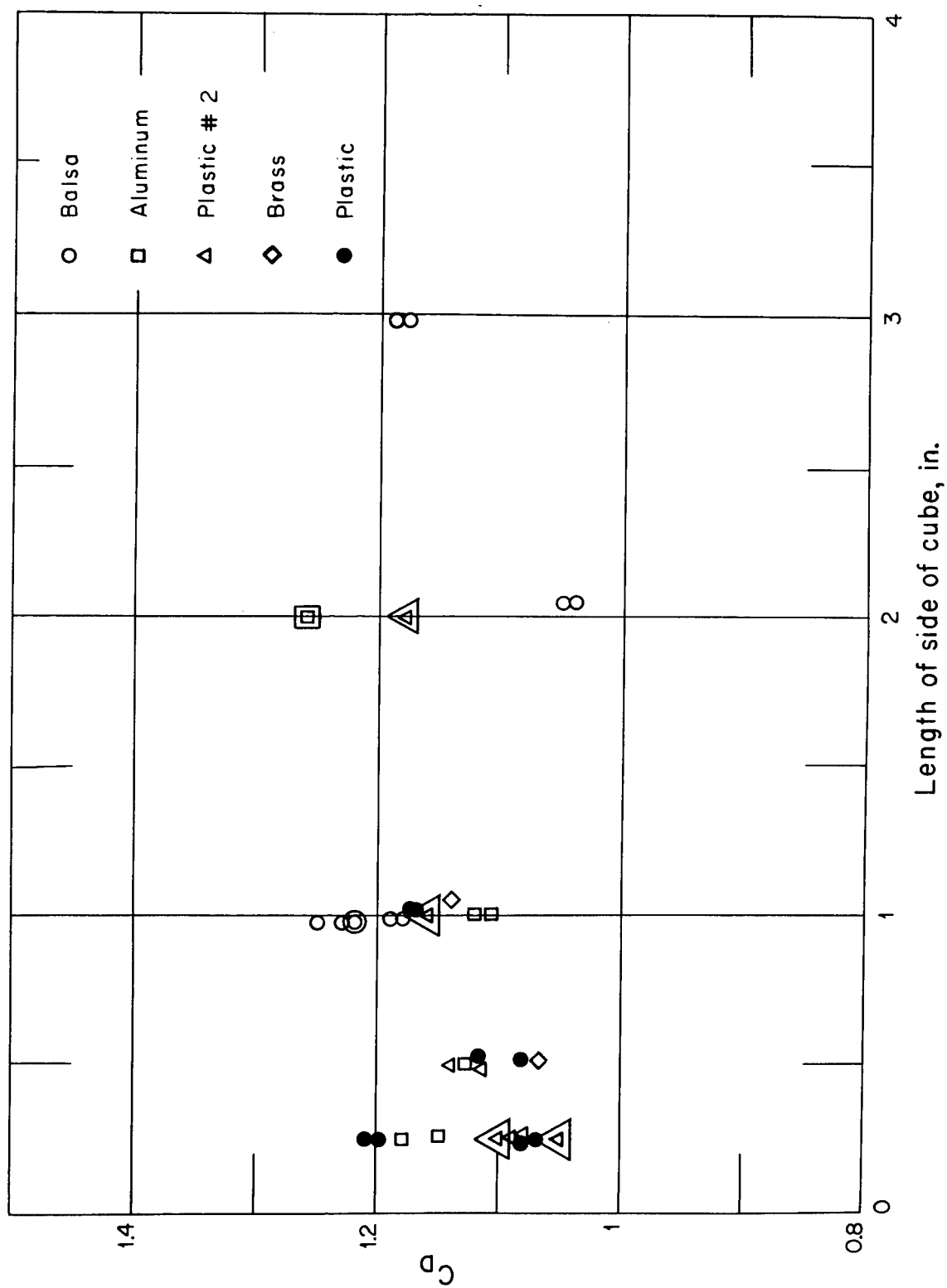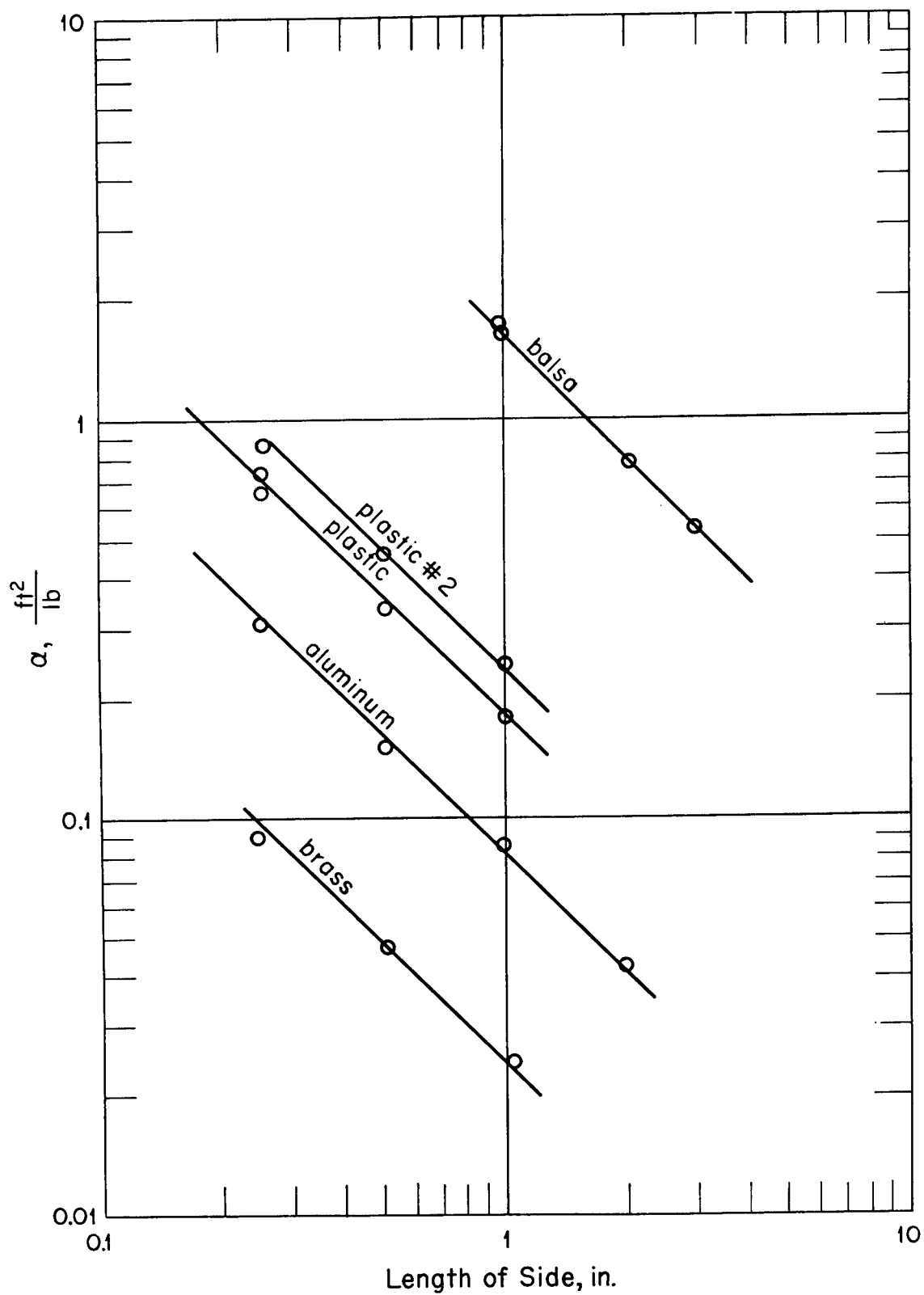
Fig. 4.15—Alpha (computed from the times of fall) of cubes vs. length of side of cubes. The lines through the points have the theoretical slope of minus one.
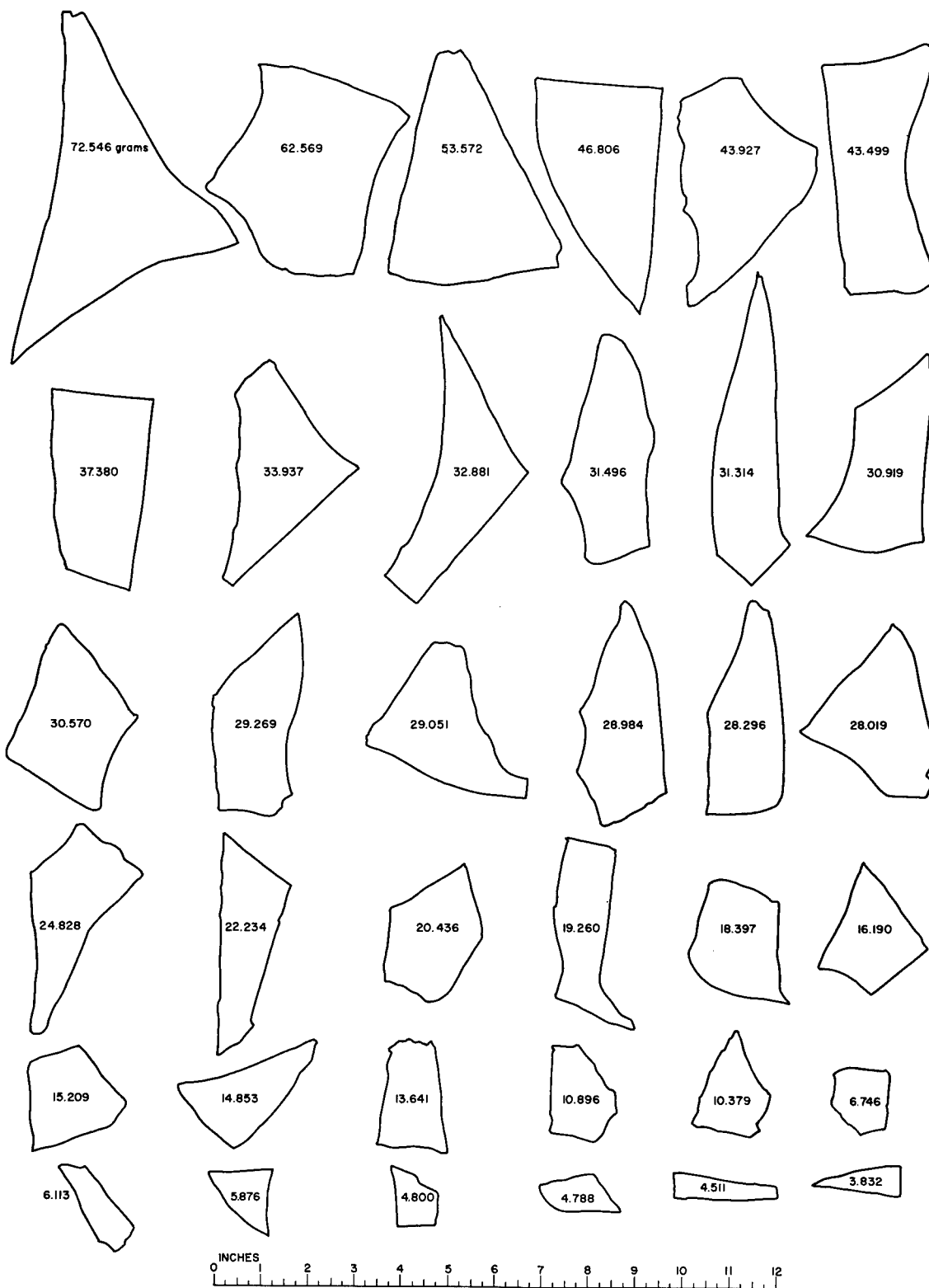
Fig. 4.16—Front views of some of the larger pieces of window glass (0.125 in. thick) used in drop-tests. Numbers indicate masses in grams.
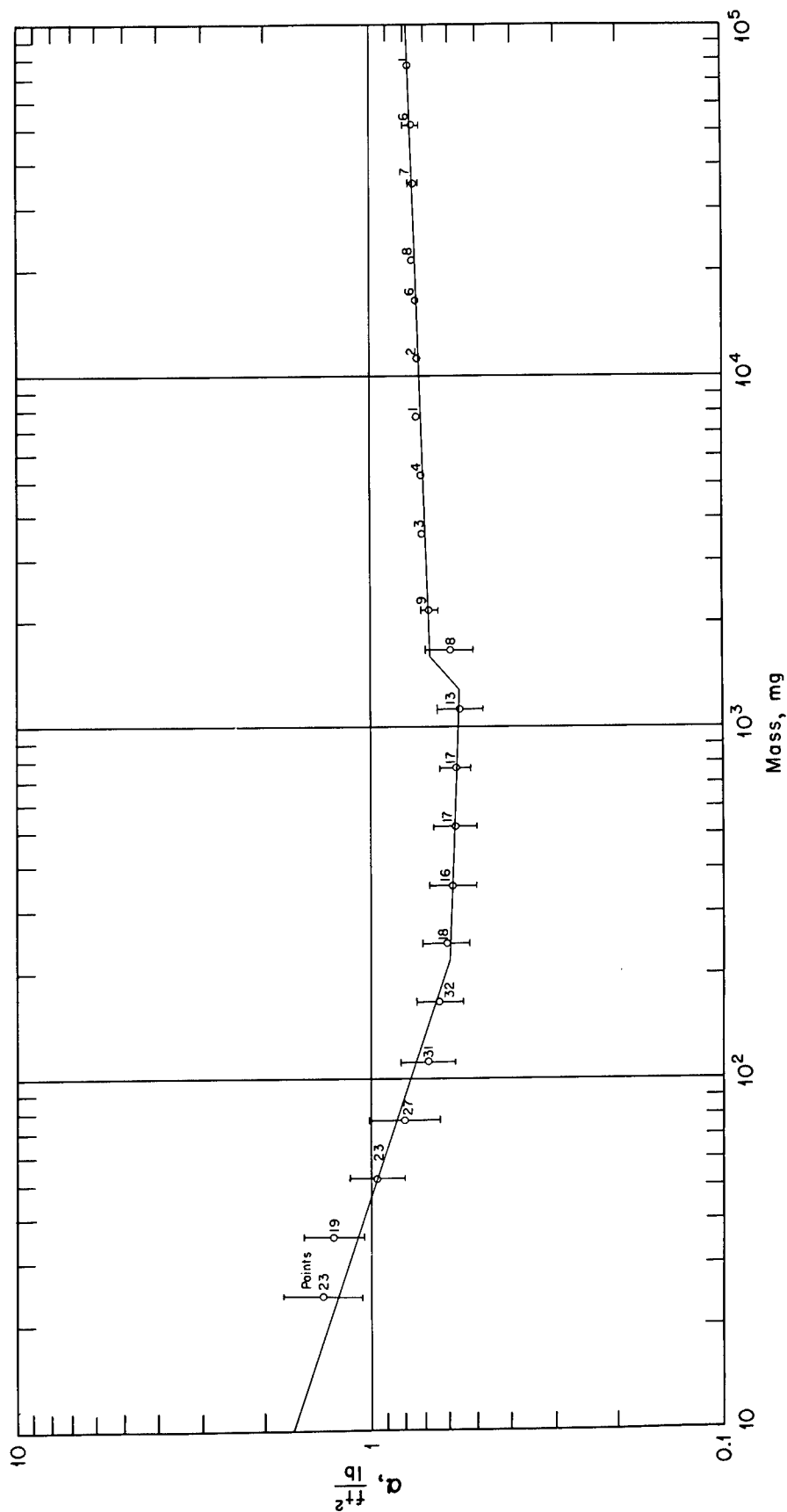
Fig. 4.17—Grouped data for window glass dropped flat showing means and standard deviations and least–squares regression lines describing α vs. mass. This figure indicates the need for four straight line segments in the analysis.
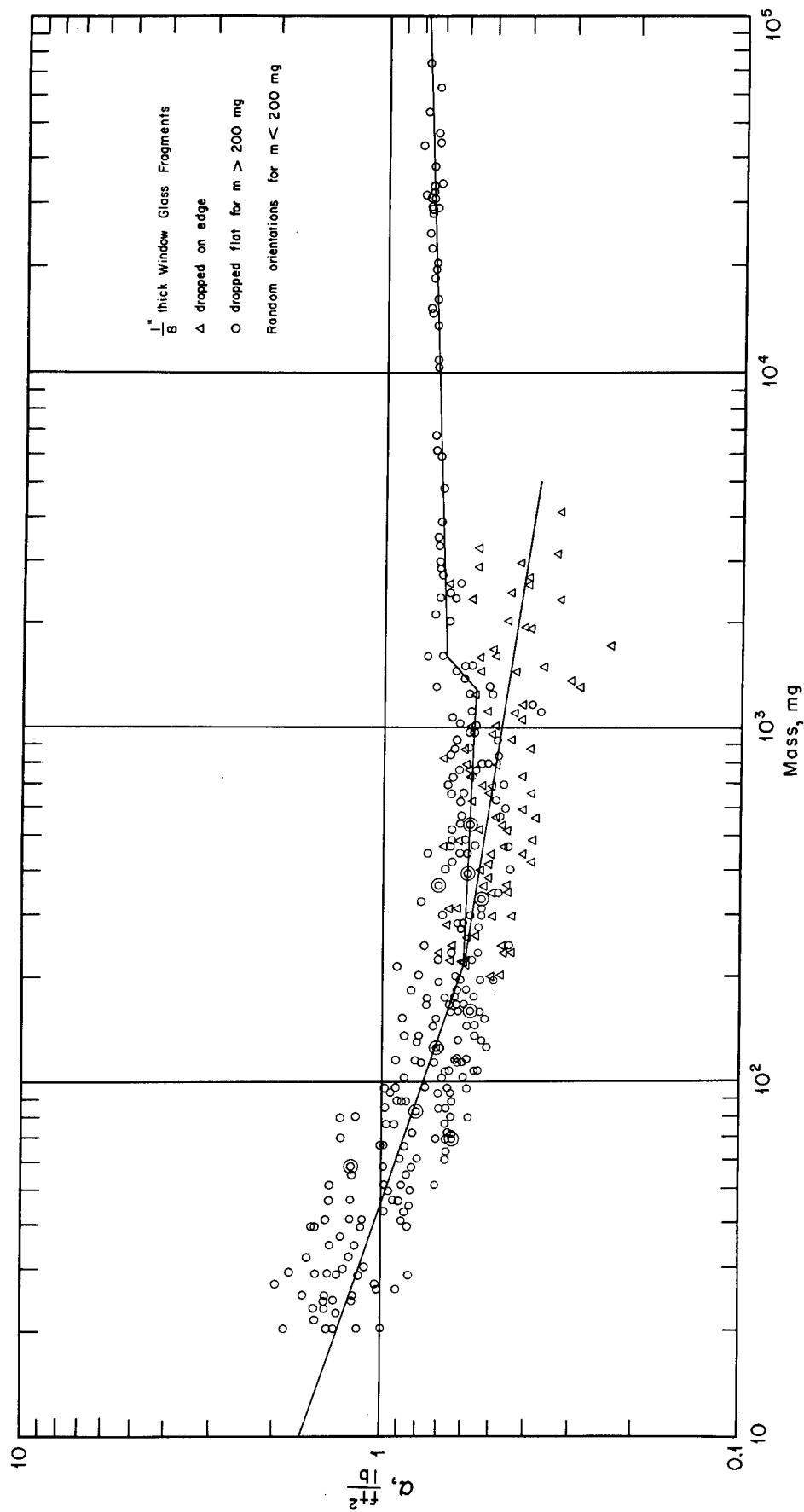
Fig. 4.18—Window-glass data for fragments dropped flat and on edge. Also included are the least-squares regression lines.
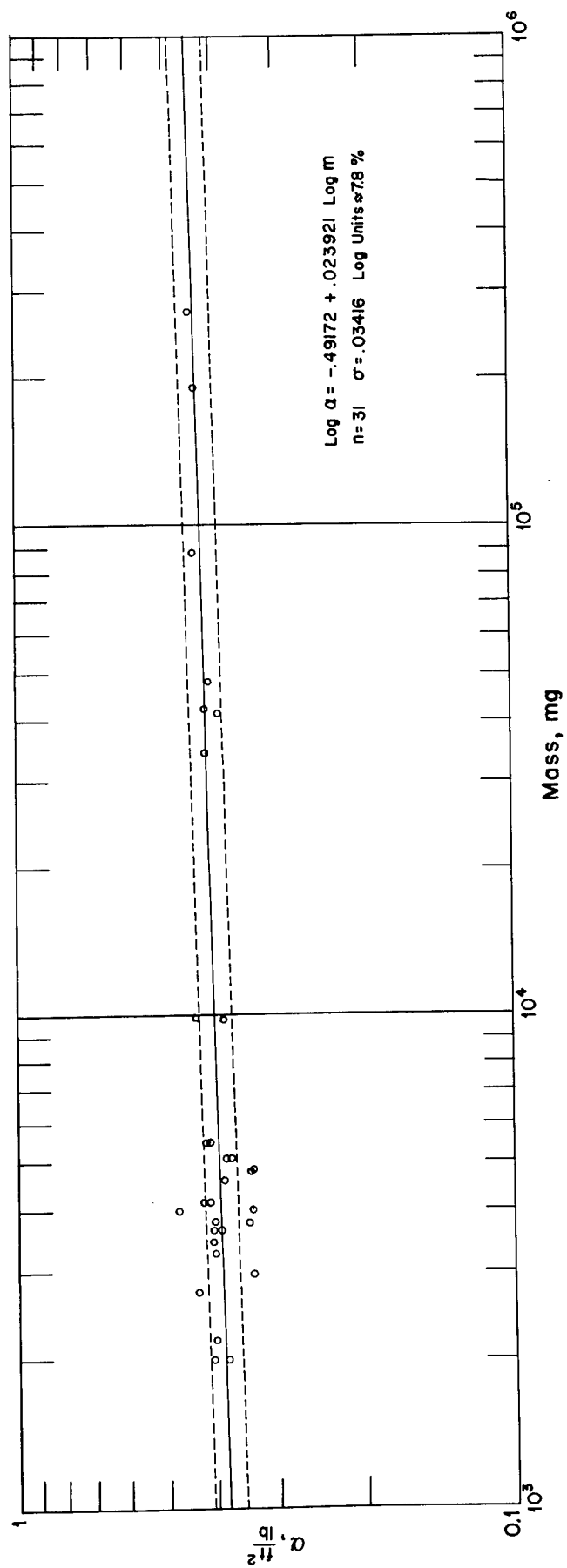
Fig. 4.19—Analysis of α vs. mass for plate-glass fragments dropped flat.

Log α = -.49172 + .023921 Log m

n=31 σ =.03416   Log Units ≈ 7.8 %

Mass, mg

α, $\frac{ft^2}{lb}$

59

All Glass

$\alpha, \frac{ft^2}{lb}$

Section 4

Mass, mg

Flat Window

3

Section 4

0.3

Section 1 $10 < m < 220$, $\log \alpha = .55659 - \frac{1}{3} \log m$
            $n = 154$ $\sigma = .09014$ log units $\approx 20.9\%$

Section 2 $220 < m < 1270$, $\log \alpha = .13874 - .036374 \log m$
            $n = 81$ $\sigma = .06348$ log units $\approx 14.6\%$

Section 3 $1270 < m < 1574$, $\log \alpha = -3.02323 + .89295 \log m$
            $n = 10$ $\sigma = .04525$ log units $\approx 10.4\%$

Section 4 $1574 < m < 10$, $\log \alpha = -.28024 + .034985 \log m$
            $n = 46$ $\sigma = .01473$ log units $\approx 3.4\%$

Edge Window

3

Section 5

0.3

Section 1 $10 < m < 220$, $\log \alpha = 55659 - \frac{1}{3} \log m$
            $n = 155$ $\sigma = .09014$ log units $\approx 20.9\%$

Section 5 $220 < m < 5000$, $\log \alpha = .12689 - .14982 \log m$
            $n = 88$ $\sigma = .1013$ log units $\approx 23.5\%$

Flat Plate

3

Section 6

0.3

Section 1 $10 < m < 860$, $\log \alpha = .55659 - \frac{1}{3} \log m$
            $n = 155$ $\sigma = .09014$ log units $\approx 20.9\%$

Section 6 $860 < m < 3(10)$, $\log = -.49172 + .023921 \log m$
            $n = 31$ $\sigma = .03416$ log units $\approx 7.8\%$

Fig. 4.20 —Summary of the glass-fragment data. This shows regression lines describing α vs. mass for (1) all the glass, (2) window glass dropped flat, (3) window glass dropped on edge, and (4) plate glass dropped flat.
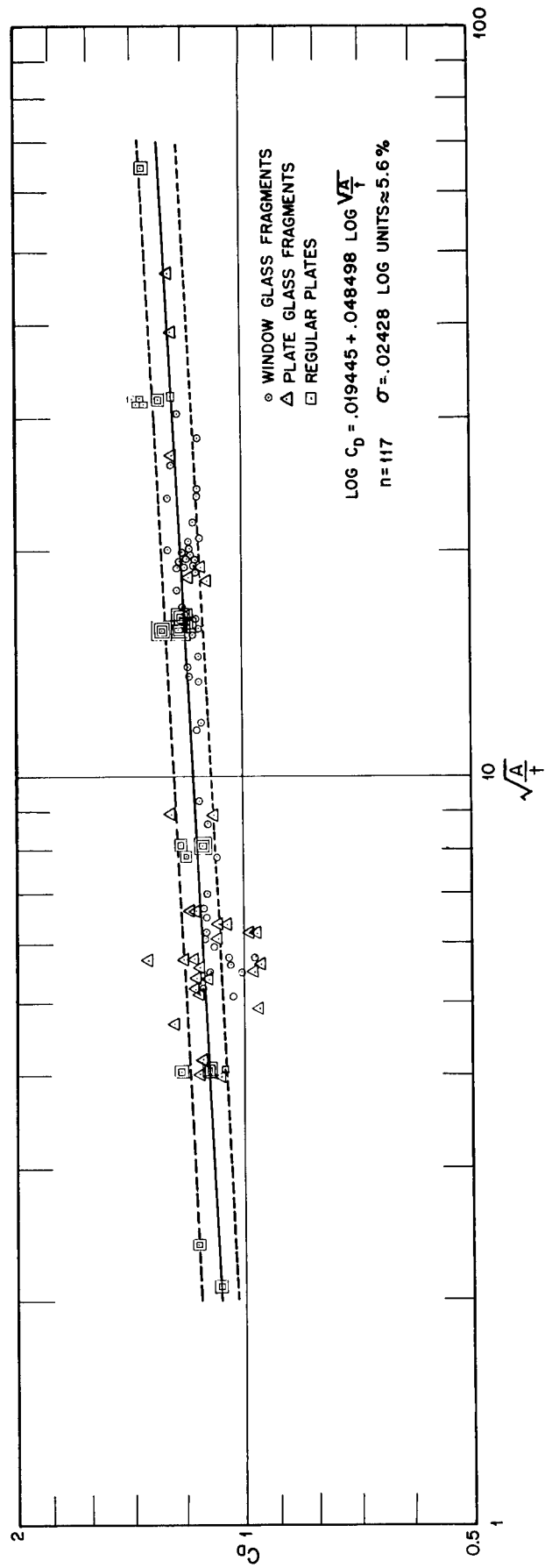
Fig. 4.21—Analysis of thick plates of random shape dropped flat. Drag coefficient vs. square root of area divided by the thickness of the plate ($s^{1/2}/t$), a dimensionless quantity representing a type of shape factor for irregular plates, is shown.

61

LATERAL POSITION   VENTRAL POSITION

MOUSE   22.45 g

RAT   192 g

GUINEA PIG   467 g

RABBIT   1829 g
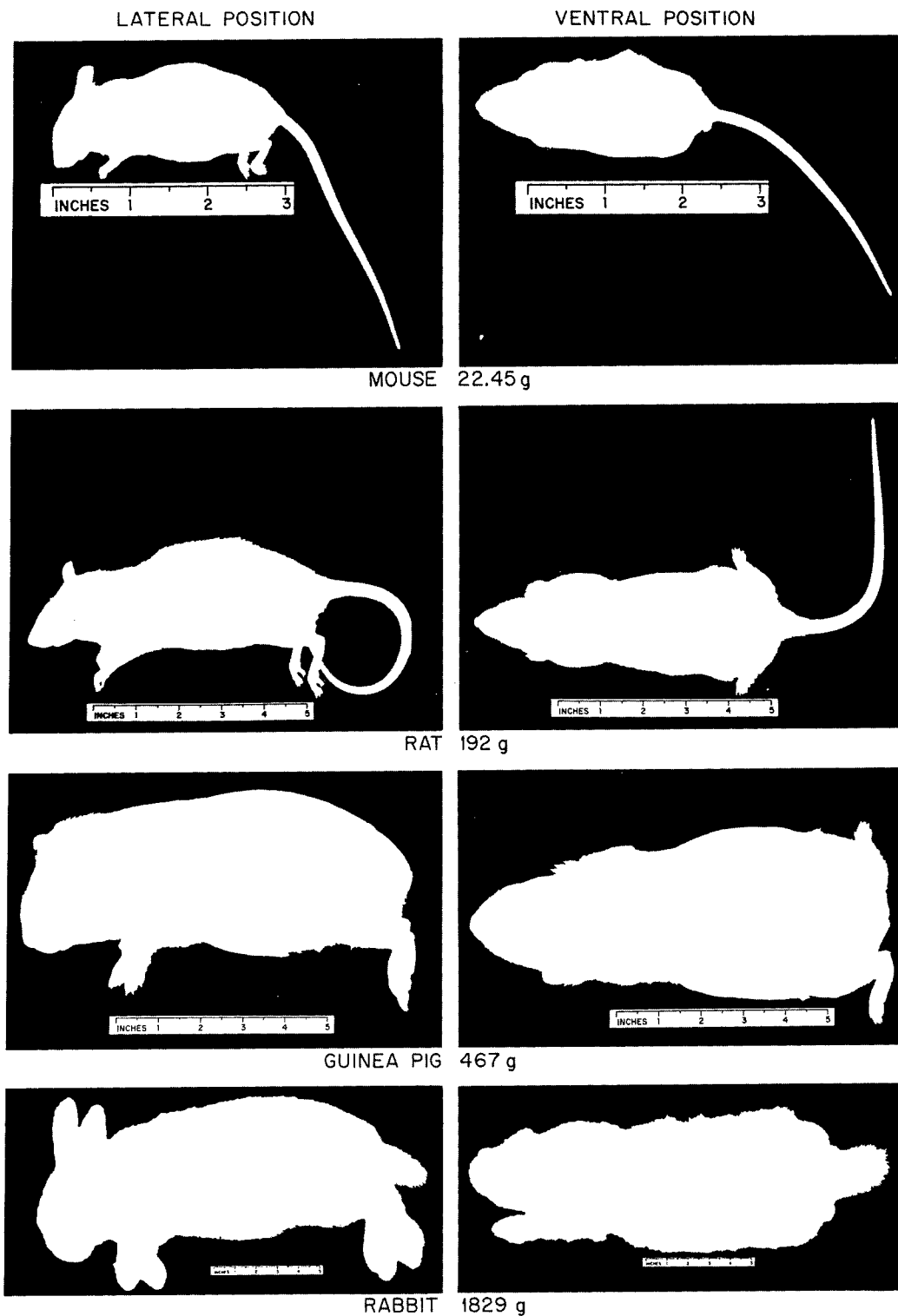
Fig. 4.22—Silhouette photographs of some of the animals used in the drop tests. The areas of the animals in the lateral and ventral positions were determined from full-scale photographs of this type.
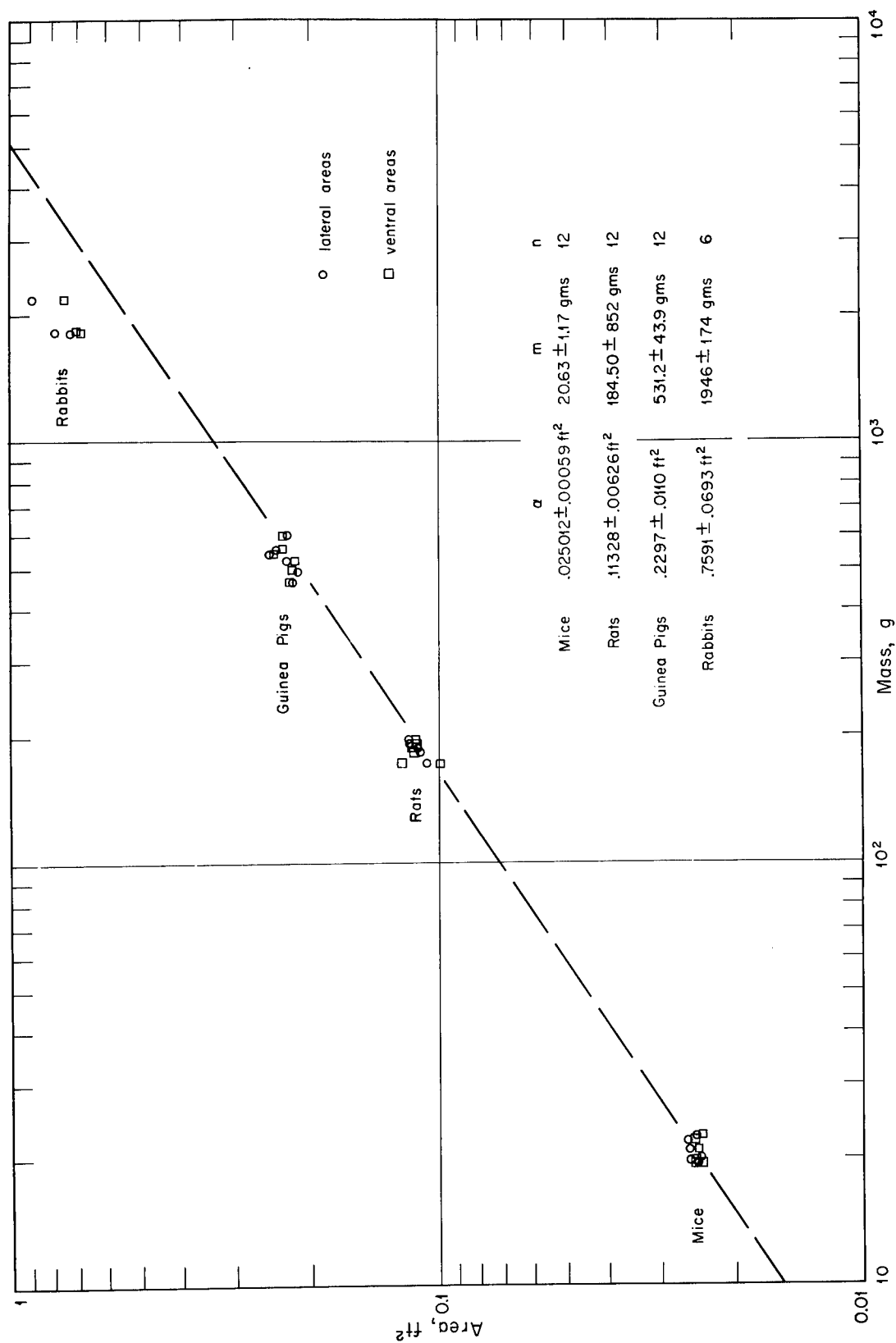
Fig. 4.23—Silhouette areas vs. mass of animals used in the lateral and ventral positions. These areas were photographically determined in the lateral and ventral positions. The line, which has a slope of $\frac{2}{3}$, is given for reference.

o lateral areas

□ ventral areas

	a	m	n
Mice	.025012 ±.00059 ft²	20.63 ± 1.17 gms	12
Rats	.11328 ±.00626 ft²	184.50 ± 8.52 gms	12
Guinea Pigs	.2297 ± .0110 ft²	531.2 ± 43.9 gms	12
Rabbits	.7591 ± .0693 ft²	1946 ± 174 gms	6

Mass, g

Area, ft²

Rabbits

Guinea Pigs

Rats

Mice

Fig. 4.24—Least-squares regression line describing α vs. mass of the animals. The masses in pounds are indicated for estimating the α of man.

64

Chapter 5

SUMMARY

The purpose of this study was to determine certain aerodynamic-drag parameters of small irregular objects, such as window-glass fragments, stones, steel fragments, and small laboratory animals. The drag parameters of interest were those necessary for the computation of the velocity vs. time history of the object when exposed to the winds associated with nuclear-produced blast waves.[1] These parameters were combined into one quantity called the acceleration coefficient (α) and defined as the product of the area presented to the wind and the drag coefficient divided by the mass.

The experimental method used to determine α was to measure the time required for a test object to free fall a given distance. To relate α to drop time, it was necessary to assume that, first, the drag coefficient and, second, the area normal to the object's motion were both constant throughout the fall; i.e., α was constant. Experimentally, the second condition was not difficult to satisfy since this only required that the object not rotate. It is well known that the drag coefficient varies with wind speed; however, it was shown from the experimental results that the error introd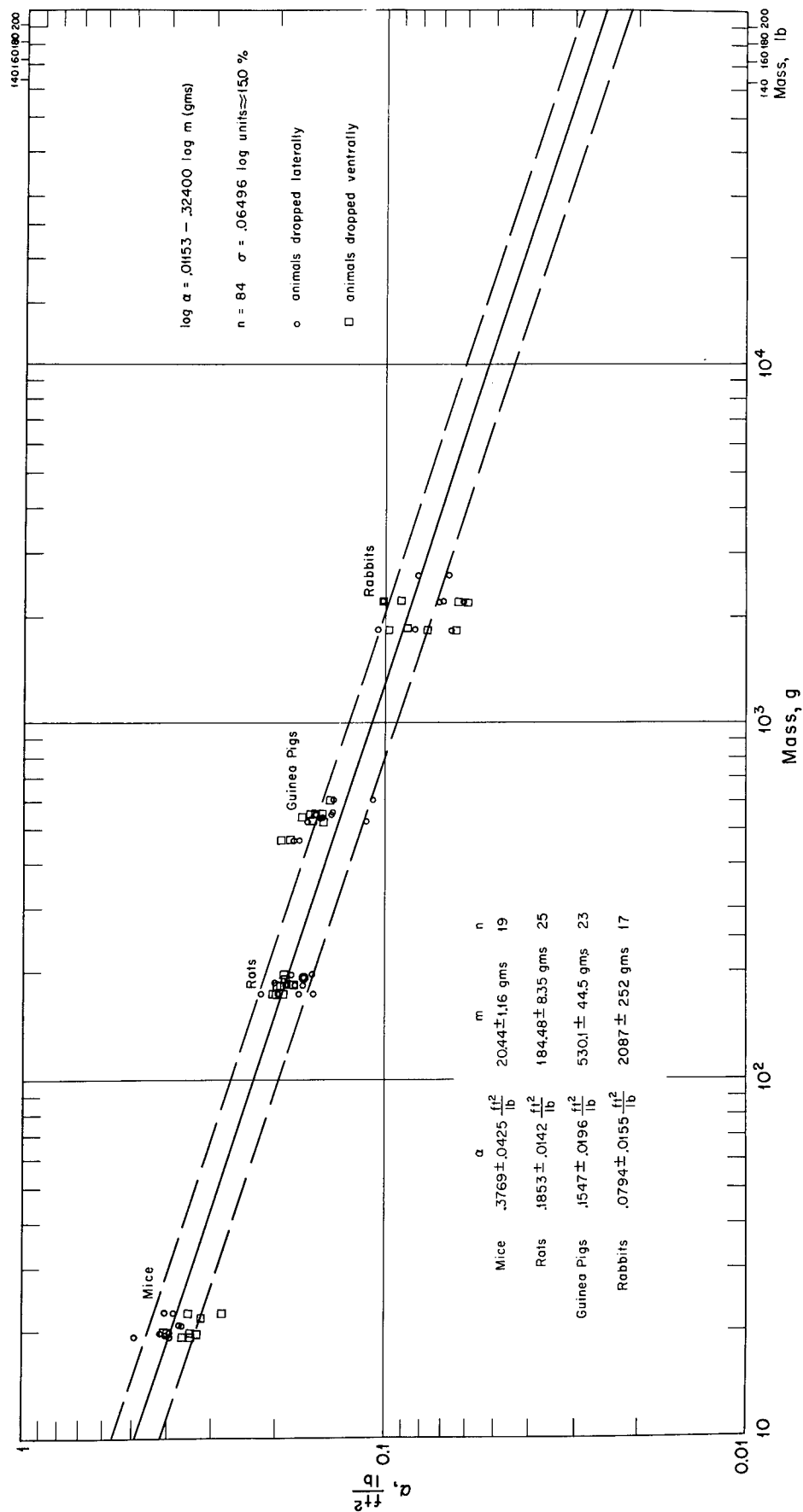uced in the measurement of α by assuming that the drag coefficient was constant was not significant, at least in so far as irregular objects were concerned. The following derived relation was used to determine α from measured drop time:

$$T = (2H/g)^{\frac{1}{2}} \, (\rho\alpha H)^{-\frac{1}{2}} \, \cosh^{-1} e^{\rho\alpha H/2}$$

where T = drop time

       g = acceleration of gravity (assumed constant)

       H = height of drop

       ρ = air density (assumed constant)

       α = acceleration coefficient (assumed constant)

The equipment used in the experiment consisted of a mechanism that would simultaneously drop the test object and start an electronic timer, an impact plate, and a contact microphone attached to the lower side of the impact plate. When the test object made contact with the plate, an electrical signal from the contact microphone stopped the timer.

The dropping technique as used in these experiments, was explored by dropping several types of regular objects (spheres, cubes, and plates); the results obtained were compared with those obtained using other techniques. The results are presented in this report for irregular objects. The drop times for two types of spheres were also used to check the experimental equipment for consistency of operation at various times during the drop tests.

Several types of stones were used as test objects. Most of the stones had been used at the NTS to study the production of secondary missiles by blast winds produced by nuclear explosions.[2,3] From 29 to 45 stones of each type were dropped, and α was determined for each. The results were analyzed by regression analyses to determine α for each type of stone, and the results are listed below. The units for α are ft^2/lb and for mass (m), mg. Sigma (σ) is used to designate the standard error of estimate in log units.

Gravel (painted):

$$\log \alpha = 0.57610 - 0.38803 \log m$$

$$30 < m < 1500 \qquad \sigma = 0.07463$$

Limestone fragments:

$$\log \alpha = 0.49926 - 0.32159 \log m$$

$$130 < m < 15{,}000 \qquad \sigma = 0.08811$$

Natural stones[3] from NTS at location 10P4:

$$\log \alpha = 0.48759 - 0.32835 \log m$$

$$11 < m < 4100 \qquad \sigma = 0.07063$$

Natural stones[3] from NTS at location 1S1a:

$$\log \alpha = 0.45171 - 0.31263 \log m$$

$$17 < m < 7100 \qquad \sigma = 0.08684$$

Natural stones[3] from NTS at location 4.3 GTS:

$$\log \alpha = 0.73833 - 0.30758 \log m$$

$$11 < m < 2300 \qquad \sigma = 0.1294$$

Pumice fragments:

$$\log \alpha = 0.63748 - 0.25466 \log m$$

$$18 < m < 2300 \qquad \sigma = 0.08948$$

Fragments of steel (mostly shrapnel) were also used as test objects, and the results were analyzed in a manner similar to that described for stones. The resulting regression equation was

$$\log \alpha = -0.74223 - 0.11315 \log (m/1000)$$

$$4500 < m < 150{,}000 \qquad \sigma = 0.09974$$

Fragments of ordinary window glass 0.125 in. thick were dropped, both with a plane surface down and edge-on, to determine the maximum and minimum α as a function of mass. In addition, plate-glass fragments 0.225 in. thick were dropped with the plane surface down. For small fragments the α values determined were independent of both orientation and type of glass (ordinary window glass or plate glass). It was found that the relation between α and mass could be represented as a straight line on logarithmic paper, but only for definite mass intervals. The regression equations derived from the experimental data are given below (n represents the number of fragments dropped; the remaining nomenclature is the same as that used previously).

Window glass and plate glass dropped flat or edgewise for $10 < m < 220$:

$$\log \alpha = 0.55659 - (1/3) \log m$$

$$n = 155 \qquad \sigma = 0.09014$$

Window glass dropped flat for 220 < m < 1270:

$$\log \alpha = -0.13874 - 0.036374 \log m$$

$$n = 81 \qquad \sigma = 0.06348$$

Window glass dropped flat for 1270 < m < 1574:

$$\log \alpha = -3.02323 + 0.89295 \log m$$

$$n = 10 \qquad \sigma = 0.04525$$

Window glass dropped flat for $1574 < m < 10^5$:

$$\log \alpha = -0.28024 + 0.34985 \log m$$

$$n = 46 \qquad \sigma = 0.01473$$

Window glass dropped edgewise for 220 < m < 5000:

$$\log \alpha = 0.12689 - 0.14982 \log m$$

$$n = 88 \qquad \sigma = 0.1013$$

Plate glass dropped flat for $860 < m < 3 \times 10^5$:

$$\log \alpha = 0.49172 + 0.023921 \log m$$

$$n = 31 \qquad \sigma = 0.03416$$

A useful formula was derived which related drag coefficient (C_D) for plates of random shapes and finite thickness to the ratio of the square root of plate surface area (s) to thickness (t). The drop-test data used in this analysis included that for window- and plate-glass fragments dropped flat as well as that for plates of regular shapes (square, circular, triangular) made of brass and plastic. The regression equation noted below was computed from data for 117 test objects whose shape factor ($s^{1/2}/t$) varied from 2 to 65.

$$\log C_D = 0.019445 + 0.048498 \log (s^{1/2}/t)$$

$$\sigma = 0.02428$$

(Note: $s^{1/2}$ and t are expressed in the same units.)

Shadowgraphs were prepared for mice, rats, guinea pigs, and rabbits in ventral and lateral positions to determine their presenting areas. In general, the areas determined (Fig. 4.23) were proportional to the mass of animal raised to the 2/3 power. The animals were then dropped ventrally and laterally to determine their α. It was found that there was no significant difference in α determined for these positions. The experimentally determined α values for each animal species were:

Mice (20.44 g)	0.3769 ± 0.0425 ft^2/lb
Rats (184.48 g)	0.1853 ± 0.0142 ft^2/lb
Guinea pigs (530.1 g)	0.1547 ± 0.0196 ft^2/lb
Rabbits (2087 g)	0.0794 ± 0.0155 ft^2/lb

These data were used to determine α as a function of animal mass.

$$\log \alpha = 0.01153 - 0.32400 \log (m/1000)$$

$$n = 84 \qquad \sigma = 0.06496$$

An estimate of the α for a 168-lb man was determined to be 0.0269 ft^2/lb by the above equation. Another estimate was made for the α of a 168-lb man using the results of a wind-tunnel study reported by Schmitt.[4] For positions corresponding to those of the dropped animals (ventral and lateral), an average α of 0.0336 ft^2/lb was obtained.

A method for estimating the average presenting area of any object in random orientations was developed. It was shown that the average presenting area is one-fourth the total surface area, provided no cavities exist. To approximate the no-cavity condition, the radiating surface area for man was used to estimate the average α for the human subjects used in the wind-tunnel study mentioned above. Assuming a drag coefficient of 1.0, a value of 0.0260 ft^2/lb for α was obtained. This value compared well with a value of 0.0281 ft^2/lb obtained by averaging the wind-tunnel data for men in various positions relative to the wind.

REFERENCES

1. I. Gerald Bowen et al., A Model Designed to Predict the Motion of Objects Translated by Classical Blast Waves, Report CEX-58.9, June 1961.
2. I. Gerald Bowen, Allen F. Strehler, and Mead B. Wetherbe, Distribution and Density of Missiles from Nuclear Explosions, Project 33.4, Operation Teapot Report, WT-1168, December 1956.
3. I. Gerald Bowen et al., Secondary Missiles Generated by Nuclear-produced Blast Waves, Project 33.2, Operation Plumbbob Report, WT-1468, in preparation.
4. Thomas J. Schmitt, Wind-tunnel Investigation of Air Loads on Human Beings, Report DTMB-892, The David Taylor Model Basin Aerodynamic Laboratory, January 1954.

Appendix

DERIVATION OF EQUATIONS

A.1 EQUATIONS OF MOTION

A.1.1 Integration of the Basic Equation

Equation 2.9 can be integrated

$$\int_{h_1}^{h_2} dh = \int_{v_1}^{v_2} \frac{v\, dv}{g\left(1 - v^2 \frac{\rho\alpha}{2g}\right)} \tag{A.1}$$

to give

$$h_2 - h_1 = \frac{1}{\rho\alpha} \ln\left\{ \frac{\left[1 - v_1\left(\frac{\rho\alpha}{2g}\right)^{1/2}\right]\left[1 + v_1\left(\frac{\rho\alpha}{2g}\right)^{1/2}\right]}{\left[1 - v_2\left(\frac{\rho\alpha}{2g}\right)^{1/2}\right]\left[1 + v_2\left(\frac{\rho\alpha}{2g}\right)^{1/2}\right]} \right\} \tag{A.2}$$

Now, solving Eq. A.2 for v_2 gives

$$v_2 = \left(\frac{2g}{\rho\alpha}\right)^{1/2}\left[1 - e^{-\rho\alpha h}\left(1 - v_1^2 \frac{\rho\alpha}{2g}\right)\right]^{1/2} \tag{A.3}$$

where $h = h_2 - h_1$ represents the height fallen from the point where the velocity equalled v_1. Substituting $v_2 = dh/dt$ in Eq. A.3 and integrating from zero height of drop to h

$$\int_{t_1}^{t_2} dt = \int_0^h \frac{dh}{\left(\frac{2g}{\rho\alpha}\right)^{1/2}\left[1 - e^{-\rho\alpha h}\left(1 - v_1^2 \frac{\rho\alpha}{2g}\right)\right]^{1/2}} \tag{A.4}$$

gives

$$t_2 - t_1 = \left(\frac{2h}{g}\right)^{1/2}\left(\left(\frac{\rho\alpha h}{2}\right)^{1/2} + \frac{\ln\left\{1 + \left[1 - e^{-\rho\alpha h}\left(1 - v_1^2 \frac{\rho\alpha}{2g}\right)\right]^{1/2}\right\}}{(\rho\alpha h)^{1/2}} - \frac{\ln\left[1 + \left(v_1^2 \frac{\rho\alpha}{2g}\right)^{1/2}\right]}{(\rho\alpha h)^{1/2}}\right) \tag{A.5}$$

Substituting $h = (h_2 - h_1)$ from Eq. A.2 into Eq. A.5 gives

$$t_2 - t_1 = \frac{1}{(2g\rho\alpha)^{1/2}} \ln\left\{ \frac{\left[1 - v_1\left(\frac{\rho\alpha}{2g}\right)^{1/2}\right]\left[1 + v_2\left(\frac{\rho\alpha}{2g}\right)^{1/2}\right]}{\left[1 - v_2\left(\frac{\rho\alpha}{2g}\right)^{1/2}\right]\left[1 + v_1\left(\frac{\rho\alpha}{2g}\right)^{1/2}\right]} \right\} \tag{A.6}$$

69

A.1.2 Dimensionless Analysis

Equations 2.4 and 2.8 of the text can be written in the form

$$v\frac{dv}{dh} = g - \frac{1}{2}\rho v^2 \frac{s}{m} f\left(\frac{vD}{\nu}\right) \tag{A.7}$$

where $f(vD/\nu) = f(R_d) = C_D$, the drag coefficient.

Now, g, D, and ν were considered constant so that they could be placed inside the differentials. Algebraic manipulations were then made on Eq. A.7 to make dimensionless quantities as follows:

$$\frac{vD}{\nu}\frac{d\left(\frac{vD}{\nu}\right)}{d\left[hg\left(\frac{D}{\nu}\right)^2\right]} = 1 - \frac{1}{2}\left[\frac{\rho}{g}\frac{s}{m}\left(\frac{\nu}{D}\right)^2\right]\left(\frac{vD}{\nu}\right)^2 f\left(\frac{vD}{\nu}\right) \tag{A.7a}$$

Defining $Y \equiv hg\,(D/\nu)^2$ (distance numeric)

$\quad\quad\quad Z \equiv vD/\nu$ (velocity numeric)

$\quad\quad\quad K \equiv (\rho/g)\,(s/m)\,(\nu/D)^2$ (acceleration-coefficient numeric)

as numeric parameters, the above dimensionless equation becomes

$$Z\frac{dZ}{dY} = 1 - \frac{1}{2}KZ^2\,f(Z) \tag{A.8}$$

By basic definition, $V = \Delta H/\Delta T$ or $\Delta T = \Delta H/V$, Eq. A.8 does not contain the time numeric. However, the incremental step of time numeric, defined as ΔX, would be the incremental step of distance numeric divided by the velocity number. Restated in terms of an equation, this is

$$\Delta X \equiv \frac{\Delta Y}{Z} \equiv \frac{\Delta h\,g\,(D/\nu)^2}{v\,(D/\nu)} = g\frac{D}{\nu}\frac{\Delta h}{v} \equiv g\frac{D}{\nu}\,\Delta T$$

Thus

$$X = g\frac{D}{\nu}\,t \qquad \text{(time numeric)} \tag{A.9}$$

Any previously derived equation can now be converted to the nondimensional form by replacing the primary parameters v, h, t, and s/m, by the numerics Z, Y, X, and K. The ρ, ν, and g quantities are dropped in the nondimensional form as they go into the numerics. C_D remains the same in the nondimensional equations.

Equations A.2 and A.6 become

$$\Delta Y = \frac{1}{KC_D}\ln\left\{\frac{\left[1 - Z_1\left(\frac{KC_D}{2}\right)^{1/2}\right]\left[1 + Z_1\left(\frac{KC_D}{2}\right)^{1/2}\right]}{\left[1 - Z_2\left(\frac{KC_D}{2}\right)^{1/2}\right]\left[1 + Z_2\left(\frac{KC_D}{2}\right)^{1/2}\right]}\right\} \tag{A.10}$$

and

$$\Delta X = \frac{1}{(2KC_D)^{1/2}}\ln\left\{\frac{\left[1 - Z_1\left(\frac{KC_D}{2}\right)^{1/2}\right]\left[1 + Z_2\left(\frac{KC_D}{2}\right)^{1/2}\right]}{\left[1 - Z_2\left(\frac{KC_D}{2}\right)^{1/2}\right]\left[1 + Z_1\left(\frac{KC_D}{2}\right)^{1/2}\right]}\right\} \tag{A.11}$$

$(T - T_{ND})$ or time-of-fall minus no-drag time-of-fall parameter* (Sec. 2.5), would now be

$$T - T_{ND} = T - \left(\frac{2H}{g}\right)^{\frac{1}{2}} \sim X - (2Y)^{\frac{1}{2}} \tag{A.12}$$

Another useful parameter (Sec. 2.5) would be

$$T - T_{ND} - \frac{\rho \alpha H}{12} T_{ND} = T - \left(\frac{2H}{g}\right)^{\frac{1}{2}} \left(1 + \frac{\rho \frac{S}{m} C_D H}{12}\right)$$

$$\sim X - (2Y)^{\frac{1}{2}} \left(1 + \frac{C_D}{12} KY\right) \tag{A.13}$$

If the approximate average value of the drag coefficient of an object is substituted for C_D in Eq. A.13, the parameter then represents the scaled time difference between the actual time above no-drag time and an approximation to the time above no-drag time considering the drag coefficient to be constant at C_D. It should be noted one can go from the variable of Eq. A.13 to that of Eq. A.12 by adding $2Y(C_D/12) KY$, which is the approximation to the time of fall minus no-drag time of fall in nondimensional form.

The no-drag equations, Eqs. 2.18 and 2.19, can likewise be put in numeric form to give

$$Z_{ND} = X_{ND} \tag{A.14}$$

$$Y_{ND} = \frac{(X_{ND})^2}{2} \tag{A.15}$$

Equations A.10 and A.11 are the equations actually used to predict the accurate drop times of two spheres (Sec. 4.2). The C_D curve was broken up into about one hundred steps over the Reynolds-number range encountered by these spheres, and the C_D values were used to integrate step by step to the total height of drop.

A.2   TERMINAL VELOCITY

Although not apropos of the present experiment, it should be noted that a useful relation can be derived from Eq. 2.13. As a body falls farther and farther, its velocity tends to reach a finite value called terminal velocity. This terminal velocity can be found from Eq. 2.13 by

$$\lim_{H \to \infty} V = \lim_{H \to \infty} (2gH)^{\frac{1}{2}} - \left(\frac{1 - e^{-\rho \alpha H}}{\rho \alpha H}\right)^{\frac{1}{2}} = \left(\frac{2g}{\rho \alpha}\right)^{\frac{1}{2}} \tag{A.16}$$

Figure A.1 is a plot of terminal velocity vs. α for two different conditions of ρ and g.

The percentage of terminal velocity reached by an object with constant α after it has fallen a distance H can be computed from Eqs. 3.13 and A.16 by

$$\%V_{terminal} = 100 \frac{V_{actual}}{V_{terminal}} = 100 \frac{(2gH)^{\frac{1}{2}} \left(\frac{1 - e^{-\rho \alpha H}}{\rho \alpha H}\right)^{\frac{1}{2}}}{\left(\frac{2g}{\rho \alpha}\right)^{\frac{1}{2}}} = 100 (1 - e^{-\rho \alpha H})^{\frac{1}{2}} \tag{A.17}$$

Figure A.2 is a plot of the above relation showing the percentage of terminal velocity as a function of α and H. Equation A.16 is independent of any initial conditions and represents the

---

*The subscript ND is used to indicate the no-drag value of a parameter; i.e., T_{ND} is the time an object would take to fall, assuming the object did not experience drag force.

71

velocity to which the instantaneous velocity is tending at any given time; whereas, Eq. A.17 requires that the velocity be zero when the height is zero and also that ρ, α, and g remain constant throughout the fall.

A.3 AVERAGE PRESENTED AREA

Consider a smooth surface, S, which has no cavities (part a, Fig. A.3); i.e., a plane that is tangent to S at any point does not cut through the surface. Then at some point on S construct a tangent plane that approximates S over a small area dA in the vicinity of the point of tangency. Let N be the normal to the plane at the point of tangency, E be oriented in any reference direction fixed in space, and θ be the angle between N and E. As N takes random orientations, not all values of θ are equally likely. To find the probability distribution of θ, one compares the area on the surface of a sphere between θ and $\theta + d\theta$ to the total area of the sphere. That is to say, consider a sphere whose center is always located at the point of tangency of the plane on the smooth surfaces. Now N can intersect the sphere in any point on the sphere, and all such points are equally likely. Then the probability that N will intersect the sphere in a specified area of the sphere is just the ratio of this area to the total area of the sphere. In the case under consideration, the specified area is the total area on the sphere between the angular limits of θ and $\theta + d\theta$ with respect to the fixed reference direction E. This area (see part b, Fig. A.3) is $2\pi(r \sin \theta) r \, d\theta$; so the probability that the angle between N and E is between θ and $\theta + d\theta$ is

$$P(\theta) \, d\theta = \frac{2\pi(r \sin \theta) \, r \, d\theta}{4\pi r^2} = \frac{\sin \theta}{2} \, d\theta \tag{A.18}$$

The presented area in the direction of E produced by dA (part a, Fig. A.3) is

$$\text{Presented area} = dA \cos \theta \qquad \text{when } 0 < \theta < \frac{\pi}{2}$$

$$= 0 \qquad \text{when } \frac{\pi}{2} < \theta < \pi \tag{A.19}$$

For $\pi/2 < \theta < \pi$, dA could not be seen from the direction of E because it is behind S. The average presented area would then be the integral of the presented area as a function of θ weighted with the probability distribution of θ, or

$$\text{Average presented area} = \int_0^{\pi_2} \frac{\sin \theta}{2} \, dA \cos \theta \, d\theta$$

$$= \frac{\sin^2 \theta}{4} \, dA \Big|_0^{\pi/2} = \frac{dA}{4} \tag{A.20}$$

For the whole surface S, the average presented area divided by the total surface area would be

$$\frac{\text{Average presented area}}{\text{Total surface area}} = \frac{\int_s \frac{dA}{4}}{\int_s dA} = \frac{1}{4} \frac{\int_s dA}{\int_s dA} = \frac{1}{4} \tag{A.21}$$

A.4 AVERAGE α FOR A RIGID MAN

Two angles were used to fix the man with respect to the wind, θ and ϕ (part c, Fig. A.3). Alpha can be computed directly from Schmitt's report[1] for $\theta = 90°$; $0° \leq \phi \leq 360°$ (upright position) or for $0° \leq \theta \leq 180°$; $\phi = 90°$ (side to the wind). For intermediate values the following formula was used to approximate α

$$\alpha(\theta, \phi) = \alpha(0°) + \frac{[\alpha(90°, \phi) - \alpha(0°)] [\alpha(\theta, 90°) - \alpha(0°)]}{\alpha(90°, 90°) - \alpha(0°)} \tag{A.22}$$

where $\alpha(0°)$ represents the α of a man head-on to the wind ($\theta = 0$) and is the same irrespective of ϕ, similarly $\alpha(180°)$ represents the α of a man feet-on to the wind ($\theta = 180°$) and also is constant for all values of ϕ. From Schmitt's report[1] $\theta(0°) = \theta(180°)$ for a clothed standing man and has a value of 0.00627 ft^2/lb. Thus Eq. A.22 holds exactly for all the conditions that can be computed directly from Schmitt's report; i.e., substituting in Eq. A.22 the various values of θ and ϕ for which α is known, the following relations for α are obtained:

$$\alpha(0°, \phi) = \alpha(0°)$$
$$\alpha(180°, \phi) = \alpha(0°)$$
$$\alpha(90°, \phi) = \alpha(90°, \phi)$$
$$\alpha(\theta, 90°) = \alpha(\theta, 90°)$$

(A.23)

Equation A.22 was arrived at by assuming $[\alpha(\theta, \phi_1) - \alpha(0)]/[\alpha(\theta, \phi_2) - \alpha(0)]$ is constant for all values of θ when ϕ_1 and ϕ_2 are fixed or, alternatively, by assuming $[\alpha(\theta_1, \phi) - \alpha(0°)]/[\alpha(\theta_2, \phi) - \alpha(0°)]$ is constant for all values of ϕ when θ_1 and θ_2 are fixed. In connection with the first assumption, one can write

$$\frac{\alpha(\theta, \phi) - \alpha(0°)}{\alpha(\theta, 90°) - \alpha(0°)} = \frac{\alpha(90°, \phi) - \alpha(0°)}{\alpha(90°, 90°) - \alpha(0°)}$$

(A.24)

for all values of θ and ϕ. Solving this for $\alpha(\theta, \phi)$ gives Eq. A.22. The second assumption will yield Eq. A.22 in a similar manner. Since θ and ϕ are independent variables, the average α would be given by

$$\overline{\alpha(\theta, \phi)} = \alpha(0°) + \frac{\left[\overline{\alpha(90°, \phi)} - \alpha(0°)\right]\left[\overline{\alpha(\theta, 90°)} - \alpha(0°)\right]}{\alpha(90°, 90°) - \alpha(0°)}$$

(A.25)

where the bars indicate average values.

The value $\overline{\alpha(\theta, 90°)}$ was computed by weighing $\alpha(\theta, 90°)$ with the probability distribution $(\sin \theta/2)\, d\theta$ (Eq. A.3) and integrating graphically from $\theta = 0$ to $\theta = \pi$ radians. The value for $\overline{\alpha(90°, \phi)}$ is just the average value of $\alpha(90°, \phi)$ with no weighing (all values of ϕ are equally likely), and $\alpha(90°, 90°)$ and $\alpha(0°)$ are particular α values computed directly from Schmitt's report. The value for $\overline{\alpha(\theta, \phi)}$ computed from Eq. A.25 represents the average α for a rigid, straight man, assuming every possible orientation with respect to the wind is equally probable. (Average α computed from Schmitt's report is 0.0281 ft^2/lb.)

REFERENCE

1. Thomas J. Schmitt, Wind-tunnel Investigation of Air Loads on Human Beings, Report DTMB-892, The David Taylor Model Basin Aerodynamic Laboratory, January 1954.
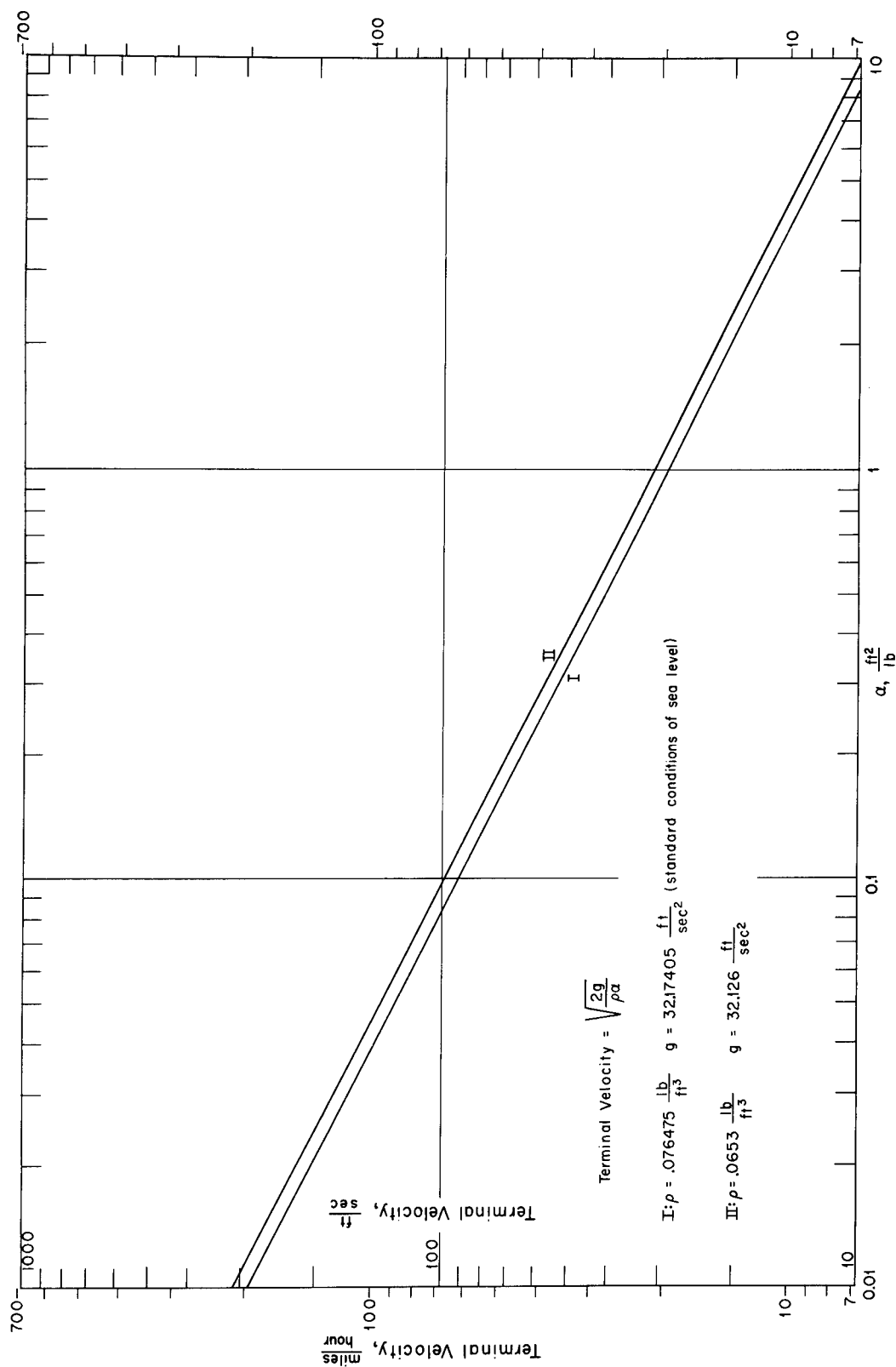
Fig. A.1—Terminal velocity vs. α for standard conditions at sea level (curve I) and typical conditions at 5300-ft altitude (curve II).

The following text appears within the figure:

Terminal Velocity $= \sqrt{\dfrac{2g}{\rho \alpha}}$

I: $\rho = .076475 \ \dfrac{lb}{ft^3}$ $g = 32.17405 \ \dfrac{ft}{sec^2}$ (standard conditions of sea level)

II: $\rho = .0653 \ \dfrac{lb}{ft^3}$ $g = 32.126 \ \dfrac{ft}{sec^2}$

$\alpha, \ \dfrac{ft^2}{lb}$

Terminal Velocity, $\dfrac{ft}{sec}$

Terminal Velocity, $\dfrac{miles}{hour}$

74

Fig. A.2—Percentage of terminal velocity vs. height of fall and α. When ρ = 0.0653 lb/ft³ (typical air density for 5300 ft above sea level), the 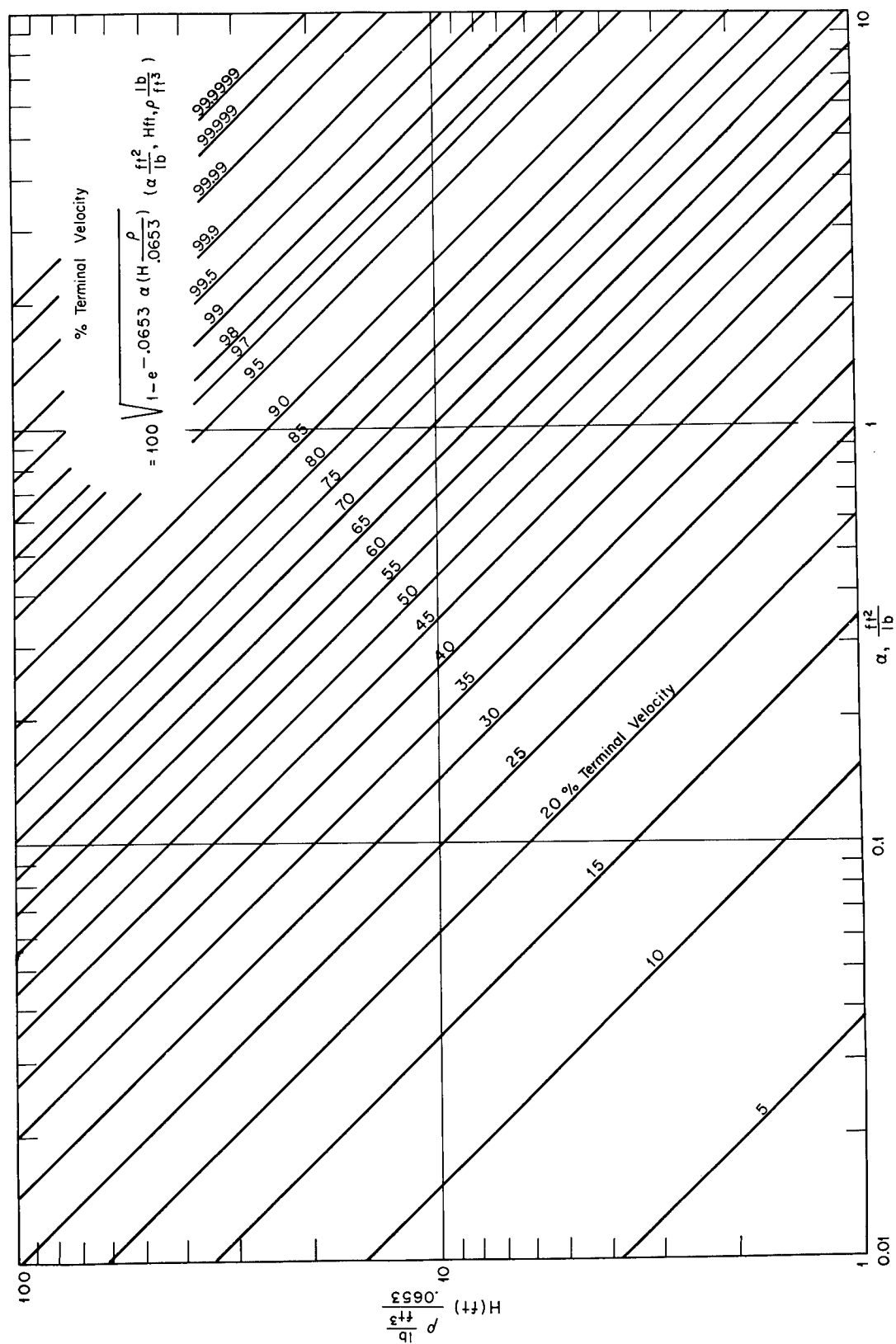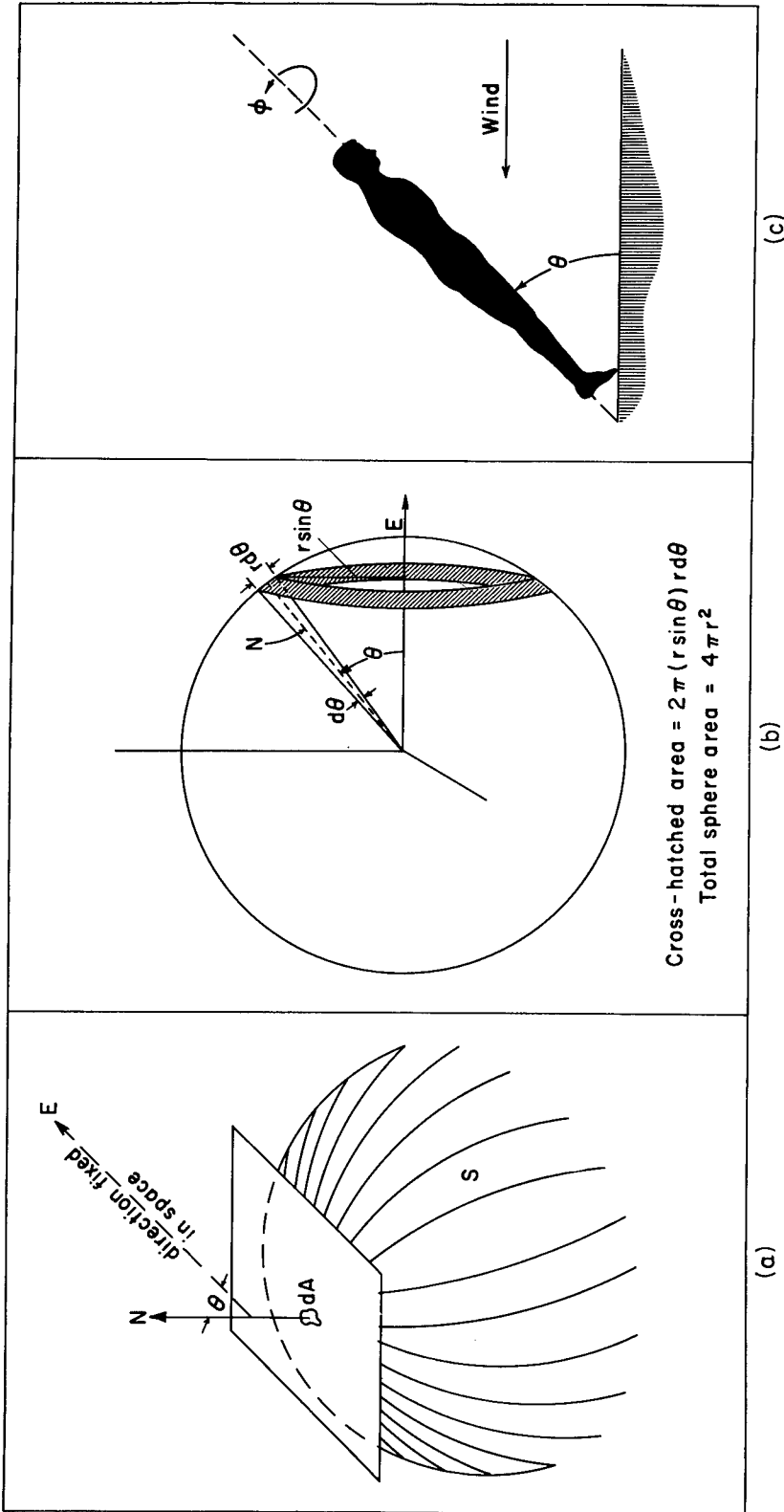height can be read directly; if ρ does not have this value, the height variable must be multiplied by the appropriate factor to convert to actual height of fall.

75

(a)

(b)

Cross-hatched area = $2\pi (r \sin\theta) r d\theta$

Total sphere area = $4\pi r^2$

(c)

Fig. A.3—(a) Drawing for the derivation of the relation between average presented area and total area for a surface with no cavities. dA is a small area that approximates S near the point of tangency. (b) Drawing for the derivation of the probability distribution of θ. (c) Drawing for the computation of the average α of a rigid clothed man. The angles θ and ϕ are used to fix the orientation of the man with respect to the wind.

CIVIL EFFECTS TEST OPERATIONS REPORT SERIES (CEX)

Through its Division of Biology and Medicine and Civil Effects Test Operations Office, the Atomic Energy Commission conducts certain technical tests, exercises, surveys, and research directed primarily toward practical applications of nuclear effects information and toward encouraging better technical, professional, and public understanding and utilization of the vast body of facts useful in the design of countermeasures against weapons effects. The activities carried out in these studies do not require nuclear detonations.

A complete listing of all the studies now underway is impossible in the space available here. However, the following is a list of all reports available from studies that have been completed. All reports listed are available from the Office of Technical Services, Department of Commerce, Washington 25, D. C., at the prices indicated.

CEX-57.1   The Radiological Assessment and Recovery of Contaminated
($0.75)   Areas, Carl F. Miller, September 1960.

CEX-58.1   Experimental Evaluation of the Radiation Protection Afforded by
($2.75)   Residential Structures Against Distributed Sources, J. A. Auxier, J. O. Buchanan, C. Eisenhauer, and H. E. Menker, January 1959.

CEX-58.2   The Scattering of Thermal Radiation into Open Underground
($0.75)   Shelters, T. P. Davis, N. D. Miller, T. S. Ely, J. A. Basso, and H. E. Pearse, October 1959.

CEX-58.7   AEC Group Shelter, AEC Facilities Division, Holmes & Narver,
($0.50)   Inc., June 1960.

CEX-58.8   Comparative Nuclear Effects of Biomedical Interest, Clayton S.
($1.00)   White, I. Gerald Bowen, Donald R. Richmond, and Robert L. Corsbie, January 1961.

CEX-58.9   A Model Designed to Predict the Motion of Objects Translated by
($1.25)   Classical Blast Waves, I. Gerald Bowen, Ray W. Albright, E. Royce Fletcher, and Clayton S. White, June 1961.

CEX-59.1   An Experimental Evaluation of the Radiation Protection Afforded
($0.60)   by a Large Modern Concrete Office Building, J. F. Batter, Jr., A. L. Kaplan, and E. T. Clarke, January 1960.

CEX-59.4   Aerial Radiological Monitoring System. I. Theoretical Analysis,
($1.25)   Design, and Operation of a Revised System, R. F. Merian, J. G. Lackey, and J. E. Hand, February 1961.

CEX-59.13   Experimental Evaluation of the Radiation Protection Afforded by
($0.50)   Typical Oak Ridge Homes Against Distributed Sources, T. D. Strickler and J. A. Auxier, April 1960.